INVESTIGATING EXTRACELLULAR MATRIX ANOMALIES AS PRECURSOR TO BLADDER COMPLIANCE DEFECTS AND VESICOURETERAL REFLUX

Fatima Tokhmafshan

Department of Human Genetics

August 2017

A thesis submitted to McGill University in partial fulfillment of the requirements of the degree of Master of Science

To Ann, Don, Lorraine and Barry, with love

Table of Contents

ABSTRACT

Bladder diverticula (BD; a pouch formation that protrudes through a weak point in the bladder musculature) and vesicoureteral reflux (VUR; abnormal retrograde of flow of urine towards the kidneys) are phenotypically and genetically heterogeneous pathologies that are discovered in patients who present with recurrent urinary tract infections and/or voiding dysfunction. Both BD and VUR can occur as part of multi-system syndromes caused by genetic abnormalities in the extracellular matrix (ECM), and have been observed in individuals with generalized joint hypermobility.

We used three mouse models to explore the ECM components that result in BD and VUR: C57Bl/6J (B6) as controls, because these mice do not reflux and do not have any documented ECM anomalies; C3H/HeJ (C3H) as a fully penetrant model of VUR with no documental systemic ECM anomalies; and *Tnxb*$^{+/-}$ and *Tnxb*$^{-/-}$ mutant mice on the B6 background, which do not exhibit VUR, but have documented ECM anomalies in their skin that models Ehlers-Danlos syndrome (EDS).

Using a bladder compliance assay, I determined that the *Tnxb*$^{-/-}$ followed by *Tnxb*$^{+/-}$ mice had the weakest bladders and ruptured at low filling pressures, suggesting a higher risk for BD formation. The C3H bladders did not rupture at any filling pressure.

Based on RNA *in situ* hybridization and RT-qPCR, *Tnxb* was expressed in the undifferentiated mesenchyme of the kidney and the smooth muscle of the ureter and bladder at E15, and the expression continued into adulthood. Histological analysis of bladder and ureter sections revealed that the bladder and ureter of newborn *Tnxb*$^{-/-}$ mice had the least amount of collagen, suggesting decreased tensile strength, while C3H mice had the most collagen, suggesting increased tensile strength. Increased α-SMA expression was observed in the bladder and ureters of *Tnxb*$^{-/-}$ and C3H newborn mice compared to B6. Elastin expression was examined and revealed that the bladder and ureter of C3H and *Tnxb*$^{-/-}$ mice had reduced elastin, suggesting impaired recoil. A reduction in both tensile strength and recoil in *Tnxb*$^{-/-}$ mice could lead to a weak bladder musculature prone to bladder diverticulum formation. An increase in tensile strength and decrease in recoil in C3H mice could lead to a stiff bladder and UVJ musculature incapable of occluding properly, thereby causing VUR.

Our lab previously identified a VUR-susceptibility locus (*Vurm1*) on the proximal end of chromosome 12 in C3H mice. An *in silico* analysis was used to identify ECM-related genes in *Vurm1* and to determine if C3H mice harboured putative disease-causing variants in these genes. Of the 16 ECM-related genes identified, only one gene, Rho-associated coiled-coil containing protein kinase 2 (*Rock2*), had a putative damaging mutation that was not observed in B6 mice. A deleterious mutation in *Rock2* could lead to increased smooth muscle contractility in the bladder, prompting an increase in α-SMA expression, a finding observed in the C3H bladder. This could increase mechanical force on the bladder musculature, which when combined with an increase in tensile strength and a decrease in recoil in the bladder of C3H mice, could maintain patency of the UVJ resulting in VUR.

Autosomal recessive mutations in *TNXB* in both humans and in mice have been shown to cause Classical-like Ehlers-Danlos syndrome (clEDS), and in humans, mutations in *TNXB* have been associated with VUR. We sequenced *TNXB* in a cohort of 47 children with VUR, BD, and generalized joint hypermobility, and identified five rare putative disease-causing variants.

In summary, these studies explore ECM anomalies as a novel cause for a defective UVJ that is prone to VUR, and a weak bladder that is prone to rupture and/or diverticulum formation.

RÉSUMÉ

Les diverticules de la vessie (BD ; formation d'une poche qui dépasse d'un point faible dans la musculature de la vessie) et le reflux vésicourétèral (VUR ; flux rétrograde anormal d'urine vers les reins) sont des pathologies phénotypiquement et génétiquement hétérogènes découvertes chez les patients présentant des infections des voies urinaires récurrentes et/ou le dysfonctionnement de mictions. Le BD et le VUR peuvent se produire dans le cadre de syndromes multi-systémiques causés par des anomalies génétiques dans la matrice extracellulaire (ECM), et ont été observés chez des individus atteints de syndrome d'Ehlers Danlos d'hyper-mobilité articulaire (HEDS).

Nous avons utilisé trois modèles de souris pour explorer les composants de l'ECM qui résultent en BD et VUR: les souris C57Bl / 6J (B6) comme contrôle, car elles ne refluent pas et n'ont aucune anomalie ECM documentée; les souris C3H / HeJ (C3H) en tant que modèle complètement pénétrant de VUR sans anomalies systémiques de l'ECM documentées; et les souris mutantes *Tnxb*$^{+/-}$ et *Tnxb*$^{-/-}$ sur fond B6, qui ne présentent pas de VUR, mais ont des anomalies de l'ECM documentées dans leur peau qui modélisent HEDS.

À l'aide d'un test de conformité de la vessie, j'ai déterminé que les souris *Tnxb* $^{-/-}$, suivies des *Tnxb*$^{+/-}$ avaient les vessies les plus faibles et se sont rompues à de faibles pressions de remplissage, ce qui suggère un risque plus élevé de formation de BD. Les vessies des souris C3H ne se sont rompues à aucune pression de remplissage.

D'après l'hybridation *in situ* d'ARN et la RT-qPCR, le *Tnxb* a été exprimé dans le mésenchyme indifférencié du rein et le muscle lisse de l'urètre et de la vessie à E15 et l'expression se poursuit jusqu'à l'âge adulte. L'analyse histologique des sections de la vessie et de l'urètre a révélé que la vessie et l'urètre des souris *Tnxb*$^{-/-}$ nouveau-nés avaient le moins de collagène, ce qui suggère une diminution de la résistance à la traction, tandis que les souris C3H ont le plus de collagène, ce qui suggère une élastance accrue. Une augmentation de l'expression de l'α-SMA a été observée dans la vessie et les urètres de souris *Tnxb*$^{-/-}$ et C3H nouveau-né comparé aux B6. L'expression de l'élastine a été examinée et a révélé que la vessie et l'urètre des souris C3H et *Tnxb*$^{-/-}$ avaient une élastine réduite, ce qui suggère une diminution de l'élasticité. Une réduction de l'élastance et de l'élasticité dans les souris *Tnxb*$^{-/-}$ pourrait conduire à une musculature de la vessie faible, susceptible de former un

diverticule de la vessie. Une augmentation de l'élastance et une diminution de l'élasticité chez les souris C3H pourraient conduire à une vessie rigide et une musculation de l'UVJ incapable d'occlure correctement, ce qui entraînerait un VUR.

Notre laboratoire a précédemment identifié un locus de susceptibilité au VUR (*Vurm1*) à l'extrémité proximale du chromosome 12 chez des souris C3H. Une analyse *in silico* a été faite pour identifier les gènes liés à l'ECM dans *Vurm1* et pour déterminer si les souris C3H présentaient des variantes qui pourraient mener à des maladies dans ces gènes. Sur les 16 gènes liés à l'ECM identifiés, un seul gène, la protéine kinase 2 associée à Rho (Rock2), a eu une mutation potentiellement néfaste qui n'a pas été observée chez les souris B6. Une mutation délétère dans Rock2 pourrait conduire à une augmentation de la contractilité des muscles lisses dans la vessie, entraînant une augmentation de l'expression de l'α-SMA, une découverte observée dans la vessie C3H. Cela pourrait augmenter la force mécanique sur la musculature de la vessie, qui, combinée à une augmentation de l'élastance et à une diminution de l'élasticité dans la vessie des souris C3H, pourrait maintenir la perméabilité de l'UVJ résultant du VUR. Il a été montré que des mutations de *TNXB* chez les humains et chez les souris peuvent causer le HEDS, et des mutations de *TNXB* chez les humains ont été associées au VUR. Nous avons séquencé le *TNXB* dans une cohorte de 47 enfants atteints de VUR, BD et d'hyper-mobilité articulaire, et nous avons identifié cinq variantes présumées responsables de la maladie.

En résumé, ces études explorent les anomalies de l'ECM comme une cause d'un UVJ défectueux qui est sujet à un VUR et d'une vessie faible susceptible de se rompre et/ou de formation de diverticules.

ACKNOWLEDGEMENTS

I am grateful to my supervisor Dr. Indra Gupta for her mentorship during the past three years. To my colleagues at the Gupta lab, I am grateful for your support.

I would like to thank the members of my supervisory committee, Drs. Danielle Malo and Mari Kaartinen, for their insight and assistance. Their constructive input was instrumental in making my project a success.

I would like to thank Drs. Rasheed Gbadegesin and Patrick Brophy for the collaborative opportunity that added a new dimension to my project, helping me hone bioinformatics and statistical genomics skills.

I am thankful to the mice as well as the animal facility technicians and veterinary staff, without whom this project would be impossible.

I am grateful to have received a studentship from Centre for Research in Reproduction and Development (CRRD) as well as a studentship in child health research from Desjardins, in support of my research.

During the past three years, the Research Institute of McGill University Health Centre (RI-MUCH) has provided me with a unique and nurturing learning environment, helping my transformation into a scholar. This transformation is the result of the mentorship of brilliant, successful and most importantly caring women scientists. I am grateful to Drs. Aimee K. Ryan, Loydie Jerome-Majewska, Cynthia Gates Goodyer, and Jacquetta Trasler for sharing their professional and personal wisdom with me. I am also grateful to many peers and colleagues at the RI-MUHC, whom I call friends and have made my graduate experience exhilarating and enriched.

As a student with disability, I would like to acknowledge and thank the Office of Students with Disability at McGill for their continued efforts in taking the stigma out of being a graduate student with disability, as well as their support in providing a fair and inclusive learning environment for students such as myself.

I would like to thank Drs. Tamara Kelly and Patricia Lakin-Thomas for igniting in me the passion for research and scientific discovery, for teaching me the tenets of good science and proper scientific practices, as well as the importance of science education and communication. I am grateful to these brilliant women of science for their continued mentorship both personally and professionally. I am grateful for their kind guidance and inputs in putting this thesis together.

Last but most certainly not least, I am grateful to Ann and Don Cooper, as well as Lorraine and Barry Kelly who have given me a second chance at having a family, and have made it their mission to see me transformed into a strong, independent and successful woman. Their constant encouragement and love is the source of my success. Without their support, I would not be able to get an education. I dedicate this thesis to them.

PREFACE AND CONTRIBUTION OF AUTHORS

This thesis is written in accordance with the guidelines provided by McGill University's Faculty of Graduate and Postdoctoral Studies.

The research reported herein was carried out by Ms. Fatima Tokhmafshan under the supervision of Dr. Indra Gupta. All results presented were generated by Ms. Tokhmafshan's experimental data, with the exception of patient recruitment, DNA preparation and the sequencing of patient cohort described; the sequencing data was analysed by Ms. Tokhmafshan. Ms. Jasmine El Andalousi and Dr. Inga Murawski were responsible for patient recruitment. Extraction of human DNA was performed by Ms. El Andalousi. She also assisted with administration of the bladder compliance assay to mice. Dr. Gupta administered the joint hypermobility test to the cohort. Experimental design, troubleshooting, animal husbandry and results analysis were carried out by Ms. Tokhmafshan with guidance from Dr. Gupta. This thesis is written by Ms. Tokhmafshan, under the supervision of Dr. Gupta, who contributed to the editing of all the chapters.

ABBREVIATIONS

α-SMA: Alpha-Smooth Muscle Actin
β2M: Beta-2-Microglobulim
µl/m: microliter/meter
ADV: Adventitia
B6: C57BL/6 inbred Mouse Strain
B-gal: Beta-galactosidase
BD: Bladder Diverticulum
BMP4: Bone morphogenetic protein
BP: Base pair
C3H: C3H/HeJ inbred Mouse Strain
clEDS: Classical-like EDS
COL 1/3/5: Type-I/Type-III/Type-V Collagen
E: Embryonic Day
ECM: Extracellular Matrix
EDS: Ehlers Danlos Syndrome
EGF: Epidermal Growth Factor
ELN: Elastin
FBN: Fibrillin
FBG: Fibrinogen
FBLN: fibulin
FGF: Fibroblast Growth Factor
FNIII: Fibronectin-Type III
GAG: Glycosaminoglycans
GJH: Generalized joint hypermobility
Het: Heterozygous
hEDS: Hypermobile Ehlers Danlos Syndrome
IF: Immunofluorescence
IHC: Immunohistochemistry
ISH: *In Situ* hybridisation
IVU: Intravesical Ureter
LP: Lamina Propria
KO: Knock-Out
MAF: Minor Allele Frequency
MMP: Matrix Metalloproteinase
MYOCD: Myocardin
P: Postnatal Day
RER: Retention in Endoplasmic Reticulum Sorting Receptor
RET: Ret Proto-Oncogene
RPL: Ribosomal Protein L
ROCK: Rho Assisted Coiled-Coil Containing Protein Kinase
RT-qPCR: Reverse Transcription Quantitative Polymerase Chain Reaction
SHH: Sonic Hedgehog
SM: Smooth Muscle
SOX: SRY-box
SRF: Serum Response Factor
TBX: T-box
TGFβ: Transforming Growth Factor beta
TNX: Tenascin-X
TSHZ: Teashirt
UPK: Uroplakin
UTI: Urinary Track Infection
v./v.: Volume in Volume
UVJ: Ureterovesical Junction
VCUG: Voiding Cystourethrogram
VUR: Vesicoureteral Reflux
WT: Wild Type
wt./v.: Weight in Volume

LIST OF FIGURES

LIST OF TABLES

1 CHAPTER ONE: INTRODUCTION

1.1 Vesicoureteral reflux: a developmental defect

The abnormal retrograde flow of the urine from the bladder in the direction of the kidney is known as vesicoureteral reflux (VUR)(1). Approximately 1% of children are affected by VUR that results in recurrent urinary tract infections. Frequent urinary tract infections scar the kidneys and lead to high blood pressure and renal failure in affected children (1-4). VUR arises due to developmental defects in the point of entry of the ureter within the bladder wall—the ureterovesical junction (UVJ). The UVJ is a critical structure in the urinary tract and consists of the submucosal length of the ureter within the bladder—the intravesical ureter (IVU), as well as the bladder musculature(5). The UVJ protects the upper urinary tract from the intermittent high pressure that arises in the bladder during micturition. The UVJ allows passage of urine into the bladder and prevents retrograde flow towards the kidneys when it is transiently occluded during micturition. Occlusion of the UVJ requires an adequate length to the IVU, an oblique angle of ureter entry into the bladder, as well as smooth muscle and extracellular matrix that compresses the ureteral orifice. Abnormalities in the development of any of these features results in VUR (1, 6).

1.2 Clinical spectrum and natural history of VUR

VUR is phenotypically heterogeneous and depending on the degree of dilation of the collecting system, it is divided into five grades using the classification proposed by the International Reflux Study (7). A number of longitudinal studies have shown that approximately 50-65% of cases of non-syndromic VUR undergo spontaneous resolution

with age (8-11). The cause of this spontaneous resolution is yet to be understood, however the elongation of the intravesical ureter (0.5 cm at birth vs. 1.5-2.5 cm in adulthood) due to somatic growth has been offered as an explanation for the improved function of the UVJ (12-14). Alternatively, morphological changes in the bladder and ureter smooth muscle layer and its supporting ECM microenvironment could be the basis for why VUR resolves over time.

The body of evidence pointing to genetic causes for VUR is overwhelming. Several studies have reported a prevalence of 27-51% for VUR in siblings of patients with VUR, and a prevalence of 66% in children whose parents had VUR (15-19). VUR also has a higher incidence in monozygotic compared to dizygotic twins (20). Candidate gene and genome-wide association approaches have been used to identify genes involved in VUR. The candidate gene approach has examined whether genes important in urogenital development cause VUR. The genome-wide analyses have determined whether specific genomic regions are linked or associated with VUR in families and cohorts of affected patients. In theory, identifying a causative gene for VUR using linkage analysis in affected pedigrees is the ideal approach, however the greatest challenge of performing such analyses is the determination of the VUR status of an individual. Mild forms of VUR can resolve spontaneously as the child grows, leaving no trace to elucidate whether an asymptomatic adult had VUR during childhood. The only way to positively determine the presence of VUR in an individual is through an invasive test known as the voiding cystourethrogram (VCUG), which involves catheterization of the urethra followed by injection of a radio-contrast dye into the bladder. Most adult members of a pedigree are not screened using a VCUG, therefore their disease-free status cannot be categorically classified as unaffected. Such a challenge has made it difficult to determine a mode of inheritance for VUR. Thus far, a range of inheritance patterns

have been suggested that include autosomal dominant with incomplete penetrance, autosomal recessive, X-linked and polygenic (21-30). The difficulty in finding multigenerational affected families makes association studies a more appropriate tool than classical linkage analysis. Association studies evaluate the relationship between alleles and phenotypes by comparing allele frequencies in affected and control populations, therefore making them applicable to related or unrelated individuals. Such association analyses have been carried out by a number of research groups and point to segregation of VUR and generalized joint hypermobility (31-36). The same studies have identified *TNXB* as a candidate gene for VUR. Autosomal recessive mutations in Tenascin-XB (*TNXB*) have been implicated in clEDS (37-40).

1.3 Congenital bladder diverticulum: a problem of bladder musculature

Bladder diverticula (BD) can be congenital (primary) or acquired (secondary), and are defined as pouches that protrude through the bladder musculature (41-43). The acquired form of BD is often associated with bladder outlet obstruction, which leads to increased intraluminal bladder pressure and ballooning of the bladder mucosa through a weak spot within the musculature. Acquired BD accounts for 90% of reported BD cases (41-45). The congenital form of BD is hypothesized to be the result of muscle hypoplasia due to defects during bladder development and accounts for 10 % of cases (41-44). Muscle weakness, atrophy and/or hypoplasia are the hallmarks of BD; however, these defects are often asymptomatic. Most BD are discovered as incidental findings when a paediatric patient with a urinary tract infection or more rarely with signs of bladder rupture undergoes a

contrast study known as the voiding cystourethrogram (i.e. VCUG). The prevalence of BD among children is approximately 1%, but this is likely an underestimation since the defect can be asymptomatic (44, 46-48). While BD can occur at any location along the bladder wall, approximately 90% of the congenital BD occur at close proximity to the ureteral orifice and are termed Hutch diverticulum (44, 47, 49-51).

1.3.1 Clinical spectrum and natural history of BD

Similar to VUR, BD is both phenotypically and genetically heterogeneous. The diverticula can range in size from 0.5-10 cm. The gold standard in diagnosis of BD, similar to VUR is performance of a VCUG, and a review of the published case studies on BD shows that in approximately 68% of cases, it co-occurs with VUR. To date there are no linkage or association studies exploring the genetic causes of isolated BD, as the majority of reported cases are syndromic (i.e. connective tissue syndromes).

1.4 Histology of the UVJ and the bladder

The UVJ in both humans and mice has three distinct layers: the urothelium, the lamina propria, and the musculature layer. The urothelium is the innermost mucosal layer of the UVJ, and consists of a highly elastic and impermeable transitional epithelium. The urothelium includes the umbrella cells, the intermediate cells and the basal cells (52, 53). The umbrella cells are a single layer of multinucleated hexagonal-shaped cells and are directly exposed to urine. The umbrella cells contribute to structural plaques seen by scanning electron microscopy. The umbrella cells express a specialized multi-protein

complex of transmembrane glycoproteins known as uroplakins (UPKs). Their function is not yet fully understood; however, they maintain the impermeability of the uroepithelium, and they facilitate bladder contractions through adjustment of the apical surface area of urothelial plaques (54-57). Uroplakins are also hypothesized to play a role in the function and/or development of the UVJ as indicated by the presence of VUR in mice with mutations in uroplakins (53, 58, 59). Protection of the urinary tract from invasion by bacteria and/or waste products in the urine is critical, and is facilitated by urothelium. The barrier function of the urothelium is, in part, dictated by glycosaminoglycans (GAGs), predominantly chondroitin and heparan sulphates, which cover the urothelial cells. The GAGs form a negatively charged and gel-like barrier against urine, and undergo turnover due to periodic shedding of the urothelium (60-64). Below the urothelium is a thin layer of loose connective tissue known as the lamina propria (LP). This layer is highly compressible and rich in nerve endings as well as fibrillary collagens. The outer most layer of the UVJ is the musculature layer, which consists of well-differentiated smooth muscle (SM) bundles. The musculature is uniform in thickness, and is longitudinal unlike the rest of the ureter that contains both circular and longitudinal muscle bundles (65, 66). The longitudinal muscles at the UVJ intercalate with the inner longitudinal muscle fibres of the bladder. A combination of these fibres and the middle circular, and outer longitudinal muscle fibres of the bladder musculature forms the roof of the UVJ. In contrast, the floor of the UVJ is made only from the inner circular, and outer longitudinal layers within the bladder. The specific arrangement of the bladder and ureter muscle bundles is vital to provide a firm support to the intravesical ureter, and to prevent VUR (14, 67).

The bladder in both humans and mice also consists of the three layers described above (i.e. urothelium, lamina propria, musculature). The smooth muscle in the bladder is known as the detrusor, which is characterized by varying arrangements of smooth muscle bundles at different points within the bladder wall. Generally, the bladder is divided into two main components: the body and the base. The bladder body is the region above the ureteral orifices, while the bladder base consists of the trigone (i.e. the triangular region that contains the ureteral and urethral orifices) (68). In humans and mice, the trigone has been shown to consist of ureteral as well as longitudinal detrusor muscles (5). The fact that the trigone consists of a thin layer of longitudinal muscle makes this region especially prone to BD formations (5, 69). The detrusor consists of three layers of smooth muscle: outer and inner longitudinal, and middle circular. These muscle fibres form bundles of varying sizes that intersect with one another. This meshwork of muscle bundles is surrounded by collagen fibres, thereby forming a strong detrusor capable of storing urine and undergoing repeated expansion and contraction (68, 70-74).

1.5 UVJ development

In mouse, the nephric duct grows caudally and induces the pronephros, followed by the mesonephros and finally the metanephros at the level of the mid-hind limb(75). The metanephric kidney forms around embryonic day (E) 10.5 when the caudal part of the nephric duct starts to form an epithelial swelling called the ureteric bud (75). The ureter develops from the ureteric bud, and is an epithelial tube surrounded by mesenchymal cells (6, 76). Until E14 in the mouse, the elongating ureter and the nephric duct remain connected

through the common nephric duct (6, 77). The insertion of the ureter into the bladder requires separation of the ureter from the nephric duct, leading to a vertical, followed by a lateral movement of the ureter towards the bladder (6, 77). Apoptosis of the common nephric duct fully severs the connection between the ureter and the nephric duct, leading to the ureter's independent insertion into the bladder at the UVJ (6, 77). The cross-talk between the ureteral epithelium and the ureteral mesenchyme is essential to the development of the ureter. In response to this cross-talk, the early cuboidal ureteral epithelial cells differentiate into urothelium around (E) 13.5-14.5 (58, 78, 79). Meanwhile the ureteral mesenchymal cells differentiate into smooth muscle and adventitial fibroblasts. The smooth muscle differentiation of the ureter occurs in a descending wave from the proximal ureter (i.e. ureteropelvic junction) to distal ureter (i.e. UVJ) (76, 80-82). A number of animal studies have pinpointed genes important for the development of the ureteral smooth muscle. Discs large homolog 1 (*Dlgh1*) is a scaffolding protein that is expressed by the ureteral epithelium and plays a role in regulating ureteral smooth muscle formation. The ureteral smooth muscle bundles in the *Dlgh1*$^{-/-}$ are misaligned, leading to impaired peristalsis (83, 84). Bone morphogenetic protein 4 (*Bmp4*), a member of the transforming growth factor beta (TGF-β) family, is expressed by the ureteral mesenchyme. BMP4 acts in concert with sonic hedgehog (Shh), a secreted signalling protein expressed by the ureteral epithelium, to regulate the differentiation of ureteral smooth muscle (76, 85-87). The transcription factor T-box 18 (*Tbx18*) is expressed in the ureter mesenchyme and is required for the ureteric mesenchyme to repond to Shh signalling (80). *Tbx18*$^{-/-}$ mice lack expression of downstream SHH signalling targets (80, 88). The ureteral mesenchymal cells in both *Tbx18*$^{-/-}$ and *Shh*$^{-/-}$ mice show reduced proliferation and fail to differentiate into smooth muscle (76, 80). Teashirt (*Tshz*)

genes code for a small family of zinc finger transcription factors, which are expressed in the ureteral mesenchyme before and after smooth muscle differentiation (89). Transcription factor *Sox9* is also expressed in the undifferentiated ureteral mesenchyme. Both *Tshz3* and *Sox9* act as downstream mediators of myocardin (*Myocd*), which is a key regulator in smooth muscle differentiation. Mutations in either *Tshz3* or *Sox9* in mice lead to mesenchymal cells that fail to differentiate into smooth muscle, and result in a dilated urinary tract described as hydroureter (82, 90-95).

1.6 Bladder development

The bladder is formed from the endodermal cloaca and from the ends of the nephric duct (5, 77, 96, 97). At embryonic day E13 in the mouse, the urogenital sinus gives rise to the bladder after the urorectal septum partitions the cloaca into the urogenital sinus and the rectum (97-100). Mesenchyme derived from splanchnopleural mesoderm surrounds the endodermal-derived epithelial lining of the lumen of the primitive bladder. The bladder mesenchyme facilitates epithelial-mesenchymal cross-talk that is critical for induction of smooth muscle differentiation from the bladder mesenchyme (101-103). The significance of this cross-talk is demonstrated by tissue recombination experiments in which E12 bladders survive and undergo smooth muscle differentiation when grown as grafts beneath the kidney capsule of mice for two weeks, while un-grafted bladders do not (101, 102). Similar to the ureter and UVJ development, SHH and BMP4 play important roles in the differentiation of the bladder smooth muscle (76, 103-105). Another signalling pathway involved in the differentiation of the bladder smooth muscle is serum response factor (SRF). SRF is a DNA-binding phosphoprotein that regulates muscle-specific gene expression and smooth muscle

differentiation (106, 107). SRF-mediated transcription of smooth muscle genes depends on interaction of SRF with cofactors such as *Myocd* (108-110). *Srf* is expressed by the bladder mesenchyme starting at E12.5; it is required for the initial differentiation of the smooth muscle cells, and has been shown to drive the expression of alpha smooth muscle actin (α-SMA) (110).

1.7 Extracellular matrix components and their functions

The extracellular matrix (ECM) of a tissue specifies its biomechanical properties, which in turn, dictates the tissue's response to internal or external forces. Tensile strength and distensibility refer to biomechanical properties of a tissue that prevent its rupture and deformation under an applied force, respectively (111). Tensile strength and distensibility are mostly dictated by the amount and type of collagens in the ECM. Compliance describes a tissue's ability to maintain a low intraluminal pressure by distending in response to an increase in the intraluminal volume. Compliance is directly related to distensibility and recoil, but inversely related to tensile strength (70, 112, 113). Recoil refers to a tissue's ability to regain its original shape and dimension after an internal or external force is removed, and is defined by the quantity and the quality of elastic fibres. Aside from the collagens and elastin, the ECM consists of many other secreted glycoproteins (e.g. fibronectin, fibrillins, laminins, proteoglycans, glycosaminoglycans), enzymes that post-translationally modify these components (e.g. lysyl oxidase), and proteinases that cleave peptide bonds (e.g. metalloproteinases) to facilitate ECM turnover, as well as cytokines such as transforming growth factor beta (TGF-β) and fibroblast growth factors (FGFs) that influence cell differentiation and growth as well as interactions with the matrix (111). The

ECM composition of each tissue type is uniquely determined during development through a dynamic biochemical and biophysical dialogue between various cellular components. Aside from its structural components, the ECM contains a number of matricellular components such as thrombospondins and tenascins (i.e. Tenascin-C and Tenascin-XB) that regulate expression, assembly and deposition of various matrix components. These matricellular components can also modulate cell function through cell-matrix interactions, which will be discussed further in Chapter 2.

1.7.1 Collagen fibrils dictate tensile strength and distensibility

Due to their great abundance in the body (~30% of total proteins), collagens are the most well-characterized components of the ECM. Thus far, 28 different collagen types have been identified, and are classified based on their ability to form fibrils (i.e. fibrillar vs. non-fibrillar) (111, 114). Type I, II, III, V, XI, XXIV, and XXVII are fibril-forming.

Each collagen molecule is composed of a triple helix of three polypeptide α-chains, which are used to distinguish the different collagen types (114-117). Collagen molecules can form homo- or hetero-trimers (i.e. made of the same or different α-chains) that are found in fibrils (10-300 nm diameter) and in fibers (1-20 μm). Collagen exists in a variety of supramolecular structures including thick parallel bundles, open weave hexagonal networks, chicken-wire lattices, membrane-bound fibrils, and beaded fibrillary strings as per each tissue's biomechanical properties. Collagen fibrillogenesis is an important process that is regulated by type-V and type-XI collagens (114-120). The fibril assembly progresses through a quarter-staggered arrangement where each collagen molecule is placed on top of or adjacent to the previous molecule at a quarter of its length, thereby leaving a space

between the head and tail of successive molecules. This arrangement is crucial to the cross-linking of fibrils through covalent bond formation between adjacent fibrils. Fibrillogenesis gives rise to either thin or thick fibrils (114-116). Thick fibrils have a larger cross-section and therefore have higher resistance against deformation due to distension—these fibrils dictate tensile strength. Thin fibrils have a smaller cross-section and have better distensibility and recoil properties (114-116). Because most tissues require both tensile strength and distensibility, both types of fibrils are usually formed.

The major contributor to tensile strength in most tissues is type-I collagen (COLI), which forms shorter fibrils with a larger cross-section (i.e. thick fibrils). Type-III collagen (COLIII) forms longer and thinner fibrils with multiple regions that can unfold, making these fibrils easily stretchable and therefore a major contributor to a tissue's distensibility. In humans and mice, COLIII forms heterotypic fibrils with COLI and is essential for COLI fibrillogenesis (114-117, 120-123).

1.7.2 Elastic fibres dictate recoil

A tissue's ability to regain its original shape and dimension when undergoing repeated cycles of stretching is dictated by elastic fibres (124-126). Elastic fibres consist of an inner core of cross-linked elastin protein surrounded by microfibrils that are made of fibrillin.

The protein tropoelastin, encoded by the elastin gene (*ELN*), is the fundamental component of elastin. The newly translated tropoelastin monomers are secreted into the extracellular environment where they are cross-linked to form elastin (126-128). The

deposition and cross-linking of elastin onto the fibrillin microfibrils is facilitated by members of the fibulin family (i.e. fibulin-4 and fibulin-5) as well as lysyl oxidases.

Fibrillins are a family of secreted glycoproteins and fibrillin-1 is the most abundant isoform (129, 130). The precise mode of assembly of fibrillin microfibrils is unknown, but they are arranged as parallel bundles of four to eight fibrillin molecules that are joined in series in a head-to-tail manner (131). The fibrillin microfibrils form a scaffold for the deposition of elastin, therefore perturbations in their synthesis will impair elastic fibre assembly (127, 131). Fibrillin microfibrils play a key role in the regulation of transforming growth factor β1 (TGF-β1) signalling in elastic tissues such as lungs and arteries (132, 133). A number of proteins associated with fibrillin microfibrils bind to and sequester TGF-β1 to prevent downstream signalling (126, 132, 133).

Fibulins are a family of seven secreted glycoproteins that interact with a variety of different ECM components to direct cell adhesion, migration, and proliferation. Fibulin-4 and -5 are crucial to elastic fibre assembly as they facilitate the deposition and cross-linking of elastin within the fibrillin microfibril scaffold (127, 134, 135). Both Fibulin-4 and Fibulin-5 interact with various members of the extracellular copper-dependent crosslinking enzyme, known as lysyl oxidases (LOX), and differentially modulate elastic fibre formation (136). Fibulin-4 binds LOX through its N-terminus, and Fibulin-5 binds lysyl oxidase-like 1 (LOXL1) through its C-terminus, thereby recruiting these molecules to the site of elastic fibre formation, resulting in elastic fibre crosslinking and therefore stabilization (136-138). Fibulin-4 is required for the development of the vasculature and the neural crest, and binds to latent TGF-β binding proteins (LTBPs), such as LTBP-4 and therefore can regulate the bioavailability of TGF-β1 (135).

1.8 ECM architecture and biomechanical components of the UVJ and the bladder

Compliance in the bladder is essential to maintain a low intraluminal pressure under the force of volume expansion from urine storage, thereby preventing potential BD formation, or VUR (49, 139, 140). Compliance in the UVJ is crucial for maintaining a steady internal fluid pressure, thereby preventing an increase in the wall tension of the IVU that could otherwise compromise the occlusion of the UVJ during micturition. Consequently, the biomechanical components of the bladder and the UVJ that facilitate compliance are indispensable to these tissues' functions.

The ureter is a fibro-muscular tube that propels urine from the kidneys to the bladder through peristalsis in a unidirectional manner. Because the amplitude and frequency of the peristaltic waves depends on the urine volume being transported, the ureter wall must have multidirectional tensile strength, distensibility and recoil. With every contractile wave, the ureter wall is distended, pushing the urine bolus forward, immediately after, the wall recoils back to its' original shape and dimension. The ureteral musculature drives the contractile waves and provides structural support. The rich array of collagen fibres present in the lamina propria as well within the muscle layer provides the required balance between tensile strength and distensibility in the ureter wall. The exact collagen composition of the ureter has not been fully explored to-date, however histological studies point to the presence of both COLI and COLIII fibres in the ureter. The higher tensile strength along the longitudinal axis of the ureter is thought to arise from the presence of more longitudinally oriented collagen fibres (141-144).

The recoil force in the ureter is dictated by the integrity and abundance of elastic fibres and is essential to restore the distended portion of the ureter containing the urine bolus into its' original shape and dimension. The elastic fibres are intertwined with collagen fibres within the lamina propria as well as within the muscle layer of the ureter (145).

The UVJ has only longitudinal muscles and therefore cannot sustain peristalsis (65, 66). The passage of urine through the UVJ is therefore, dependent on the pressure gradient between the extravesical and intravesical portions of the ureter. Because the UVJ is narrower than the extravesical ureter, maintaining low pressure in the UVJ is highly dependent on tensile strength, which is dictated by the amount and composition of collagen fibres.

The bladder's function is to store the urine at low pressure and expel it periodically by undergoing repeated cycles of expansion and contraction. The continuous distension and recoil, as well as the requirement for maintenance of low pressure, depend on the integrity of the detrusor muscle bundles, the tensile properties of the collagen fibres and the recoil properties of the elastic fibres. A number of studies have shown that the lamina propria is responsible for bearing most of the mechanical load of the bladder, as it is rich with collagen fibres (70, 146, 147). Histological analyses of both human and mouse bladders show that the collagen fibre composition is 75% COL I with the remaining 25% of fibres consisting of COL III. The thick COLI fibres are important for tensile strength, while the thin COL III fibres facilitate distension (148). As with the ureter, the elastic fibres facilitate bladder recoil post-micturition and are found abundantly in the lamina propria as well as the muscle layer of the bladder.

1.9 ECM defects associated with VUR and urinary tract phenotypes

As described above, the integrity of ECM components of the UVJ and the bladder and the balance between biomechanical forces such as tensile strength, recoil and compliance are essential for proper functioning of these structures. The significance of this balance is vividly illustrated by the presence of urinary tract phenotypes such as bladder diverticula and vesicoureteral reflux in a range of syndromes arising from genetic abnormalities in the ECM, such as Cutis Laxa, Ehlers-Danlos, Marfan, and Williams syndromes (Table 1)(149).

Table 1 ECM-related syndromes with VUR and BD as a common urinary tract phenotype.

Syndrome	Inheritance	Gene	Characteristic features	Renal and urinary tract phenotypes
Cutis Laxa	Autosomal dominant, Autosomal recessive	*ELN* *FBLN4, FBLN5* *ATP6V0A2,* *ATP7A,* *EFEMP2*	Lax and inelastic skin, vascular anomalies, gastrointestinal diverticula, abdominal hernia, genital prolapse	VUR, bladder diverticula
Ehlers-Danlos	Autosomal dominant, Autosomal recessive	*ADAMTS2, COL-I-A1, COL-I-A2, COL-III-A1,* *COL-V-A1,* *COL-V-A2,* *PLOD1,* *TNXB*	Hyperextensible skin, joint hypermobility, poor wound healing, easy bruising and scarring, molluscoid pseudotumors, subcutaneous spheroids, muscle hypotonia	VUR, bladder diverticula
Marfan	Autosomal dominant	*FBN1*	Increased height, disproportionately long limbs and digits, anterior chest deformity, joint laxity, vertebral column deformity, highly arched palate	VUR, bladder diverticula
Williams	Autosomal dominant	*ELN*	Cardiovascular defects, mental retardation, joint, skin and facial abnormalities	VUR, bladder diverticula, renal artery stenosis, renal agenesis, renal ectopia,

Adapted from Tokhmafshan et al., 2016

1.9.1 Cutis Laxa syndrome

Cutis Laxa (prevalence of ~1:400,000) refers to a spectrum of genetically heterogeneous rare connective tissue disorders (150). Cutis Laxa is characterized by the presence of sagging and inelastic skin and has both autosomal dominant and recessive forms of inheritance (150). The autosomal dominant form is caused by mutations in elastin (*ELN)* or more rarely in fibulin 5 (*FBLN5*) and presents later in life, typically with the following features: inelastic and redundant skin, aged appearance, high forehead, large ear lobes, cardiac disease, and pulmonary disease including bronchiectasis and emphysema (150). The autosomal recessive form is caused by mutations in fibulins, namely fibulin-4 and -5 genes, and presents in early childhood with a number of features including: severe cardiac disease (i.e. aortic aneurysm), pulmonary emphysema, inguinal and umbilical hernias, gastro-esophageal reflux, and diverticula formation in the intestines (150). Most children with the recessive form die in early childhood from cardiac or pulmonary failure (150). Urinary tract defects are described in a number of case series and include VUR and bladder diverticula (151-154). Pathogenic mutations of *FBLN4* and *FBLN5* result in abnormal protein folding that prevents secretion of the protein so that it is not available to cross-link elastic fibres. This leads to a shortage of elastic fibres and a reduction in tissue recoil (150, 151).

1.9.2 Marfan syndrome

Marfan syndrome (prevalence of ~1:10,000) is a multisystem disorder characterized by musculoskeletal (e.g. hypermobility), cardiovascular, and ocular abnormalities. Marfan has an autosomal dominant mode of inheritance and is caused by mutations in the fibrillin-1 (*FBN1*) gene. The mutations in humans often alter protein folding, secretion and/or assembly thereby destabilizing the FBN1 protein leading to its rapid degradation (130, 155, 156). The reduction in FBN1 impairs the synthesis of the fibrillin microfibrils that form the scaffold to assemble the elastic fibres (130, 155, 156). From case series, the reported urinary tract phenotypes in Marfan syndrome include: VUR, BD, and rare cases of voiding dysfunction (157-160).

1.9.3 Williams syndrome

Williams syndrome (prevalence of ~1:10,000) is a disorder caused by the hemizygous deletion of a specific region of chromosome 7 that removes 26 to 28 genes, which typically includes the elastin (*ELN*) gene (161, 162). Haploinsufficiency for the elastin gene, results in 50% less elastin protein, a reduction in the formation of elastic fibres, and impaired recoil for all tissues. This leads to systemic phenotypes that include a range of connective tissue and cardiovascular symptoms. Affected individuals exhibit intellectual disability, unique personality characteristics, distinctive facial features, cardiovascular and joint problems, as well as fragile and sagging skin. The urinary tract phenotypes reported for this syndrome are bladder diverticula and VUR. Amongst the connective tissue disorders discussed, urinary tract phenotypes in Williams syndrome are best characterized. These

studies collectively show that BD and VUR are present in approximately 60% of reported cases (163-167).

1.9.4 Ehlers-Danlos Syndrome

Ehlers-Danlos syndrome (EDS) constitutes a spectrum of monogenetic disorders that primarily affect the skin, ligaments, joints, blood vessels and internal organs (168, 169). EDS was classified into six subtypes in 1998 (169). In 2017, this classification was updated to reflect the most up-to-date understanding of the molecular basis of EDS, and includes 13 subtypes (170). The majority of EDS subtypes are linked to mutations in fibrillary collagens or enzymes involved in post-translational modifications of collagen proteins.

Studies using skin biopsies and fibroblast cultures from individuals with various subtypes of EDS point to defects in collagen fibrillogenesis as indicated by irregular and loosely packed collagen fibrils (171-174). There are at least 30 reported cases of bladder diverticula (BD) among individuals with various subtypes of EDS, making BD the most commonly reported urinary tract phenotype (48, 173, 175-190). Besides BD, VUR, urinary incontinence, recurrent urinary tract infections (UTIs) and reflux nephropathy are commonly reported urinary phenotypes (48, 173, 175-177, 179-181, 188, 190). Thus far, no large-scale studies have been conducted to elucidate the incidence of BD and VUR among patients with EDS.

Van Eerde *et al.* (2012) studied 50 children with VUR and found that they had a four-fold greater likelihood of having joint hypermobility than age-matched controls without VUR (34). These results have been echoed by Pournasiri et al., Beiraghdar et al., and Adib et al.,

who demonstrated that patients with joint hypermobility have an increased likelihood of having VUR compared to the general population (31-33). Furthermore, BD is frequently reported in individuals with EDS (48, 173, 175-190). Given the reported high prevalence of generalized joint hypermobility among children with VUR, we evaluated presence of generalized joint hypermobility in a cohort of children with VUR.

1.10 Generalized joint hypermobility (GJH) is a hallmark of Classical-like EDS (clEDS) due to mutations in *TNXB*, as well as hypermobility-type EDS (hEDS)

Generalized joint hypermobility (GJH) is seen in approximately 40% of school-age children, and 2-5% of the general public depending on ethnicity and gender (i.e. more common in females) (191). The diagnostic criteria for joint hypermobility were established by Beighton and colleagues (1998) (191-196). GJH is the hallmark phenotype clEDS and hEDS(170).

The recent identification of a number of putative disease-causing *TNXB* mutations among individuals with VUR and GJH is in line with our hypothesis that ECM anomalies can lead to VUR (35, 36).

1.11 TNXB, a matricellular protein

Tenascin-XB gene is located on chromosome 6 in humans and 17 in mice, and is translated into a large glycoprotein with five domains: a signalling domain at its N-terminus, heptad repeats, epidermal growth factor (EGF)-like repeats, fibronectin type III (FNIII) repeats, and a fibrinogen (FBG)-like globular domain at its C-terminus (197) (Figure 1). The heptad repeats are the site of homo-trimerization of TNXB, the FNIII repeats are responsible for the protein's conformational flexibility and facilitate its physical interaction with other ECM components, the FBG domain interacts with α1β1 integrin receptor and can modulate cell adhesion (198, 199). The human TNXB has 32 FNIII repeats with an RGD motif located between the 10th and the 11th FNIII repeats (Figure 1.A). The murine TNXB has 31 FNIII repeats and lacks the RGD motif (Figure 1.B), which is known to facilitate cellular and molecular attachment through interaction with integrins.

It has been shown that TNXB can interact with types I, III, V, XII and XIV collagens via its EGF-like, FNIII repeats, and FBG-like domains (198-203). The functional significance of these interactions has been extensively studied using both mouse models and in tissue samples from humans harbouring *TNXB* mutations. These studies have shown that *Tnxb*$^{-/-}$ mice and humans with both heterozygous and homozygous *TNXB* mutations have hyperextensible skin with loosely packed and sparse collagen fibrils, as well as reduced type I collagen (COLI) expression (40, 204-213).

TNXB also interacts with tropoelastin, the main component of elastic fibres, and it has been shown that both mice and humans with TNXB defects have slender and fragmented elastic fibres in their skin (214, 215). TNXB plays a regulatory role in cell attachment, matrix turnover and bioavailability of TGF-β1. *In vitro* studies have shown that TNXB has

anti-adhesive properties and can cause cell detachment (216, 217). Both *in vivo* and *in vitro* studies have shown that TNXB can negatively regulate matrix metalloproteinases (MMPs), and therefore modulate ECM turnover (218, 219). TNXB interacts with vascular endothelial growth factor B (VEGF-B) through its FN III repeats, and this promotes endothelial cell proliferation (220, 221). Finally, TNXB has been shown to modulate the bioavailability of TGF-β1 through interaction of its FBG domain with the latent form of TGF-β1 (221). Taken together, these findings demonstrate that TNXB is a matricellular protein capable of altering the biomechanical properties of tissues.

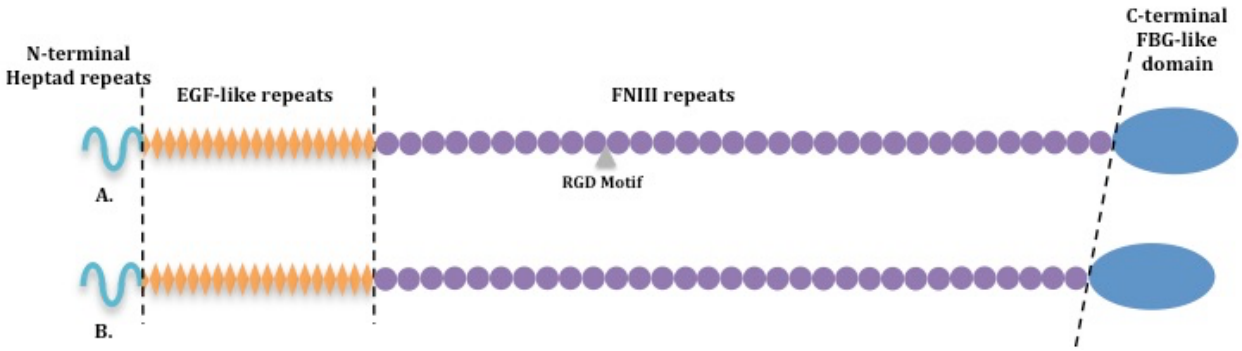

Figure 1 Schematic representation of human and murine TNXB monomer.

TNXB has four distinct domains: heptad repeats at the N-terminal, followed by epidermal growth factor (EGF)-like repeats, fibronectin type III (FNIII) repeats, and fibrinogen-like globular domain at the C-terminal. The human TNXB has 32 FNIII repeats as opposed to 31 in mouse, and also contains a RGD motif that facilitates its interaction with integrins.

1.12 Mouse models of VUR and EDS

Studying the underlying mechanisms of genetically-driven developmental defects, such as VUR, BD and EDS using human cells and tissues is limited to *ex vivo* analyses. The phylogenetic relatedness and physiological similarities between humans and mice, the ease of maintaining and breeding mice in the laboratory, the availability of many inbred strains, and the versatility of methods for creation of transgenic, knockout and knockin lines, makes *Mus musculus* (i.e. the house mouse) an appropriate model. However, use of mice as model organisms should be entwined with the understanding that all too often, mice respond to experimental intervention differently from humans, and might not fully recapitulate the human phenotype. These differences are expected given that the lineages leading to modern rodents and primates have diverged from a common ancestor approximately 85 million years ago (222).

To date, various mouse models of VUR have been described, some of which have abnormally formed uro-renal systems, while others have VUR without any apparent kidney or urinary tract defects. No mouse model of BD has been reported. Although BD is a common urinary tract phenotype seen in humans with connective tissue syndromes, the animal models of such syndromes have not been evaluated for the presence or absence of BD; this could be due to the fact that compared to the systemic connective tissue phenotypes, BD is less severe and does not impact the survival of the animals. A number of mouse models for various types of EDS have been described. These include the *Col3a1*$^{+/-}$ model for vascular EDS, the *Col5a1*$^{+/-}$ for classic EDS, and the *Col1a1*$^{Jrt/+}$ that is a model for both osteogenesis imperfecta and EDS (223-225). None of the above-mentioned mouse models have been

assessed for joint hypermobility, but the *Col5a1*$^{+/-}$ mice have hyperextensible skin, while the *Col1a1*$^{Jrt/+}$ mice have fragile skin and tendons (223-225).

Below is a classification and brief description of mouse models of VUR and hEDS.

1.12.1 Mouse models of VUR with renal and urinary tract malformations

I. *Hoxb7/Ret*$^{+/-}$: this transgenic mouse is a misexpression model for the receptor tyrosine kinase, RET, which is essential for the formation of the ureteric bud and therefore, the kidney. *Ret* is normally expressed in the nephric duct and the ureteric bud (226, 227). In the *Hoxb7/Ret*$^{+/-}$ mice, Ret is constitutively expressed throughout the ureter and the collecting ducts (77). As a result, these mice have renal dysplasia, short intravesical ureters (IVU) and VUR (228, 229).

II. *Pax2*$^{1Neu+}$: *Pax2* encodes for a transcription factor expressed in the ureter, collecting ducts and condensing metanephric mesenchyme (230). These mice exhibit VUR, short IVUs and a delay in urinary tract development (231, 232). The mutation in these mice is identical to a mutation in humans that leads to renal coloboma syndrome in which patients also present with VUR (232-234).

III. Conditional *Fgfr2*$^{-/-}$: *Fgfr2* encodes for a receptor tyrosine kinase important for ureteric bud induction (235). These mice were generated using a *Pax3-Cre* system that selectively ablates *Fgfr2* in the metanephric mesenchyme leading to a range of uro-renal phenotypes such as renal hypoplasia and dysplasia, multiple ureteric buds, urinary tract obstruction and VUR (235, 236).

IV. *Agtr2*$^{-/-}$: *Agtr2* encodes the angiotensin type II receptor, which is important for kidney and urinary tract development (237). These mice exhibit a range of uro-renal

phenotypes that include: double ureteric buds, renal agenesis, renal hypoplasia, duplex systems, VUR, obstruction, and hydroureter (237-239).

V. Conditional *Lim1*$^{-/-}$: *Lim1* encodes a homeobox transcription factor important for ureteric bud formation (240). Because *Lim1*$^{-/-}$ mice die at E10 due to abnormal head development, conditional *Lim1* knockout, were established using a *Pax2-Cre* system which ablates *Lim1* expression only in the nephric duct and the ureteric bud (240). These mice exhibit unilateral renal agenesis, renal hypoplasia, VUR, and duplex systems (240).

VI. *Upk2*$^{-/-}$ and *Upk3*$^{-/-}$: *Upk2* and *Upk3* encode for two transmembrane proteins of the uroplakin family (241, 242). These proteins are the subunits of the urothelial plaques that cover the apical surface of the urothelium and contribute to the impermeability of the barrier (241, 242). Both *Upk2*$^{-/-}$ and *Upk3*$^{-/-}$ mice exhibit hydronephrosis, VUR, obstruction, and renal failure (53, 58, 59, 78, 243).

1.12.2 Mouse models of VUR without renal malformations

To date six inbred mouse models of VUR without renal malformations have been identified: DDD, CBA, DBA, AKR, C3H/HeN, C3H/HeJ (244). All of these mice have normally formed kidneys and therefore recapitulate the phenotype observed in most children with VUR that have normally formed kidneys (245).

Of importance to this study is the C3H/HeJ mouse line, which has a 100% incidence of VUR at birth, with significantly shorter IVUs compared to the non-refluxing C57BL/6J (B6) mouse line (244, 245).

1.12.2.1 Vesicoureteral reflux model 1 *(Vurm1):* a 22Mbp reflux susceptibility locus in the C3H/HeJ mice

As mentioned above mouse models of VUR have been instrumental in furthering our understanding of VUR. The C3H/HeJ mouse is a fully penetrant model of VUR without renal malformations. This mouse model is consistent with the phenotype observed in most children with VUR who also have normally developed kidneys (1, 246-248). Using genome-wide mapping and linkage analysis, Murawski and colleagues (2010) identified a VUR susceptibility locus on the proximal arm of chromosome 12 spanning from position 11,207,819bp to 16,380226bp, called *Vurm1*(245). We performed a validation linkage analysis using Illumina mouse medium density linkage panel (GoldenGate Genotyping Assay, Illumina, San Diego, California), which consists of 1,449 thoroughly screened and validated SNP loci selected from the Wellcome Trust Sanger Institute's Mouse Genome Project (http://www.sanger.ac.uk/). The results of the validation analysis led to the revision of the genomic coordinates of the *Vurm1* region to 24,728,980bp to 37,010,797bp.

1.12.3 *Tnxb*$^{+/-}$ and *Tnxb*$^{-/-}$ mice have skin phenotypes of clEDS

Tnxb$^{+/-}$ and *Tnxb*$^{-/-}$ mice have hyperextensible skin (Figure 2) (204-210). Analysis of the skin of these mice has revealed that the collagen fibrils within the skin are not tightly packed, but spaced further apart, and this is associated with a decrease in the expression of COLI (208, 210-213). In addition, there is a reduction in the quantity and quality of the elastic fibres that appear slender and fragmented (214, 215). Eggings et al., (2006) tested these mice for joint hypermobility by measuring the stiffness of the medial collateral ligament (MCL) of the knee, and investigated the tail laxity in these mice by attempting to tie

a knot in their tail. While their MCL measurements were lower than the wild type (WT) littermates, the difference was not significant. Also, formation of a knot in the tail of *Tnxb*$^{+/-}$ and *Tnxb*$^{-/-}$ was not possible (212). Voermans and colleagues (2011), have tested the functional muscle strength of the *Tnxb*$^{-/-}$ mice using a paw-fall-through test and a hang-time test, by placing these mice as well as their WT littermates on a mesh wire and recording the number of times their limbs falls through the mesh, as well as the time it takes for the mice to fall off the mesh once it is inverted. The paw-fall-through and hang-time tests results revealed a significant decrease in the functional muscle strength of *Tnxb*$^{-/-}$ mice. Histological analysis of the quadriceps muscle revealed increased fibre size, consistent with increased matrix turnover. This was further confirmed by gene expression profiling results that showed a significant up-regulation of genes involved in matrix synthesis and degradation (208). The nuclei of muscle fibres in these mice were more internally positioned, which is indicative of unhealthy muscles (208, 249).

Tnxb$^{-/-}$ adult male

Tnxb$^{+/+}$ adult male

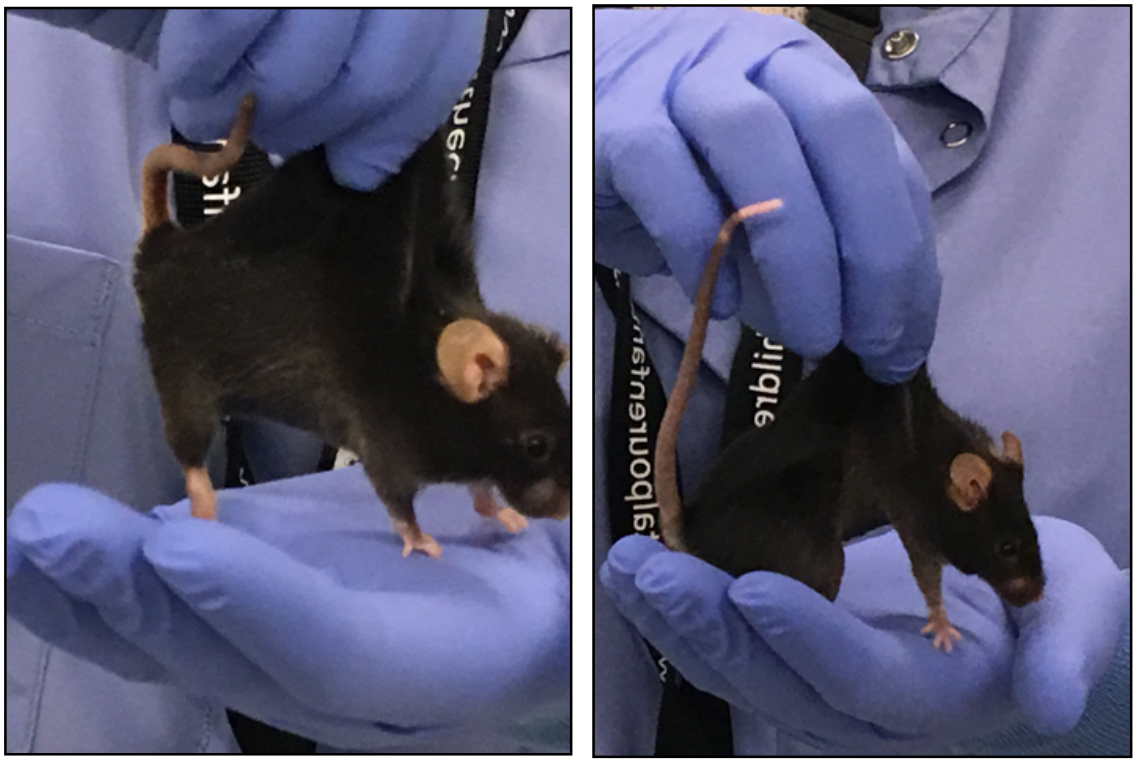

Figure 2 Hyperextensible phenotype of TNXB mutant mice.

Six-month old *Tnxb*$^{-/-}$ (left) and *Tnxb*$^{+/+}$ littermate (right) were anesthetised and held by the skin of the back. The hyperextensible skin of the *Tnxb*$^{-/-}$ is apparent.

1.13 Hypothesis and objectives:

Biomechanical forces such as compliance, tensile strength and recoil are important facilitators of the functions of the bladder and the UVJ. Given the role of TNXB in regulation of collagen fibre formation, as well as modulation of matrix homeostasis based on the dermatological phenotypes (i.e. hyperextensible and fragile skin, reduced collagen expression, aberrant elastic expression) observed in the *Tnxb*$^{+/-}$ and *Tnxb*$^{-/-}$ mice, I hypothesized that the bladder in these mice would exhibit compliance defects due to reduced collagen expression. To test this hypothesis, I first described the expression pattern of *Tnxb* in the bladder and ureter of mice, which has not been previously characterized. I then characterized the extracellular matrix defects in the bladder and ureter of newborn *Tnxb*$^{+/-}$ and *Tnxb*$^{-/-}$ mice in comparison to their WT littermates.

The C3H/HeJ mice are a fully penetrant model for VUR without kidney malformations, and linkage studies have led to the identification of a reflux susceptibility locus called *Vurm1* in these mice. I hypothesize that the anomalous expression of ECM components in the bladder and UVJ of these mice can cause VUR. I compare the ECM components in the ureter and bladder of C3H mice, compared to the C57BL/6J (B6) mice that are resistant to VUR. I further hypothesized that the *Vurm1* locus in the C3H mice includes matrix-related genes, and that the C3H mice might harbour damaging variants in some of these genes, which give rise to their ECM phenotypes. To test this hypothesis, I performed *in silico* analyses to describe the matrix genes located in *Vurm1* and to determine if the C3H strain has damaging variants, using the Wellcome Trust Sanger Institute Mouse Genome Project database.

Given the significant co-prevalence of VUR and joint hypermobility, I hypothesized that deleterious *TNXB* variants are enriched in children with joint hypermobility and VUR.

To test this hypothesis, we sequenced *TNXB* in a cohort of paediatric patients with VUR some of whom have joint hypermobility as well as BD.

2 CHAPTER TWO: MATERIALS AND METHODS

2.1 C57BL/6J (B6), C3H/HeJ (C3H), C57BL/6J$^{Tnxb+/-}$ (*Tnxb*$^{+/-}$), C57BL/6J$^{Tnxb-/-}$ (*Tnxb*$^{-/-}$) Mouse colonies:

2.1.1 Animal breeding and tissue collection

B6 and C3H inbred strains were purchased from Jackson laboratories at six weeks of age. *Tnxb* mutant mice were generated by Mao et al., (2002) on the 129SvJ background (210). Because 129SvJ strain is susceptible to VUR, the *Tnxb* null allele was transferred to the non-refluxing B6 background by backcrossing 129SvJ$^{Tnxb+/-}$ with B6 mice for five generations (Fillion ML., M.Sc. thesis, McGill University 2015). For all mouse lines, the embryos were generated by mating mice overnight and visualization of a vaginal plug was recorded as embryonic day E0.5. Timed-pregnant females were euthanized using a combination of Isoflurane and CO_2, followed by cervical dislocation, dissection and collection of embryos. Pups were euthanized by decapitation. All genotyping was performed using tail DNA. All mice were housed in the Research Institute of McGill University (RI-MUCH) vivarium. All animal studies were performed in accordance with the regulations of the Canadian Council on Animal Care (CCAC). Animal protocols were approved by the McGill University Animal Care Committee (UACC, AUP #4120).

2.1.2 VUR status

C3H mice are a fully penetrant model for recessively inherited VUR, while the B6 strain has been shown to be resistant to VUR (245). The *Tnxb*$^{+/-}$ and *Tnxb*$^{-/-}$ newborn and adult mice on the B6 background were tested for VUR using the VUR assay previously described by our laboratory (250). Neither the *Tnxb*$^{+/-}$ nor the *Tnxb*$^{-/-}$ mice exhibit VUR at birth or adulthood.

2.2 Genotyping *Tnxb*$^{+/-}$ and *Tnxb*$^{-/-}$ mice

The null allele was generated by Mao et al., (2002), through insertion of a lacZ and neomycin resistance cassette, replacing exons 3 to 6 of the *Tnxb* gene. To generate heterozygous (Het) and homozygous knockout (KO) tissue, I set up Het x Het, as well as KO x KO crosses. WT tissue was collected from the WT littermates of Het x Het crosses. Genotyping of both newborn and adult mice was carried out using tail DNA. The WT allele was detected using primers for exon 5 that generate a 238bp fragment, while the null allele was detected using primers for the LacZ cassette that generate a 234bp fragment (Table 2, Figure 3). Therefore, the PCR amplification of DNA from a WT mouse will generate only a WT amplicon, while a KO mouse will generate only a KO amplicon, and a Het mouse will generate both WT and null amplicons (Figure 3).

Table 2 *Tnxb* primers used for genotyping *Tnxb* mutant mice

Primer	Forward Sequence	Reverse Sequence
KO allele	TTGAAAATGGTCTGCTGCTG	TATTGGCTTCATCCACCACA
WT allele	ACTACTGAGCCCTCTTCTGTCT	ATACTCCACACCAGGCATCA

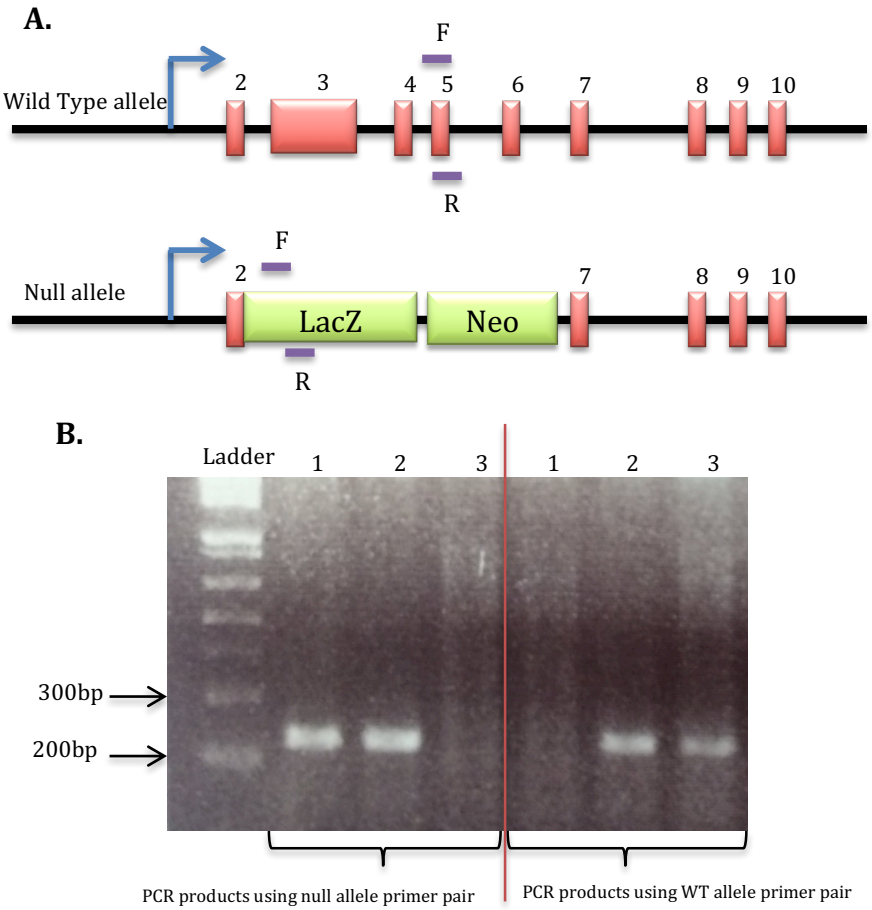

Figure 3 *Tnxb* WT and null allele genotyping PCR.

Schematic representation of the first ten exons of wild type (WT) and null alleles of *Tnxb*, depicting the position of primer pairs used to genotype mice (A). A representative image of *Tnxb* genotyping results for three mice (samples 1-3) run on a 4% agarose gel. Sample 1 is DNA from a $Tnxb^{-/-}$ mouse as it has generated a KO amplicon, but not a WT one. Sample 2 is DNA from $Tnxb^{+/-}$ mouse because it has both the KO and WT amplicons. Sample 3 is DNA from a $Tnxb^{+/+}$ mouse as it has only a WT amplicon (B).

2.3 Bladder compliance assay

We designed an assay to detect defects in bladder compliance by exposing bladders to a gradient of increasing intraluminal pressure. Postnatal day one (P1) pups were euthanized by decapitation. The urethra of the pups was occluded using Vetbond tissue adhesive (3M cat # 1469Sb). Using dissection scissors, a midline incision was created from the thorax to the abdominal cavity, exposing the internal organs. From the midline, two additional incisions were made toward each hind limb, exposing the urinary tract. Methylene blue dye was added to a 60ml syringe (i.e. dye column) connected to intravenous tubing attached to a 30-gauge ½ needle. Forceps were used to securely hold the sides of the hind limbs, therefore immobilizing the bladder. The needle was inserted in the anterior of the bladder, proximal to the UVJ. At the site of needle insertion, the dye column was kept at the same level as the dissection table, ensuring equal pressure within the system, thereby preventing the dye flow. The dye column was then raised at 30 cm increments causing the dye to flow. The incremental increase in height occurred only after the pressure inside the bladder had reached equilibrium with the pressure of the dye column and the dye flow into the bladder had stopped. The pressure (i.e. equal to the height of dye column) at which the bladder ruptured, along with the sex of the pups, and the fullness of their bladder prior to start of the assay were recorded.

2.4 Beta-galactosidase (β-gal) expression assay to determine *Tnxb* expression

Because the *Tnxb* null allele was generated through insertion of a LacZ cassette, I performed β-galactosidase (β-gal) assay using X-gal (Sigma Cat# 94433) on P1 tissue to describe the expression pattern of *Tnxb* in the urinary tract of mice. Kidney, bladder and ureters were dissected from P1 *Tnxb*$^{+/-}$ and *Tnxb*$^{-/-}$ as well as WT littermates. The tissues were fixed in X-gal fixative (4% PFA, 1M $MgCl_2$, 0.5M EDTA, 10% NP-40) for two hours on ice, followed by washes in X-gal wash buffer (1M $MgCl_2$, 1% sodium deoxycholate, 10% NP-40, 1M PBS pH 8). The tissues were then incubated with X-gal staining buffer (50mg/ml X-gal, 200mM potassium ferricyanide, 200mM potassium ferrocyanide, 1M Tris pH 8) at 37°C till β-gal activity was detected. The stain was then removed and the tissues were washed in the X-gal wash buffer, and analyzed as whole-mounts, followed by paraffin embedding for sectioning.

2.5 *Tnxb* RNA *in situ* hybridisation (ISH)

To establish the mRNA expression pattern for *Tnxb*, I generated a DIG-labelled *Tnxb* antisense probe. Mouse reference sequence NM_031176.22 with the primers described in Table 3 and Figure 4 were used to generate the template *Tnxb* cDNA, which was subsequently cloned into pCRII-TOPO vector (ThermoFisher Cat# 450641). The plasmids were linearized using *Hin*dIII (NEB Cat# R0104S), and sequenced to ensure the direction and identity of the insert. *In vitro* transcription was carried out using T7 RNA polymerase. The final antisense probe was 836bps long. Whole-mount RNA ISH was performed using kidney,

bladder, ureter and skin dissected from (E) 15 B6 embryos. The dissected tissues were fixed overnight at 4°C in 4% PFA. The following day, the tissues were washed in PBST, and partially permeabilised using 10µg/ml proteinase K for 15 minutes at room temperature. The digestion was stopped by washing the tissues with 2 mg/ml of glycine in PBST, followed by a re-fixation step in 4% PFA. The embryos were then washed and incubated with hybridization solution at 65°C for 3 hours (50% (v./v.) formamide, 1% (wt./v.) embryo powder, 5X SSC, 1 mg/ml yeast RNA, 0.1 ng/ml heparin, 0.1% (wt.,/v) CHAPS, 5mM EDTA). Subsequently the tissues were incubated with the *Tnxb* antisense probe (i.e. 100 µl probe in 1ml of hybridization solution) at 65°C overnight. The following day the probe was removed and the tissues were washed with 2X SSC with 0.1% CHAPS at 65°C, followed by PBST washes at room temperature. The tissues were then incubated with blocking buffer (10% (v./v.) heat inactivated sheep serum in PBST) for 2 hours at 4°C, followed by overnight incubation with 1:500 dilution of anti-DIG antibody (Sigma Cat# 11093274910) at 4°C. The following day the antibody was removed and the tissues were washed with PBST. The colourimetric detection step was performed using the 1-Step™ NBT/BCIP substrate solution (ThermoFisher Cat# 34042). The tissues were then analyzed as whole-mounts, followed by paraffin embedding to generate sections.

Table 3 Sequence of the primer pair used to generate cDNA template for *Tnxb* antisense RNA probe.

Table 3 *Tnxb* cDNA primers

Primer	Forward Sequence (5'-3')	Reverse Sequence (5'-3')
***Tnxb* mRNA**	CTCCCGTGCTCACTTCCTTT	CCCCCTGTAAACATGGTGCT

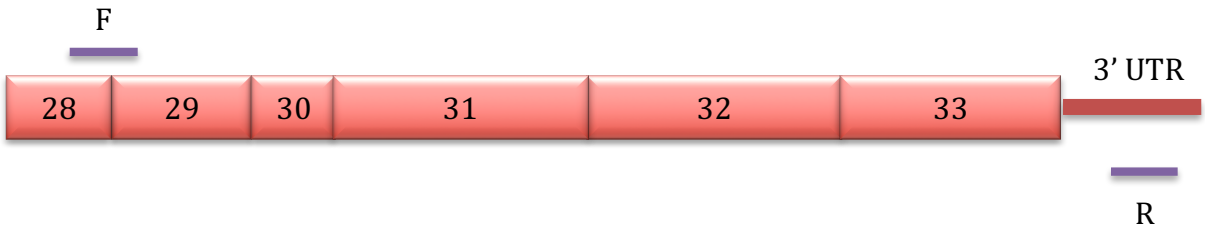

Figure 4 Location of *Tnxb in situ* hybridization probe.

Schematic representation of *Tnxb* mRNA spanning exons 28 to 33, and the position of primer pair used to generate cDNA template for RNA probe generation. The forward primer spans exon junction, while the reverse primer is located in the 3'UTR of the transcript.

2.6 RNA isolation and quantitative Reverse-Transcription PCR (RT-qPCR)

To examine expression levels of *Tnxb* mRNA in the urinary tract, I performed RT-qPCR on kidney, bladder, ureter, as well as skin. Total RNA was extracted from frozen tissue of newborn and adult mice. TURBO DNA-free™ kit (ThermoFisher Cat# AM1907) was used to ablate genomic DNA. cDNA synthesis was performed using QuantiTect Reverse Transcription kit (Qiagen Cat# 205311). RT-qPCR was performed in duplicates using QuantiTect SYBR® Green (Qiagen Cat# 204143) and Roche LightCycler® 96 system. Reference genes were selected using the geNorm v. 3.4 algorithm as described by Hellemans

and Vandesompele (2014), and in accordance with MIQE guidelines (251, 252). β-2 microglobulim (*β2m*), ribosomal protein L13a (*Rpl13a*), and retention in endoplasmic reticulum sorting receptor 1 (*Rer1*) were selected as reference genes, from a total of ten candidate genes, because they are stably expressed in all tissues of interest. The normalization factor for *Tnxb* gene expression was calculated by geNorm using the data from the three reference genes. The primers for the reference genes and *Tnxb* as well as their annealing temperature are described in Table 4. The normalized relative quantity (NRQ) of the *Tnxb* was calculated according to the qBase+ method described by Hellemans et al., (2007) (253).

Table 4 RT-qPCR primers and annealing temperatures

Primer	Forward Sequence (5'-3')	Reverse Sequence (5'-3')	Reference Sequence	Amplicon size (bp)	T_m (°C)
Tnxb	GTGGATCACCAGGGAGTGAG	TCAGTGCTCGGCAGTCATAC	NM_031176.22	162	58
β2m	ATGCTATCCAGAAAACCCCTCAA	GCGGGTGGAACTGTGTTACG	NM_009735.3	100	58
Rpl13a	AGGGGCAGGTTCTGGTATTG	TGTTGATGCCTTCACAGCGT	NM_009438.5	123	58
Rer1	GATTTTTCTCACGGCTTGGA	GGCTGTGTAGGGGGTAGACTT	NM_026395.1	182	58

2.7 Collagen detection by Sirius Red Staining

To examine the collagen content in the ureter, bladder and skin of embryonic day E15, newborn and adult mice, 5μm sections of paraffin-embedded bladder, ureter and skin were stained with picro-sirius red (Polysciences Inc., Cat# 24901B). Digital images of stained sections were obtained using the Zeiss Axiophot® microscope with polarized filters and analyzed using Image-Pro Plus software (Media Cybernetics) to quantify total collagen based on the degree of birefringence detected. For each tissue type, three sections from three individual mice were analyzed. For each section, three randomly selected microscopic fields were used to examine birefringence, and for each microscopic field the intensity distribution was used to set a background intensity threshold. In each microscopic field, the signal intensity of five rectangular areas of equal size were analyzed by the software. Consequently, a total of 15 regions were analyzed per section. The total area analyzed, as well as the total area yielding signal intensity over the threshold was established for each section and tissue type. The average intensity was calculated for each section, and then for each tissue type. The ratio of collagen expression for each tissue was calculated by diving the average intensity by the total area analyzed for each tissue. This ratio was expressed as a percentage and plotted. The collagen content of the skin for each mouse strain was used as the indicator of presence or absence of systemic defects in collagen deposition.

2.8 Immunofluorescence

To visualize alpha smooth muscle actin (α-SMA), and tropoelastin (Eln) expression in paraffin-embedded bladder and ureter sections, the following antibodies were used: (α-SMA rabbit polyclonal Abcam 5694) (Eln rabbit polyclonal Abcam 21600). Heat-induced epitope retrieval was performed using 10mM sodium citrate buffer, pH 6.0, for 30 minutes. Slides were then blocked in 10% normal goat serum for 1 hour at room temperature, and incubated overnight at 4°C with a 1:100 dilution of the primary antibody. The following day, slides were washed in PBS and incubated for 2 hours at room temperature with fluorescently-conjugated secondary antibody (goat anti-rabbit, 1:500 dilution). After final washes, slides were mounted and the sections were visualized using a Leica® DM 6000 Fluorescence microscope.

2.9 Semi-quantitative Western blot

Flash-frozen kidney, bladder, ureter, and skin samples pooled from four pups for each mouse strain was used for protein extractions. The protein extracts were prepared as follows: flash-frozen tissues were ground into powder using a chilled pestle and mortar. The lysis buffer consisted of protease and phosphatase inhibitor cocktail (AG Scientific Inc., Cat# T-2495) and a modified RIPA, optimized to better solubilize ECM proteins with the following ingredients: 150mM NaCl, 1% Triton X-100, 0.1% SDS, 10mM Tris-HCl, 1% Na-Deoxycholate, 5mM EDTA, 1mM EGTA, 100mM Na-orthovanadate, 5% glycerol, 1mM PMSF. The *DC* ™ colourimetric protein assay (Bio Rad Cat# 5000112) was used to determine the protein concentration of the extracts. Electrophoresis was performed using Bio Rad TGX Stain-Free™

FastCast™ 7.5% acrylamide solutions (Cat# 1610181), and 30 µg of protein was loaded per sample. The blots were first detected for Col1 protein using 1:1000 dilution of rabbit polyclonal antibody (Abcam 21286), then stripped using Millipore ReBlot Plus Mild (Cat# 2506), and detected for Col3 protein using 1:1000 dilution of rabbit polyclonal antibody (Abcam 7778). In all cases the secondary antibody (Cell Signalling 70745) was used at a 1:10000 dilution. The chemiluminescence detection was performed using Luminata Forte (Millipore Cat# WBLUF0100). The protein abundance was normalized to the total protein using Bio Rad's Image Lab™ software. The software creates a multichannel image using the digital image of the blot taken immediately post protein transfer (i.e. stain-free image of total protein) and the digital image of the blot post chemiluminescence detection (i.e. image of the band intensities). The software then associates each detected band with its corresponding lane on the stain-free image of total protein. To adjust for variation in the protein loading between different lanes, the software automatically selects the first nonstandard (i.e. not a protein ladder) as the reference lane against which all other lanes are compared, generating a normalization factor. The normalized intensity of each band is calculated by multiplying the normalization factor with band intensity. This value is reported as the amount of protein present in each tissue type.

2.10 *Vurm1 in silico* analysis

List of elements present in the *Vurm1* region was generated using USCS Table Browser data retrieval tool and mouse mm10 alignment (254). Information on gene and protein functions was retrieved from Gene database of the National Centre for Biotechnology Information (NCBI, Bethesda, MD, https://www.ncbi.nlm.nih.gov/genome), The Universal Protein Knowledgebase (UniProt, Oxford, UK, http://www.uniprot.org/), GeneCards database (Weizmann Institute of Science, Rehovost, Israel, http://www.genecards.org/), and The Extracellular Matrix Interaction database (MatrixDB, Lyon, France, http://matrixdb.univ-lyon1.fr/). The Mouse Genome Project (Wellcome Trust Sanger Institute, Oxford, UK, http://www.sanger.ac.uk/) was used to generate a list of SNPs in genes with matrix-related functions. The Mouse Genome Project database was used to investigate presence or absence of these variants in C3H, as well as other mouse models of VUR without kidney malformations (i.e. AKR/J, CBA/J, DBA2/J). The predicted functional effects of coding variants were determined using pre-computed values of the PROVEAN and SIFT algorithms. Figure 5 is a description of the data analysis workflow.

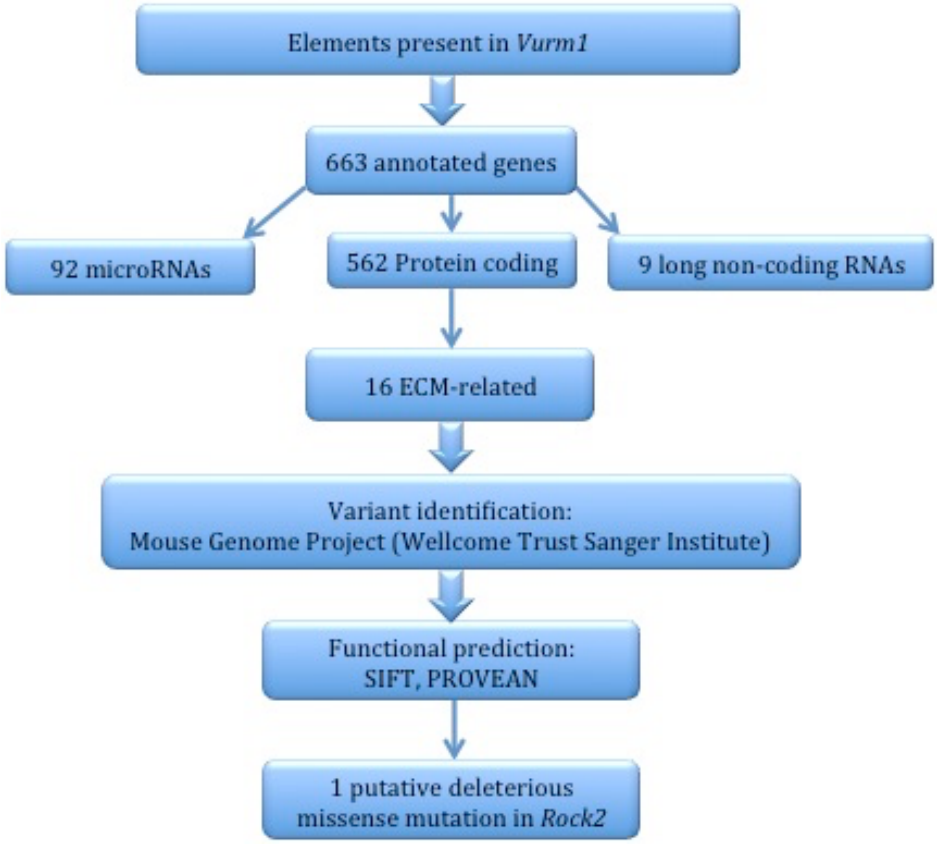

Figure 5 Workflow of variant analysis for ECM-related genes in the *Vurm1* locus

2.11 Human DNA samples

Our laboratory previously recruited, phenotype and obtained saliva samples from a cohort of children with VUR (255).

2.12 PCR and Sanger sequencing

The human *TNXB* is ~68Kbps long and has 44 exons with many internal repeats and high GC content. Its longest coding exon, exon 3, is the site of numerous CpG islands. Exons 32 to 44 have undergone duplication, resulting in a pseudogene (i.e. *TNXA*). *TNXA* is located upstream of *CYP21A2* gene, which is implicated in congenital adrenal hyperplasia, and flanks *TNXB* on its 3' end, in opposite transcriptional direction. *TNXA* is transcriptionally active and codes for a truncated version of *TNXB,* containing partial FNIII repeats and intact FBG-like domain (256). The combination of these characteristics has posed a challenge in sequencing *TNXB*. In collaboration with Voermans and colleagues, as well as Gbadegesin and colleagues, I designed a set of 41 primer pairs, as well as long-range PCR primers to cover the duplicated region of *TNXB* (i.e. exons 32-44) (Table 5) (36, 38).

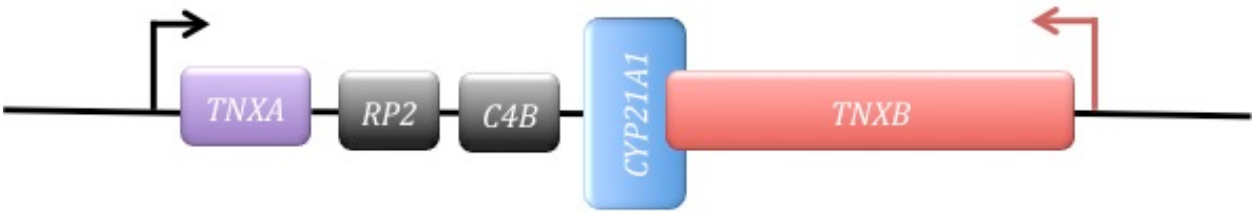

Figure 6 Arrangement of *TNXB* and *TNXA* on human chromosome six.

The red arrow shows the direction of *TNXB* transcription, while the black arrow shows the direction of transcription of all other genes in that region. *CYP21A1* encodes the steroid 21-hydroxylase, and flanks the 3' end of *TNXB. RP2* is a pseudogene for *RP1*, which encodes a serine/threonine nuclear kinase. *C4B* encodes the basic form of complement factor 4.

Table 5 *TNXB* Sanger primers

Exon	Forward Primer (5'-3')	Reverse Primer (5'-3')
3	ATGCCACAGTCGTCACCA	AGAGCAGAGCTGGGCTACAT
3	GCAATCGGTTCCAGTGTACC	GGTCGTTGCGTGTGCTTT
3	GCAGTCTTCCCCTGAGTAGC	GAATGCATTTGCGACACG
3	AGGCACACTCCTTGCACAC	GAGAACGGCGTGTGTGTTT
3	CCCTCTACACACACACACTGG	GGAAGGCTACGTGAGTGAGG
3	CATGCTCTCCCTCCACTCTT	GTGCAAGGAGTGTGCCTGT
4	GCCATCTGGACTCAACCAAT	CTGAGTAAAAGGGGCTGTGG
5	GGCAGATTCCCTCTCTAGTCC	GAGATAAGGGGGATTGAGCA
6	CCAGAAGCATTCAGAGGAGTC	TGGACTAGAGAGGGAATCTGC
7	CCAATAACCCCAGCTCCTC	GGACTGGGGATTCCTTTCTAGT
8	CCCAAAGCACTGAGAAAACC	ATCCAGGATGGAGTGAGGTG
9	CTGACACAGCCAGGGTATGA	CCTATGTGGGATTTGGCTTC
10	GGCAAAATGAGCTGAGAAGG	TGTCAGGCTTCCCAGAAGTT
11	CTGGAGCAAGGAGAGCAACT	TTTCCATGGCTGTCATCTGT
12	GGAGGAGTAAAGGGGTCAGG	GGTGACAGCGAGACTCCATC
13	CAGGTGGACAAAGGGAAGAC	CCCCATCTCAGTTCACAGC
14	CTGGGGCCAAATAATGGTAA	GCAGTTCTGGGTTTTTCCAG
15	AAAGGGGCACAAGGAAACTT	CCCAGTCTTCCAGAAACAGC
16	TTCTGAAGGCTTCTCCTCCTC	TTTCGATTGCTGACTGCTTG
17	ACCAAAGAGCAAGAGGGTGA	CTTTCAGATGGCTGGGAGAG
18	AGGAGATGCTGGAGGCTGTA	CCAGTCATAGCCTTGGCTTC
19	AGTGAAGGCACCAGCAGAA	CCTCAACACCTCCTTGCAG
20	ACCAAAGAGCAAGAGGGTGA	GCACCAGCATCCAGACTGT
21	GGTACCCATGAGGGAAAGGT	CCACGACGTAAGCACATCC
22	ACTGTGAGCCCCATCAAGAC	AGCAAAGCAAGTTGCCCTTA
23	ACCAAAGAGCAAGAGGGTGA	GGGCACTTTGTGTTTTGTGA
24	CATGGAAACGTGCAAAAGAA	CTTGAAGACCTGAGCACATCC
25	GTCAGTCCTCAGGGAAGTGG	AACAAAAGATGGCGAGGAGA
26	CGAAGACTGGAGAGACAGCA	CCTTCCTCACAAGACCCAAG
27	CCTGTTCTTGGGCACTTTGT	CCTCTGCAGTGGAGAAGGAG
28	AAGAGGTGCCAAGATCCAAA	CCAGTCATAGCCTTGGCTTC
29	ATCAGTGGGTGCTGAGGACT	GCCGCTAAGAAATGCTCACT
30	GAGGGACTCACTTTCGGAGTT	ATAGCAGCCCAGGAAGCTC
31	TTGTCTTCAGCCCAAATGC	CTCGATCACAGCAGGGAAG
32 (start of Pseudogene region)	GGCCAAGCCTGGAAGATAAA	GATTGGAGACAGAAGCACAC
33	CCAGGGAGAGAGGATGGAT	GTCCCCAGGAATGGAAGT
34, 35	GACCTAGTGCCTCAGCCA	GGCTCTCTCTACTCCGTG
36, 37, 38	ATGGGTGGGAGTTGAGAG	TGGAAGCTGAGCAGGTAG
38, 39, 40	TCTCCTCTTCCTGCTTTCCC	CCCCATCAGTCTCCATGTC
40, 41, 42, 43	CAGGACCAGCACCATCTT	TTGAGGTTGGCGTAGTGG
43, 44	GCTGTCTCCTACCGAGGG	GCAGAGAAGGCTTCCTCC
Long range primers for Pseudogene region	GTCTCTGCCCTGGGAATGA	TGTAAACACAGTGCTGCGA

2.13 *TNXB* sequencing data analysis

Sequenced reads were mapped to the hg19 human reference genome using Phred alignment tool. Variants in each sample were determined using Atlas-SNP2 to detect single nucleotide variants. Variants were annotated using the following data sources: 1000 genome database, ExAC, dbSNP, ESP5400, NIEHS exomes, RefSeq, and dbNSFP. Variants not reported in these databases were considered novel. Non-synonymous variants with a minor allele frequency (MAF) of ≤1% when compared to the frequency in ethnically matched populations were considered as rare variants. The ethnicity of our cohort was self-reported and consisted of 40% French Canadians, 30% European (non-Finnish), 8% South Asian, and 22% mixed race. For the purpose of data analysis, we utilized the population groups described in ExAC and therefore categorized French Canadians as European non-Finnish, and the mixed-race individuals as other, because they did not unambiguously cluster with the major populations described in ExAC. The predicted functional effects of rare variants were determined using pre-computed values of the PHAST, SIFT, Polyphen2 and Mutation Taster algorithms. ClustalW2 alignment tool (The European Bioinformatics Institute, EMBL-EBI, Cambridge, UK) was used to align the human *TNXB* with its murine orthologue. Figure 7 is a description of the data analysis workflow.

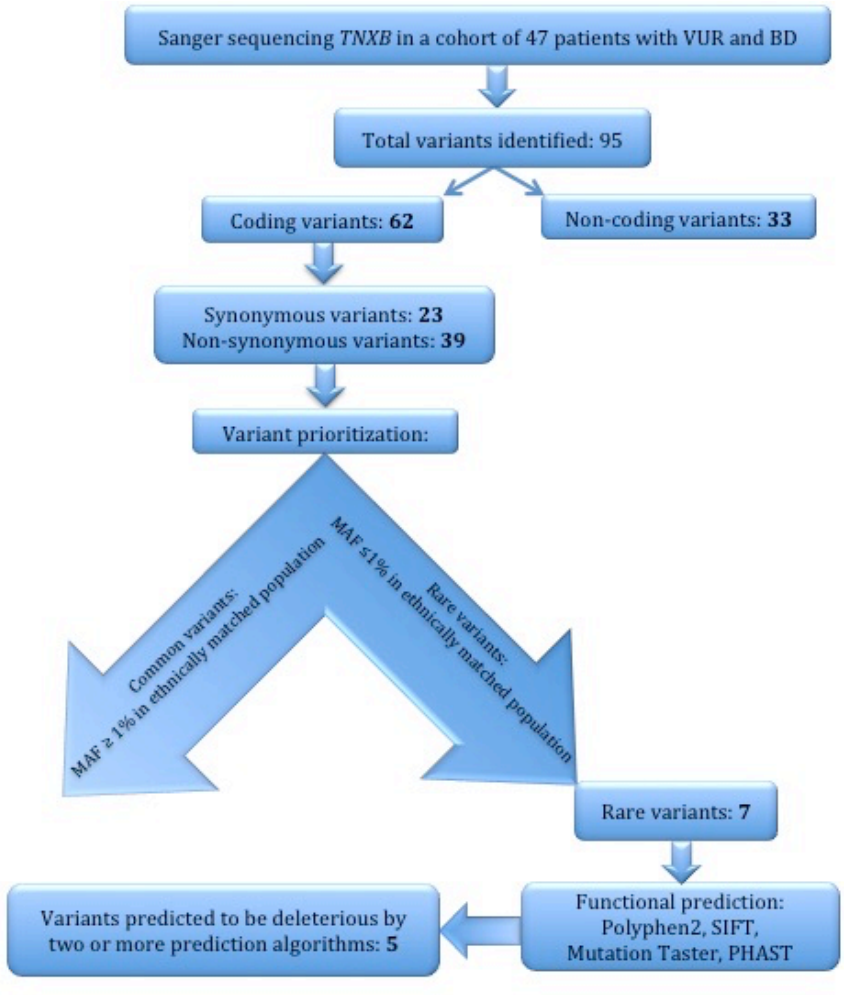

Figure 7 Workflow of *TNXB* variant prioritization.

2.14 Statistical analysis

All results with samples size≥ 3 are expressed as mean ± standard error. One-way ANOVA followed by Dunnett's multiple comparisons (Graphpad Software, La Jolla, California USA) was used for statistical analysis involving three experimental groups (i.e. B6, *Tnxb*$^{+/-}$, *Tnxb*$^{-/-}$). Paired t-test (Graphpad Software, La Jolla, California USA) was used for statistical analysis involving two experimental groups (i.e. B6, C3H). In all analysis genotype was the independent variable. The cut-off for significance was p-value ≤ 0.05. All results with sample size = 2 are expressed as a mean, with the error bar corresponding to the range of the plotted data. Statistical significance will be analyzed pending increase in sample size.

3 CHAPTER THREE: Results

3.1 Matrix defects in the bladder and ureter in a mouse model of VUR (C3H), as well as *Tnxb*$^{+/-}$ and *Tnxb*$^{-/-}$ mice

3.1.1 The bladder of newborn *Tnxb*$^{+/-}$ and *Tnxb*$^{-/-}$ mice exhibits a compliance defects

I used the bladder compliance assay described in **13.3**, to evaluate the ability of P1 bladders of B6 (i.e. *Tnxb*$^{+/+}$, and no VUR controls), C3H, *Tnxb*$^{+/-}$ and *Tnxb*$^{-/-}$ mice to withstand increasing intraluminal pressures (Table 6).

The results indicate that 40% of *Tnxb*$^{+/-}$ bladders ruptured at an intraluminal pressure of 90 cm, 53.3% ruptured at 60 cm, and 6.7% ruptured at 30 cm. For the bladders of *Tnxb*$^{-/-}$ mice, 50% of ruptured at 60 cm and 50% at 30 cm. The majority of *Tnxb*$^{+/+}$ (i.e. B6) bladders, 91.7%, ruptured at 120 cm, while 8.3% ruptured at 90 cm. Interestingly, the bladder in C3H pups did not rupture even at a pressure of 120 cm. I did not find any correlation between the pressure at rupture and the gender of the pups. Similarly, there was no correlation between the bladder content prior to start of the assay and the pressure at rupture. The bladders of *Tnxb*$^{+/-}$ and *Tnxb*$^{-/-}$ mice rupture at lower pressures than wildtype mice and this suggests there is a defect in the tensile strength and compliance of these bladders that could predispose to the development of bladder diverticula in the setting of sustained and elevated intraluminal pressure.

Table 6 Compliance of occluded newborn mouse bladder.

The rupture pressure is equal to the height of the dye column measured in cm. All pups were tested at postnatal day one.

Strain	Total pups tested	Rupture Pressure			
		30 cm	60 cm	90 cm	120 cm
B6	12	0	0	1	11
	% Ruptured	0%	0%	8.3%	91.7%
Tnxb$^{+/-}$	15	1	8	6	0
	% Ruptured	6.7%	53.3%	40%	0%
Tnxb$^{-/-}$	8	4	4	0	0
	% Ruptured	50%	50%	0%	0%
C3H	8	0	0	0	0
	% Ruptured	0%	0%	0%	0%

3.1.2 The LacZ cassette used to create the *Tnxb* null allele is not expressed

The β-galactosidase expression assay was performed multiple times by modifying several experimental conditions (i.e. pH, temperature and duration of X-gal incubation) on P1 tissue, however I was unable to detect an expression pattern in *Tnxb*$^{+/-}$ and *Tnxb*$^{-/-}$ tissue that differed from the endogenous β-galactosidase activity observed in *Tnxb*$^{+/+}$ tissue (Figure 7). We contacted the group (J. Bristow, personal communication) who had originally created the null allele, and were informed that their efforts to express the LacZ cassette were also unsuccessful.

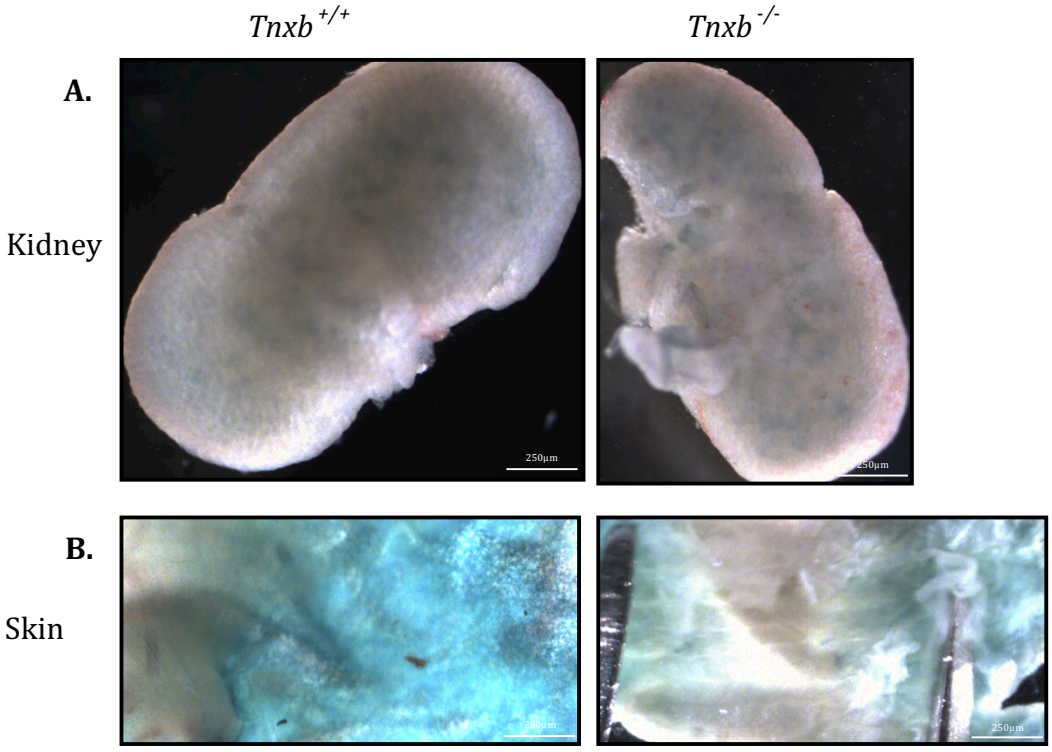

Figure 8 β-galactosidase expression assay in *Tnxb* mutant mice.

Bright-field microscopic images of representative β-gal expression assay performed on WT (left) and KO (right) kidney (A) as well as skin (B). Endogenous β-gal activity is shown in the WT (left) image and is similar to the signal detected in the *Tnxb*$^{-/-}$ kidney (right). Scale bar= 250µm, N= 5.

3.1.3 The commercially available TNXB antibodies are not specific in mouse

I used two commercially available antibodies (Proteintech rabbit polyclonal Cat# 13595-1-AP and Santa Cruz rabbit polyclonal Cat# sc-25717) to describe the expression of Tnxb in mouse urinary tract using semi-quantitative Western blotting and immunohistochemistry (IHC). I used protein extracts from *Tnxb*$^{-/-}$ pups to control for antibody specificity. With both antibodies, I observed bands corresponding to the predicted molecular weight of TNXB, as reported by the makers of the antibodies (i.e. 75kDa and 200kDa for Proteintech, 200kDa and 400kDa for Santa Cruz) in the KO samples. It is worth mentioning that the 75kDa and the 200kDa bands correspond to the plasma isoform of TNXB, while the 400kDa corresponds to the interstitial isoform of TNXB.

IHC experiments carried out on *Tnxb*$^{-/-}$ kidney, bladder and ureter sections produced a signal similar to that of the *Tnxb*$^{+/-}$ littermates. These experiments suggested that neither antibody could be used to detect the protein.

A non-commercially available rabbit polyclonal anti-TNXB antibody was created by Bristow et al., (1997)(204). We were given a 10 µl aliquot of this antibody, however this was insufficient to perform analysis and we were unable to procure more.

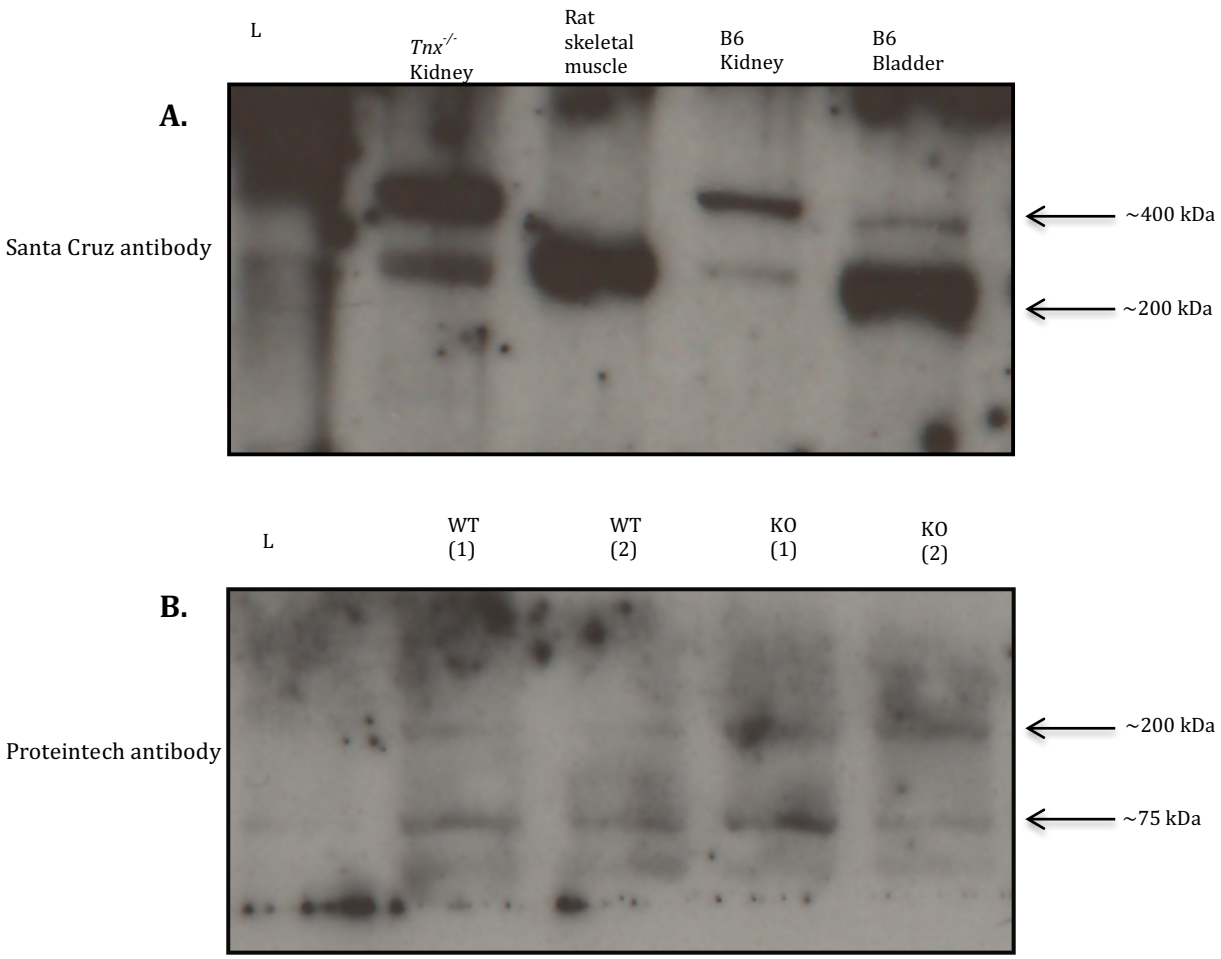

Figure 9 Tnxb Western blot analysis.

A representative Western blot experiment performed using Santa cruz (A), and Proteintech (B) anti-TNXB antibody. The Santa Cruz antibody is predicted to generate bands at 400kDa and 200kDa, while the Proteintech antibody is predicted to generate bands at 75KDa and 200kDa. L represents protein ladder, TNX KO1 and TNXKO2 represent protein extracts from two different pools of *Tnxb*$^{-/-}$ kidneys, while WT1 and WT2 represent protein extracts from two different pools of WT kidneys. With both antibodies, bands corresponding to the predicted molecular weight of Tnxb were observed in the null samples.

3.1.4 *Tnxb* mRNA expression in the urinary tract

The expression pattern of *Tnxb* in the urinary tract of mice is not well established. Due to the unavailability of a reliable antibody, I endeavoured to establish the expression pattern of *Tnxb* mRNA using RNA *in situ* hybridisation (ISH) and reverse transcription quantitative PCR (RT-qPCR).

I performed the *Tnxb* ISH analysis from B6 E15 embryonic tissue, as this is the onset of urine production in the mouse embryo. The newborn and adult analyses are on going. The temporal and spatial expression of *Tnxb* is well established in mouse skin, using the non-commercially available antibody created by Bristow et al., (1997)(204). I therefore used skin as a control.

At E15, expression was observed in the kidney, bladder and ureter, and the skin (Figure 10-13). At E15, *Tnxb* was expressed in the undifferentiated mesenchyme surrounding epithelial structures of the kidney (Figure 10). In the bladder and ureter, the expression was observed in the basal periphery of smooth muscle as well as the adventitia (Figure 11,12), which are the sites of induction of smooth muscle cell proliferation, as bladder smooth muscle forms first in the outer zone (adventitial side), and then proceeds towards the lumen (257). The peripheral cells in the bladder and ureter are known to express α-SMA and other matrix components (257). In the bladder some signal was detected on the lumen face of the urothelium. Gbadegesin et al., (2013) have performed immunohistochemistry on resected human UVJs using Proteintech anti-TNXB antibody, and reported presence of TNXB in urothelium(36).

In the skin, *Tnxb* expression was limited to the dermis (Figure 13), which is consistent with the protein expression profile previously reported by Egging et al., (2006)(212).

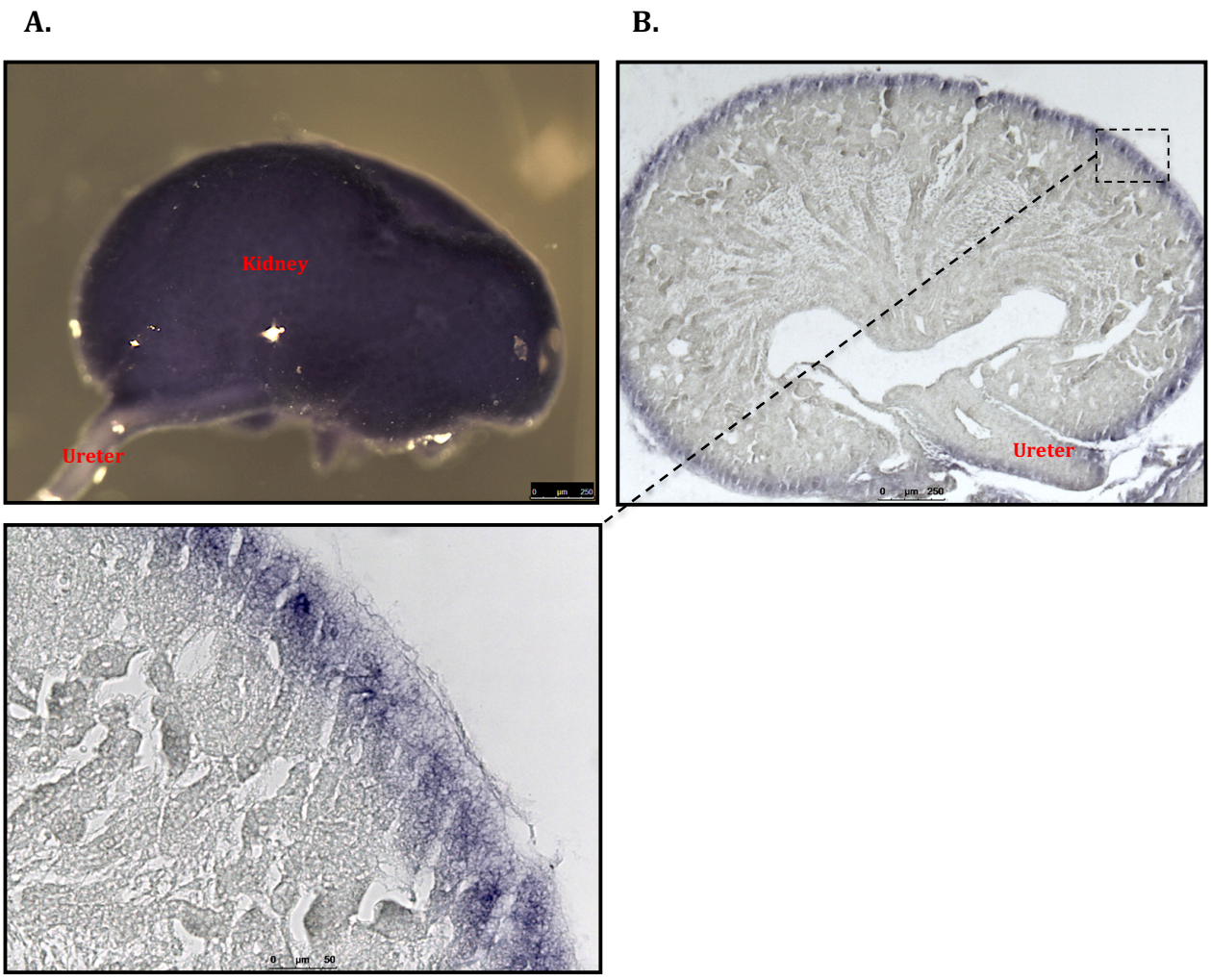

Figure 10 *Tnxb in situ* hybridisation in E15 mouse kidney.

Whole-mount RNA ISH in E15 kidney shows presence of *Tnxb* mRNA in cap mesenchyme (A). Bright-field microscopic image of paraffin section of whole-mount kidney confirms presence of *Tnxb* mRNA in the undifferentiated mesenchyme of the kidney (B). Panel (C) is a high magnification image of panel (B). Scale bar=250 µm (A, B), or 50 µm (C). N= 2.

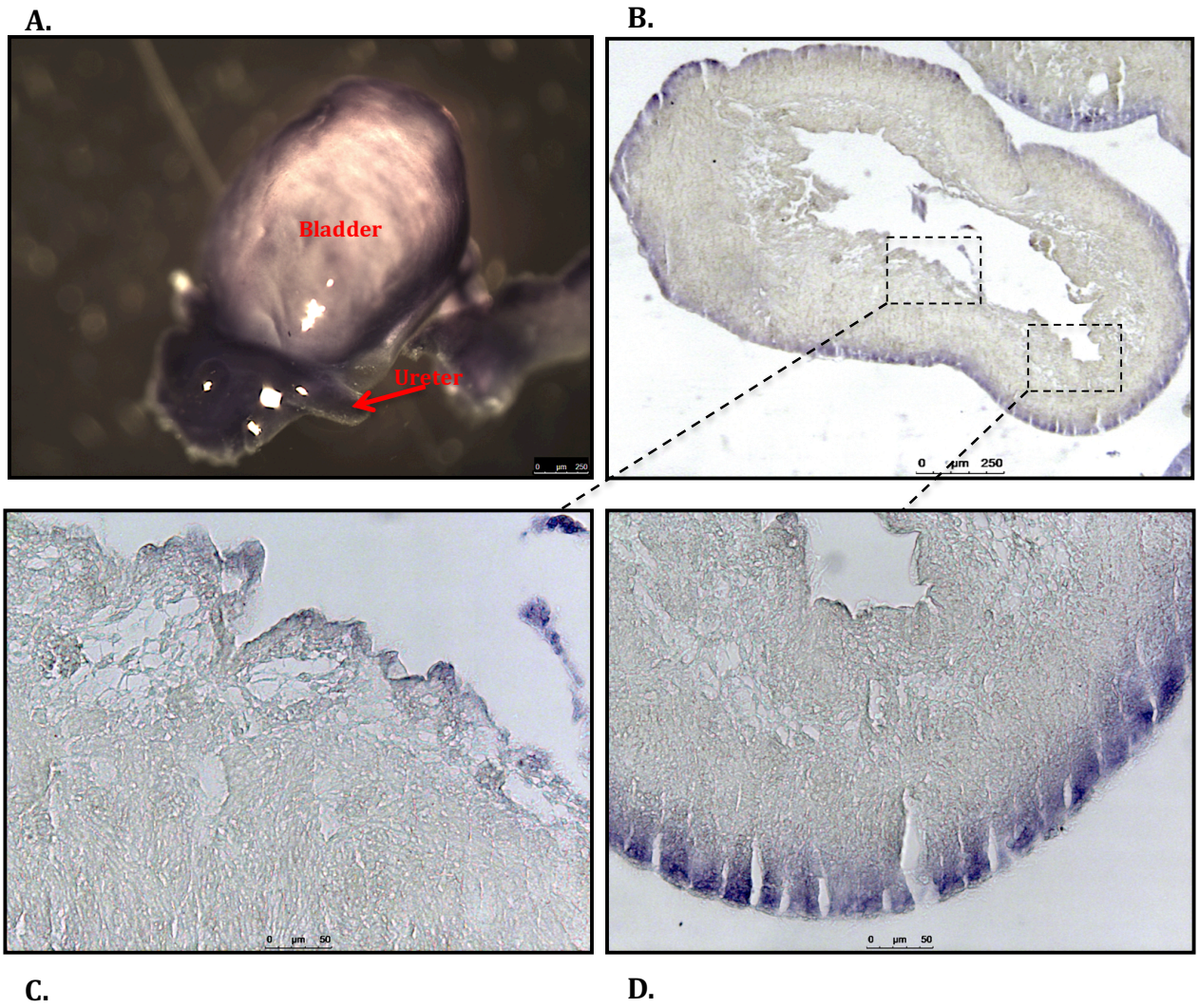

Figure 11 *Tnxb in situ* hybridisation in E15 mouse bladder.

Whole-mount RNA ISH of bladder shows the presence of *Tnxb* mRNA in the bladder (A). Bright-field microscopic images of paraffin section of whole-mount bladder confirms the presence of *Tnxb* mRNA in the basal periphery of bladder smooth muscle (B). Faint signal is defected on the luminal face of the urothelium (C). Panel (D) is a high magnification image of bladder smooth muscle. Scale bar=250 µm (A, B), or 50 µm (C, F). N= 2.

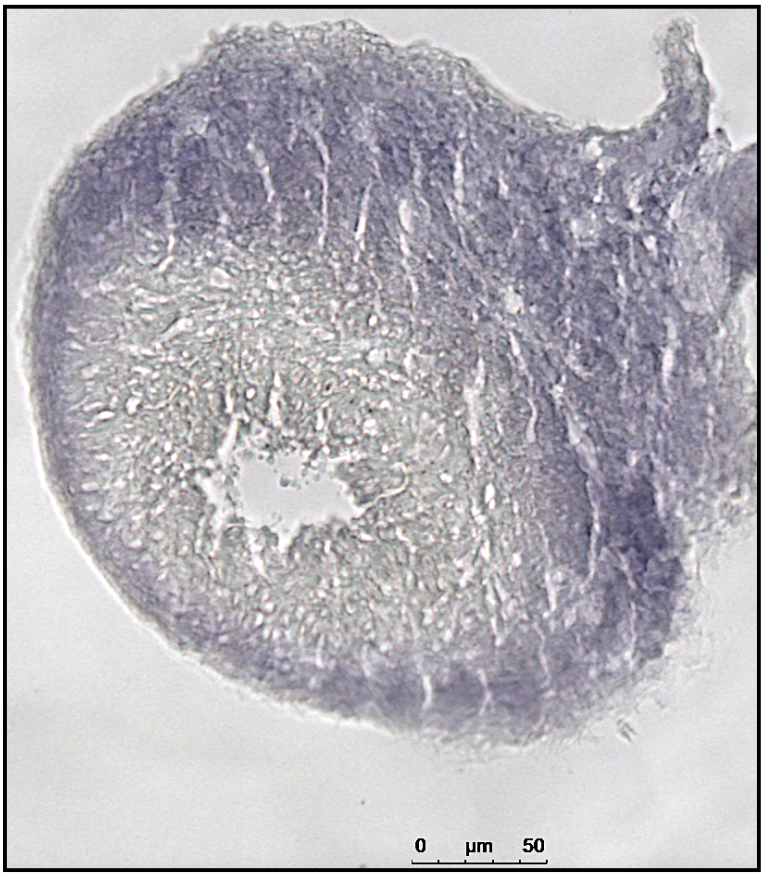

Figure 12 *Tnxb in situ* hybridisation in E15 mouse ureter.

Bright-field microscopic images of paraffin section of ureter confirms the presence of *Tnxb* mRNA in the basal periphery of bladder smooth muscle as well as adventitia. Scale bar= 50 µm. N= 2.

A. B.

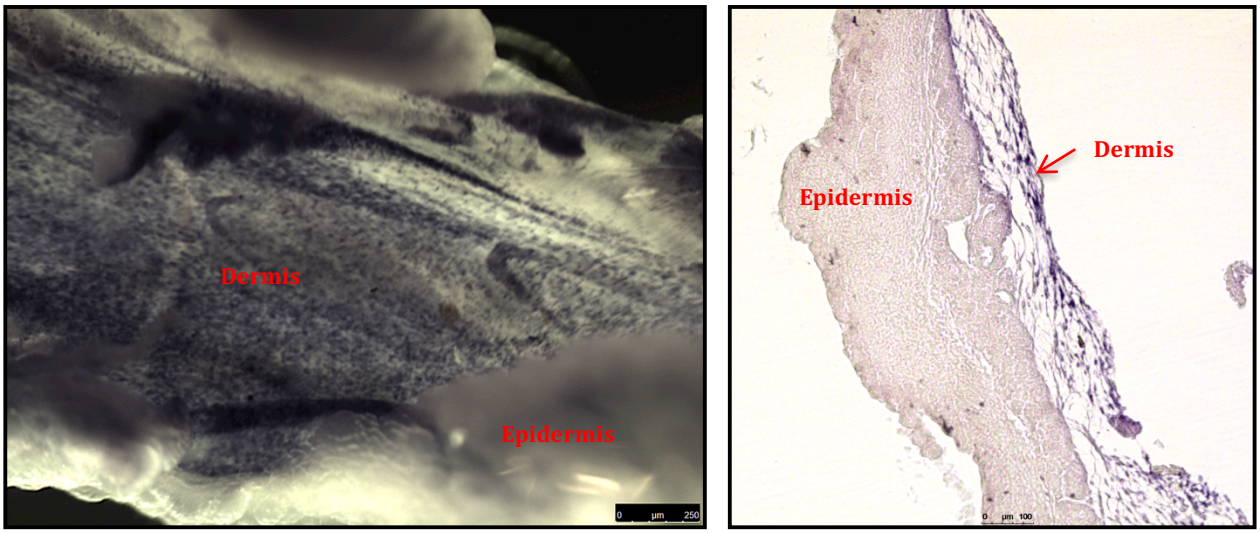

Figure 13 *Tnxb in situ* hybridisation in E15 mouse skin.

Whole-mount RNA ISH of skin shows the presence of *Tnxb* mRNA is limited to the skin dermis (A). Bright-field microscopic image of paraffin section of whole-mount skin confirms presence of *Tnxb* mRNA in the dermis. Scale bar=250 µm (A), or 100 µm (B), N= 2

Using RT-qPCR I analysed the mRNA expression of *Tnxb* in newborn and adult B6 kidney, bladder, ureter and skin normalized to reference genes (i.e. β*2m, Rer1, Rpl13a*) (Figure 14). At birth, *Tnxb* was expressed in kidney, bladder, ureter and skin, with the lowest expression level observed in the kidney, and the highest expression observed in the bladder (Figure 14A). Similar expression levels were noted in adult mice (Figure 14B). The analysis in E15 embryonic tissue is ongoing.

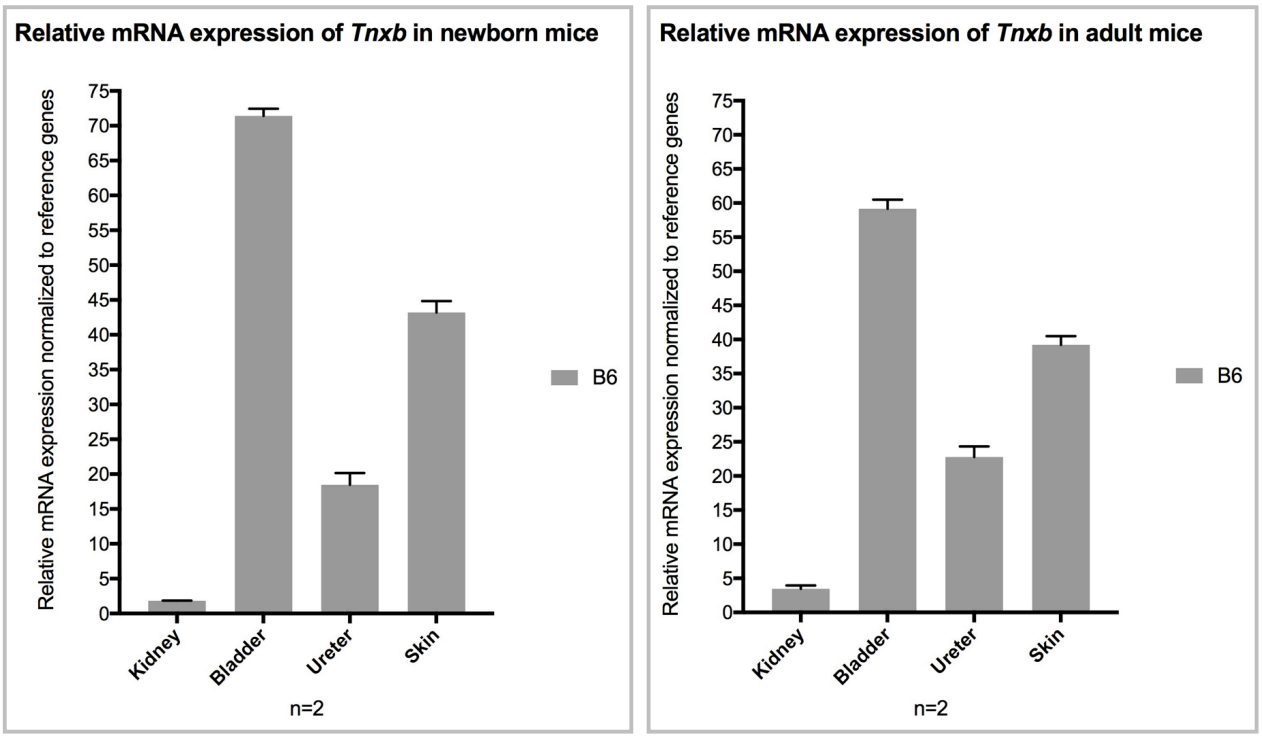

Figure 14 Normalized *Tnxb* mRNA expression.

***Tnxb* mRNA expression in newborn (A), and adult (B) B6 mouse kidney, bladder, ureter and skin, normalized to reference genes.**

3.1.5 Collagen content in the bladder and ureter of *Tnxb*$^{+/-}$, *Tnxb*$^{-/-}$, and C3H mice compared to controls

Fibrillary collagens have birefringence qualities, which when viewed under polarized light produce an array of colours depending on the type and thickness of collagen fibres. Yellow-orange colours are associated with thicker fibres (i.e. Col I), while blue-green colours are associated with thinner fibres (i.e. Col III). Visualization of Sirius red-stained bladder, ureter and skin of P1 *Tnxb*$^{+/-}$, *Tnxb*$^{-/-}$ and C3H mice under polarized light demonstrated differences in the collagen content compared to age and sex-matched B6 controls (Figure 15).

In the case of *Tnxb*$^{+/-}$and *Tnxb*$^{-/-}$ mice a reduction in the birefringence intensity was observed in the bladder, ureter and skin compared to WT littermates (Figure 15). In the C3H pups, an increase in the birefringence intensity was observed in the bladder and ureter compared to sex and age-matched B6 pups (Figure 15). The birefringence intensity in the skin of C3H pups was similar to that of B6 pups.

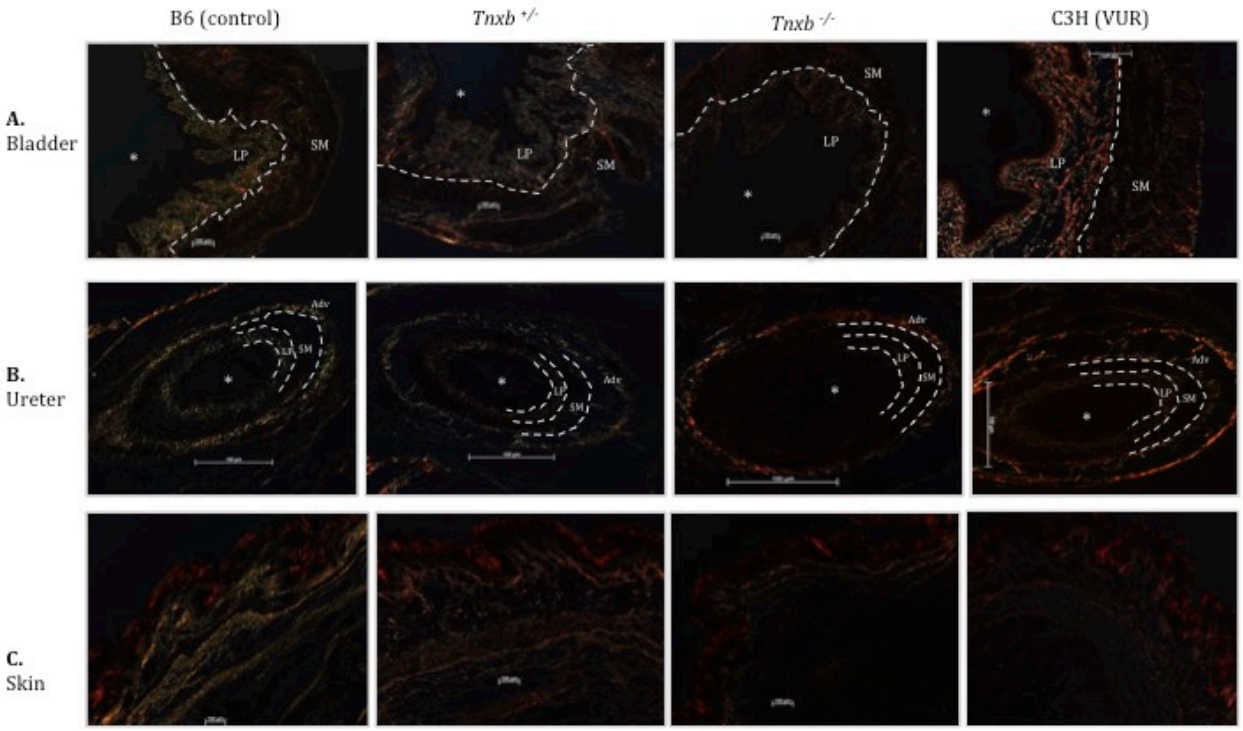

Figure 15 Polarized light images of Sirius Red-stained newborn bladder, ureter and skin.

The lamina propria in the bladder and ureter *Tnxb*$^{-/-}$ and *Tnxb*$^{+/-}$ pups has less collagen as indicated by the decrease in the degree of birefringence detected (A, B). Skin is used as control and demonstrates the previously reported skin phenotype in the *Tnxb*$^{+/-}$ and *Tnxb*$^{-/-}$ mice (C). The lamina propria in the bladder and ureter of C3H pups has more collagen as indicated by the increase in the detected birefringence (A, B). No difference was detected in the birefringence intensity of skin in C3H and B6 pups. LP: lamina propria, SM: smooth muscle, Adv: adventitia. Scale bar = 100 µm. N=2 for *Tnxb*$^{+/-}$ and *Tnxb*$^{-/-}$, and 3 for C3H.

Quantitative analysis of birefringence was performed. The analysis showed that the bladder and ureter of *Tnxb*$^{-/-}$ and *Tnxb*$^{+/-}$ pups had less collagen content compared to WT littermates. No statistical significance was calculated due to the small sample size (Figure 16A). Because the collagen deficiency in the skin of these mice has been well characterized, skin was used as a control, and my analysis confirmed a reduction in collagen content of the skin in *Tnxb*$^{-/-}$ and *Tnxb*$^{+/-}$ pups that is consistent with previously published data.

By performing a similar quantitative analysis on C3H sections, I showed that the bladder and ureter of C3H pups had significantly more collagen content compared to B6 pups (p-value = 0.0022 and 0.0002 respectively)(Figure 16B). However, the collagen content in the skin of C3H and B6 pups was similar, demonstrating that the defect in collagen deposition is not seen in all tissues.

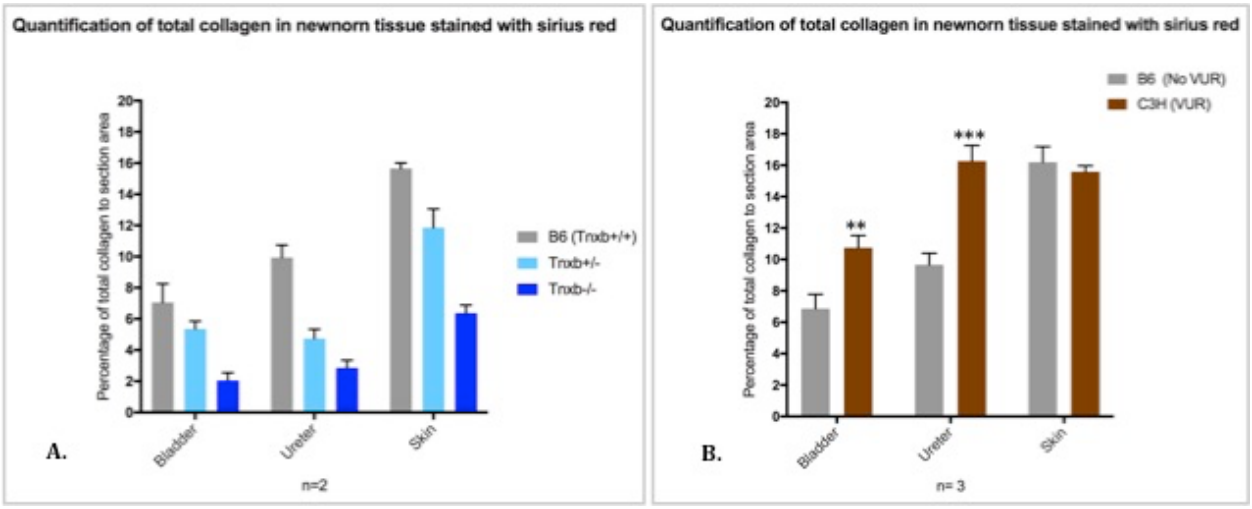

Figure 16 Quantification of birefringence as a measure of total collagen expression.

The collagen content in the bladder, ureter and skin of *Tnxb*$^{-/-}$ and *Tnxb*$^{+/-}$ pups is reduced compared to B6. The bladder and ureter of C3H pups have significantly more collagen compared to B6. *P ≤ 0.05, **P ≤ 0.005, ***P ≤ 0.0005. N=2 for *Tnxb*$^{+/-}$ and *Tnxb*$^{-/-}$, and 3 for C3H.

The bladder and ureter of C3H mice showed more yellow-orange birefringence, which corresponds to thicker collagen fibres (i.e. Col1). To distinguish differences in the abundance of different collagen types, I performed Western blot analysis using antibodies for ColI and ColIII (Figure 17A). Quantitative analysis of Western blot experiments showed that there is indeed more Col I present in the bladder of C3H mice (Figure 17B). The ureter of C3H mice on the other hand, had more Col III compared to B6 (Figure 17C). Once again, these differences were limited to the bladder and ureter, as the levels of Col I and Col III in the skin of C3H and B6 mice were similar.

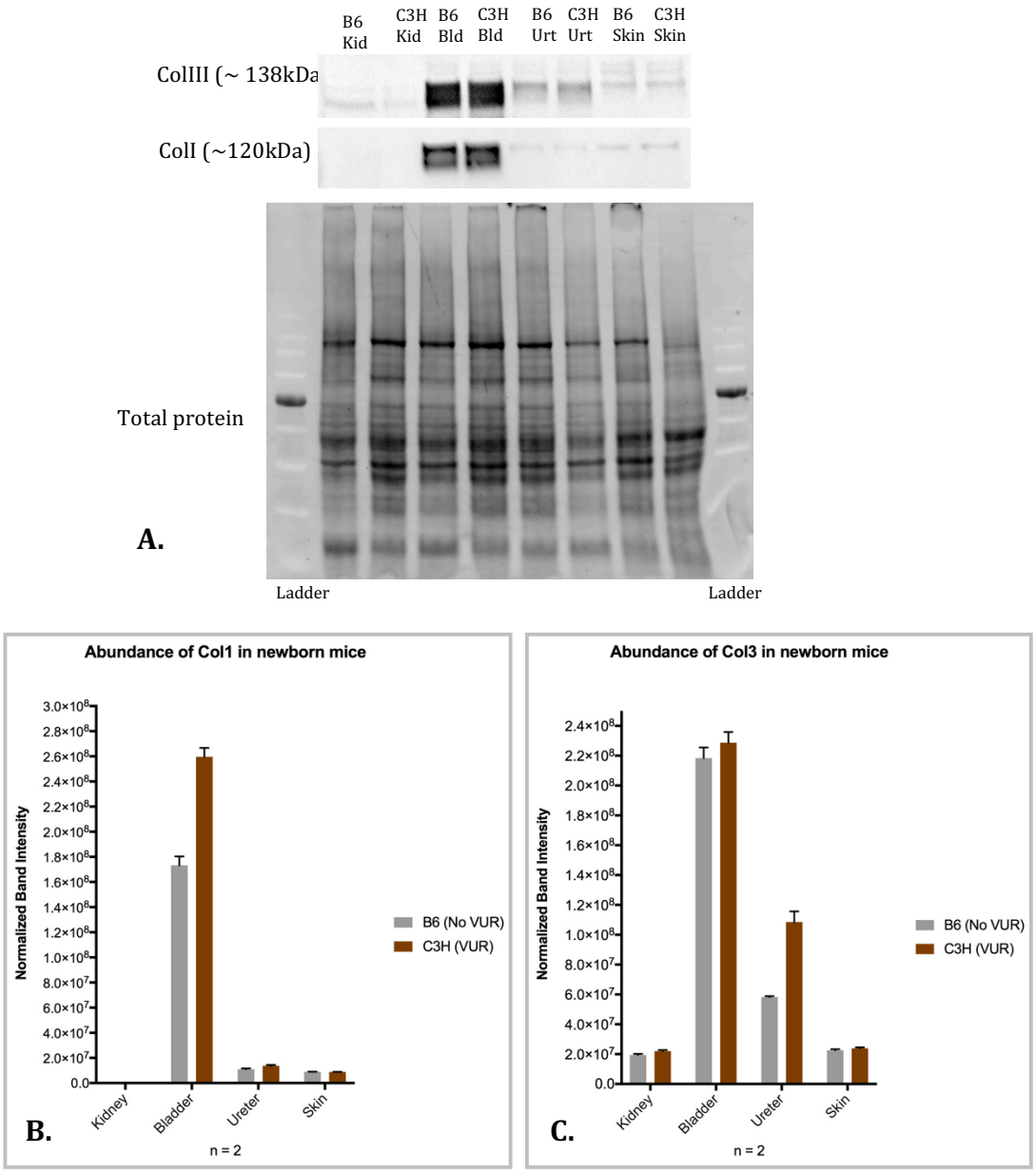

Figure 17 Western blot analysis of Col I and Col III expression.

Col I and Col III expression in the kidney, bladder, ureter and skin of newborn C3H and B6 mice, normalized to total protein (A). Quantitative analysis of the Col I Western blots shows the bladder of C3H mice has more Col I, which is consistent with the birefringence signal (B). Quantitative analysis of Col III western blots shows that the ureters of C3H mice have more Col III compared to B6. (C). The Western blots confirm the observation that the difference in collagen abundance is limited to the bladder and ureter, as the skin of these mice contains similar collagen levels.

3.1.6 α-SMA expression in the bladder and ureter of *Tnxb*$^{+/-}$, *Tnxb*$^{-/-}$, and C3H mice compared to controls

The bladder and ureter are muscular systems that rely heavily on their smooth muscle for structural support as well as regulation of tissue biomechanics (i.e. contraction, distension). Because actin is a major component of smooth muscle cells, and because its α isoform is the major component of smooth muscle cells' contractile machinery, I performed immunofluorescence (IF) of α-SMA on ureter and bladder of P1 *Tnxb*$^{+/-}$, *Tnxb*$^{-/-}$ and C3H mice (Figure 18). No difference was observed in the α-SMA detected in the bladder musculature of *Tnxb*$^{+/-}$ mice compared to WT littermates (Figure 18A). However more α-SMA was detected in the bladder musculature of *Tnxb*$^{-/-}$ mice compared to WT littermates (Figure 18A). In the ureter, more α-SMA was observed in both *Tnxb*$^{+/-}$ and *Tnxb*$^{-/-}$ mice; this increase was more pronounced in the ureter musculature of *Tnxb*$^{-/-}$ mice (Figure 18B).

In C3H mice, more α-SMA was detected in both the bladder and ureter, compared to B6 mice (Figure 18A,B).

Because increased α-SMA is often associated with a pro-fibrotic environment in a tissue, I used Masson's Trichrome to investigate collagen deposition in the musculature of the bladder and ureter as an indication of a pro-fibrotic environment (Figure 18C). Masson's Trichrome staining of the bladder showed increased collagen fibres in the musculature of *Tnxb*$^{-/-}$ and C3H mice compared to B6 controls (Figure 18C). The Masson's Trichrome staining of the ureters was unremarkable.

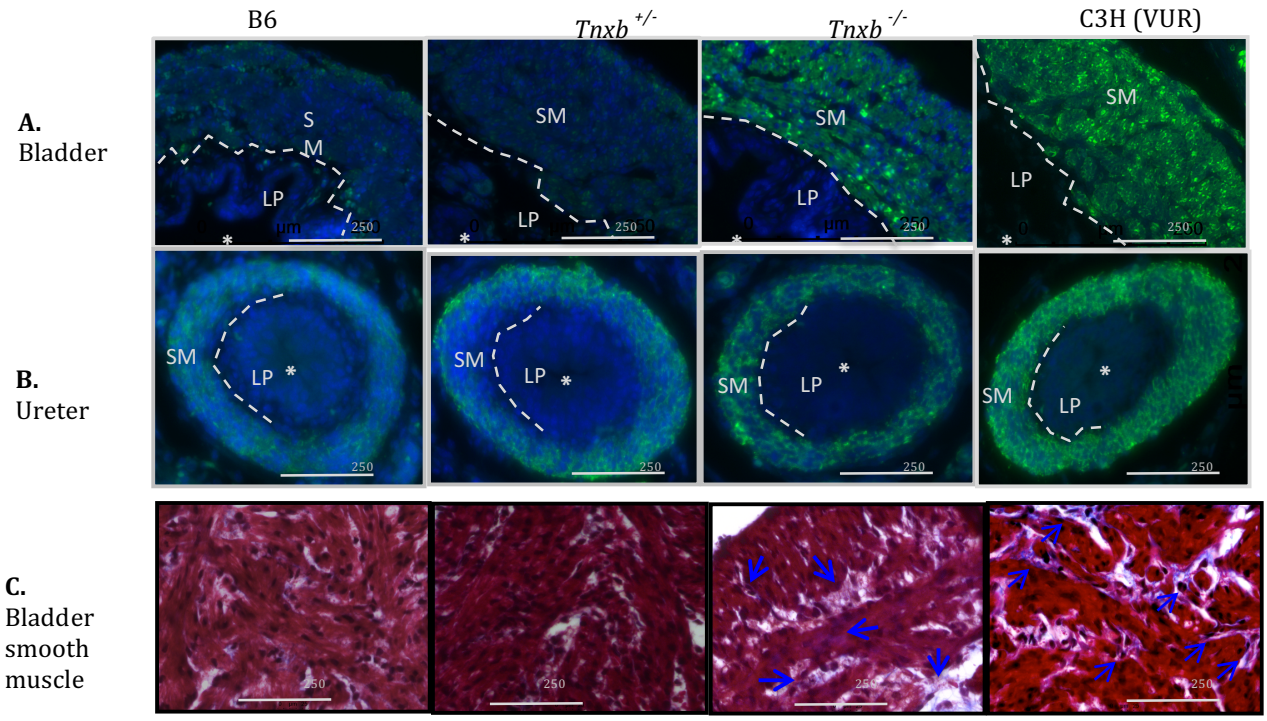

Figure 18 α-SMA expression in the bladder and ureter and newborn mice

Immunofluorescence (IF) detection of α-SMA protein in the bladder and ureter (A, B) of newborn mice. α-SMA is green, DAPI is blue. α-SMA is highly expressed in the bladder of *Tnxb*$^{-/-}$ and C3H mice (A). In the ureter, this overexpression in seen in *Tnxb*$^{+/-}$ and *Tnxb*$^{-/-}$, and C3H mice (B). Masson's Trichrome staining of the bladder of newborn mice (C). Muscle is stained red, collagen fibres are stained blue. Masson's Trichrome staining of the bladder shows increased collagen in the bladder of *Tnxb*$^{-/-}$, and C3H mice. The blue arrows point to areas with prominent collagen fibres. LP: lamina propria, SM: smooth muscle. Scare bar = 250 µm (A,B), or 25 µm (C). N= 2 (IF). N = 5 (Masson's Trichrome).

3.1.7 Elastin expression in the bladder and ureter of *Tnxb*$^{+/-}$, *Tnxb*$^{-/-}$, and C3H mice compared to controls

Because TNXB is known to interact with elastic fibres and in order to evaluate the recoil properties of the bladder and ureter, I performed elastin immunofluorescence.

Elastin was mostly observed in the smooth muscle layer of the bladder, and the periphery of musculature, as well as adventitia of the ureter. In the bladder, a decrease in the amount of elastin detected was observed compared to WT littermates, with *Tnxb*$^{-/-}$ mice having the least amount of elastin (Figure 19A). In the ureter, the amount of elastin present appeared similar, however the expression pattern in the ureter of *Tnxb*$^{-/-}$ mice appeared diffuse throughout the musculature (Figure 19B). Because the skin of *Tnxb*$^{+/-}$ and *Tnxb*$^{-/-}$ mice is reported to have slender, fragmented elastic fibres with aberrant expression pattern, I used skin as a control (Figure 19C). The reduced elastin signal detected in the skin of these mice is consisted with previously published data (Figure 19C).

In C3H mice, less elastin was detected in both the bladder and ureter compared to B6 mice (Figure 19A, B). Interestingly, the skin of C3H mice appeared to have less elastin as well (Figure 19C).

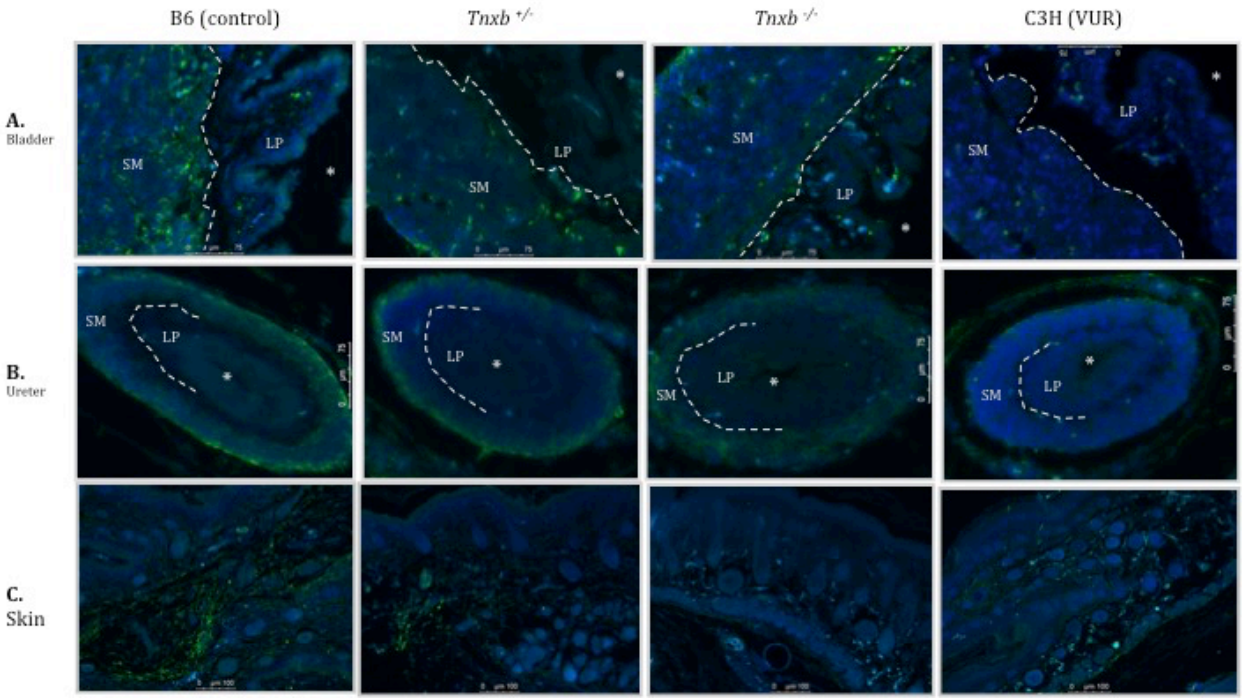

Figure 19 Elastin expression in the bladder, ureter and skin on newborn mice.

Elastin is green, DAPI is blue. In the bladder elastin is mostly observed in the musculature and on the edges of the lamina propria. The elastin expression is decreased in the bladder of *Tnxb*$^{+/-}$, *Tnxb*$^{-/-}$ and C3H mice (A). In the ureter, elastin is mostly observed in the periphery of musculature as well as adventitia. No difference was detected in the amount of elastin present in the ureter of *Tnxb*$^{+/-}$ and *Tnxb*$^{-/-}$ mice, however the expression of elastin in *Tnxb*$^{-/-}$ ureter appeared diffuse. The ureter of C3H mice had less elastin compared to B6. LP: lamina propria, SM: smooth muscle. Scale bar = 75 µm (A,B), or 100 µm (C). N=2.

3.2 Extracellular matrix-associated genes in *Vurm1*

As reported in **14.1**, the C3H mice present a host of ECM anomalies in their urinary tract that include increased collagen and α-SMA expression in their bladder and ureter, as well decreased elastin expression. Thus, I examined the *Vurm1* locus to determine if any genes within the locus might be relevant for the formation and/or maintenance of the extracellular matrix, and whether the C3H strain harbours deleterious mutations in these genes.

Vurm1 contains 663 annotated genes, of which 9 transcribe long non-coding RNAs, 92 transcribe microRNAs, and the remaining 562 are protein coding.

I identified 16 ECM-related genes within the *Vurm1* region, which are described in Table7. These genes are all are protein coding, and can be divided into three main categories based on their function as described below:

I-genes that code for proteins that are structural components of the matrix: *Matn3, Lamb1*, *Fbln5*.

II-genes that code for proteins that are involved in the proper expression, assembly and deposition of matrix components: *Ctage5*, *Ltbp2*, *Tgfb3*.

III-genes that code for proteins that play an important role in cell-matrix interaction through regulation of interaction of cell's cytoskeleton with the matrix, as well as cell adhesion and migration: *Itgb8, Sdc1*, *Rock2*, *Cfl2*, *Ctage5*, *Flrt2*, *Inf2, Itgb1b, Sntg2, Actn1*.

Table 7 Matrix-related genes in the *Vurm1* locus

Genomic position on Chromosome 12		Gene ID	Gene Name	Function
8771395	8793687	Sdc1	Syndecan 1	Cell surface heparin sulfate proteoglycan, participates in cell-matrix interactions through its function as an ECM receptor
8947928	8972028	Matn3	Matrilin 3	Structural component of the matrix; may play role in formation of extracellular filamentous networks.
16894977	16958431	Rock2	Rho-associated coiled-coil containing protein kinase 2	Protein kinase, key regulator of actin cytoskeleton and cell polarity. Involved in regulation of smooth muscle contraction and actin filament organization.
21269805	21286111	Itgb1bp1	Integrin beta 1 binding protein 1	Key regulator of the integrin-mediated cell-matrix interaction by binding to integrin beta 1. Plays a regulatory role in cell proliferation, differentiation, spreading, adhesion and migration. Stimulates cell proliferation in a fibronectin-dependent manner.
30174556	30243351	Sntg2	Syntrophin, gamma 2	Adaptor protein that binds to and modulates properties/functions of actin filaments
31265293	31268860	Lamb1	Laminin B1 (Lamb1), mRNA.	Mediates attachment, migration and organization of cells during developments by interacting with other ECM components.
54858818	54862877	Cfl2	Cofilin 2	Reversibly controls actin polymerization /depolymerisation in a pH-sensitive manner. Required for muscle maintenance
59129745	59163019	Ctage5	CTAGE family, member 5	Required for collagen VII (COL7A1) secretion by loading COL7A1 into transport carriers.
75308312	75395817	Rhoj	Ras homolog family member J	Induces formation of F-actin-rich structures.
80167541	80172144	Actn1	Actinin, alpha 1	F-actin crosslinking protein
84783211	84816036	Ltbp2	Latent transforming growth factor beta binding protein 2	Plays role in assembly and architectural organization of elastic fibres.
86056742	86079041	Tgfb3	Transforming growth factor, beta 3	Regulates assembly of non-fibre forming matrix components. Activates matrix metalloproteinases.
95692225	95785213	Flrt2	Fibronectin leucine rich transmembrane protein 2	Important for cell adhesion and cell migration.
101746564	101819119	Fbln5	Fibulin 5	Essential for elastic fibre formation.
112588783	112615557	Inf2	Inverted formin 2	Plays a role in actin filament polymerization
119162802	119238276	Itgb8	Integrin beta 8	A receptor for fibronectin

3.2.1 Coding variants in ECM-related genes within the *Vurm1* region

I identified a total of eight coding variants in *Rock2*, *Lamb1*, *Inf2*, and *Itgb8* (Table 8). *In silico* analysis of the impact of these variants using the pre-computed values of the PROVEAN and SIFT algorithms, indicated that except for T16A in *Rock2*, the rest are tolerated. None of these variants are annotated in the non-refluxing B6 strain. Evaluation of the presence of these variants in the C3H/HeJ, AKR/J, CBA/J and DBA2/J, which are all mouse models of VUR without kidney malformations, showed that all of these variants are found in the C3H/HeJ, AKR/J and CBA/J, while only two of these variants are present in the DBA2/J.

Table 8 Coding variants in matrix-related genes located in *Vurm1* locus.

Presence or absence of these variants in other mouse strains is noted by Yes and No, respectively. Variants predicted to be deleterious are coloured yellow, while variants predicted to be tolerated are coloured blue.

Gene	dbSNP	Variant	PROVEAN	SIFT	C3H/HeJ	AKR/J	CBA/J	DBA/2J	C57BL/6J (B6)
Rock2	rs216367646	T16A			Yes	Yes	Yes	Yes	No
Lamb1	rs13481376	A207T			Yes	Yes	Yes	No	No
	rs49685907	I617V			Yes	Yes	Yes	No	No
	rs13471814	E1041D			Yes	Yes	Yes	No	No
	rs29489998	V1441A			Yes	Yes	Yes	No	No
Inf2	rs29159504	A1036T			Yes	Yes	Yes	No	No
	rs13469487	R1165Q			Yes	Yes	Yes	No	No
Itgb8	rs48942401	R140H			Yes	Yes	Yes	Yes	No

3.3 *TNXB* variants in a cohort of children with VUR, BD and hEDS

As described above, the *Tnxb*$^{+/-}$ and *Tnxb*$^{-/-}$ mice have bladder compliance defects that manifest as bladder rupture when the intraluminal pressure of the bladder increases. These mice exhibit a decrease in the content of their fibrillary collagens as well as elastin, in their bladder, ureter, and skin. In the context of the urinary tract, this reduction can translate into the compliance defect described above. While these mice do not exhibit VUR, many studies have reported a co-prevalence of VUR and joint hypermobility. Given the bladder weakness observed in the *Tnxb+/-* and *Tnxb-/-* mice, we set out to explore the damaging effect of *TNXB* mutations in a cohort of children with VUR, BD and joint hypermobility.

3.3.1 Cohort demographics

Our cohort included 47 paediatric VUR patients ranging in age from 6-17 years. The clinical characteristics of the cohort are outlined in Table 9. We tested 40 children for generalized joint hypermobility using the Beighton scoring system. The remaining seven children have not been tested because they have not yet attended a follow-up clinic. Of the 40 children tested for generalized joint hypermobility, 26 were diagnosed with hypermobility based on Beighton score cutoff of six out of a total possible score of nine for pre-pubertal children (170, 258).

Table 9 Clinical and demographic characteristics of cohort of children sequenced for *TNXB* variants.

Presence of a clinical feature is denoted by yes, while absence and unavailability of information is denoted by No and NA, respectively. Beighton scores greater than six are highlighted yellow.

PATIENT ID	AGE AT HYPERMOBILITY DIAGNOSIS	SEX	POPULATION	UTI AT VUR DIAGNOSIS	FAMILY HISTORY OF HYPERMOBILITY	FAMILY HISTORY OF VUR	BLADDER DIVERTICULUM	VUR GRADE	BEIGHTON SCORE
6	9	F	Other	No	NA	**Yes**	No	3	4
9	13	M	European (Non-Finnish)	No	NA	No	No	3	6
17	17	M	South Asian	**Yes**	NA	No	No	4	2
23	17	F	Other	**Yes**	NA	No	No	3	8
31	7	F	Other	No	NA	No	No	5	7
37	8	M	European (Non-Finnish)	**Yes**	NA	No	No	2	5
41		M	Other	**Yes**	NA	No	No	3	Not tested
43	7	F	Other	**Yes**	NA	No	No	5	5
45	6	M	European (Non-Finnish)	**Yes**	NA	No	No	2	2
51	7	M	Other	No	NA	No	No	3	6
60	11	F	European (Non-Finnish)	No	NA	No	No	4	6
65	6	F	European (Non-Finnish)	No	NA	**Yes**	No	3	7
68	8	M	European (Non-Finnish)	**Yes**	NA	No	No	5	5
69	6	F	European (Non-Finnish)	**Yes**	NA	No	No	4	9
82	16	F	European (Non-Finnish)	No	**Yes**	No	No	2	6
86	9	F	European (Non-Finnish)	**Yes**	**Yes**	No	No	4	8
88	10	F	European (Non-Finnish)	**Yes**	NA	No	No	4	6
89	12	F	European (Non-Finnish)	**Yes**	NA	**Yes**	**Yes**	2	5
95	7	F	European (Non-Finnish)	**Yes**	NA	**Yes**	No	3	9
103		F	European (Non-Finnish)	**Yes**	NA	No	No	3	Not tested
105	12	F	European (Non-Finnish)	No	NA	No	No	2	8
110	11	M	European (Non-Finnish)	**Yes**	**Yes**	No	No	4	3
115	6	F	European (Non-Finnish)	**Yes**	**Yes**	**Yes**	No	5	6
116	7	M	European (Non-Finnish)	**Yes**	NA	No	**Yes**	2	9
120		M	European (Non-Finnish)	**Yes**	NA	No	No	5	Not tested
122	7	M	South Asian	**Yes**	NA	No	No	4	7
124		F	Other	No	NA	No	No	5	Not tested
126	7	M	South Asian/European	No	NA	No	No	4	6
129	8	M	European (Non-Finnish)	**Yes**	NA	No	No	3	6
130	7	F	European (Non-Finnish)	No	NA	No	No	4	4
134	8	M	Other	**Yes**	NA	No	No	5	6
142	12	F	European (Non-Finnish)	**Yes**	NA	No	No	2	Not tested
151		F	European (Non-Finnish)	**Yes**	NA	**Yes**	No	4	Not tested
155	7	F	European (Non-Finnish)	**Yes**	**Yes**	No	No	5	4
159	7	M	Other	**Yes**	NA	NA	No	3	8
164	17	F	European (Non-Finnish)	No	NA	No	No	1	6
167	12	M	European (Non-Finnish)	No	NA	**Yes**	No	4	6
169	7	F	European (Non-Finnish)	No	**Yes**	No	No	3	8
172	12	F	European (Non-Finnish)	**Yes**	NA	No	No	2	2
177	15	F	European (Non-Finnish)	**Yes**	NA	No	No	2	3
179		M	Other	No	NA	No	No	4	Not tested
191	14	F	European (Non-Finnish)	No	NA	No	No	3	4
193	12	M	European (Non-Finnish)	No	NA	**Yes**	No	4	2
199	10	F	European (Non-Finnish)	**Yes**	**Yes**	No	No		9
208	8	M	European (Non-Finnish)	No	NA	No	No	2	6
216	8	F	European (Non-Finnish)	No	**Yes**	No	No	2	9
223	10	M	South Asian	No	NA	No	No	3	6

3.4 Putative disease-causing *TNXB* variants:

I identified five rare non-synonymous variants that are predicted to be deleterious by at least two prediction algorithms (Table 10). R4171Q, W3673STOP, M3775T, and R3719W were identified in hypermobile individuals, while G878D was identified in an individual with a Beighton score of 4 (i.e. not hypermobile) (Table 9). G878, W3673STOP, R3719W, R4171Q are variants that affect evolutionarily conserved amino acid residues, while M3775T occurs in a non-conserved amino acid (Figure 20). G878, W3673STOP, R3719W, and M3775T are within the FNIII domain of the TNXB, while R4171Q is within the FBG domain; both of these domains are the site of TNXB interaction with matrix components such as fibrillary collagens and elastic fibres (Figure 21).

In order to identify whether W3673STOP and M3775T mutations are in cis (i.e. same allele) or in trans (i.e. different alleles) in patient 86, we Sanger sequenced the DNA from parents. However, we were unable to detect either mutation in the parents. A repeat of the Sanger sequencing performed on a freshly extracted DNA of patient 86, also failed to reveal either mutation. These mutations occur at the pseudogene region, and the sequencing strategy for this region involved generation of a long-range amplicon, coupled with Sanger sequencing of the long-range amplicon. We suspect that the W3673STOP and M3775T mutations are a consequence of low fidelity in the original long-range amplicon.

Table 10 List of rare putative disease-causing *TNXB* variants.

Variants predicted to be deleterious are coloured yellow, while tolerated variants are coloured blue.

PATIENT ID	HYPERMOBILITY STATUS	POPULATION	REFERENCE SNP	PROTEIN VARIANT	MINOR ALLELE FREQUENCY (ExAC POPULATION)	SIFT	PolyPhen 2	Mutation Taster
37	Hypermobile	European (non-Finnish)	Novel	R4171Q	0%			
86	Hypermobile	European (non-Finnish)	Novel	W3673STOP	0%			
86	Hypermobile	European (non-Finnish)	Novel	M3775T	0%			
105	Hypermobile	European (non-Finnish)	Novel	R3719W	0%			
130	Not hypermobile	European (non-Finnish)	rs201647307	G878D	0%			

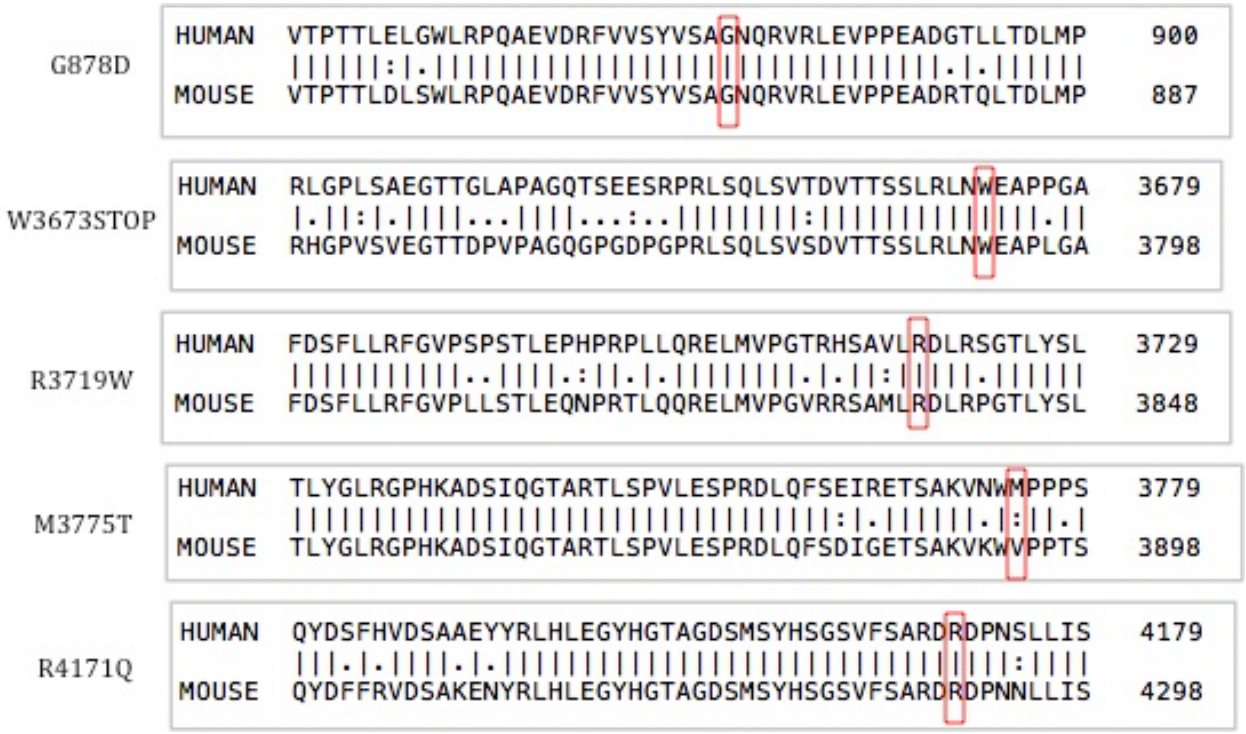

Figure 20 Alignment of human *TNXB* with its murine orthologue.

The aligned sequences correspond to the location of the five identified rare putative disease-causing variants. All variants except for M3775T affect evolutionarily conserved sequences.

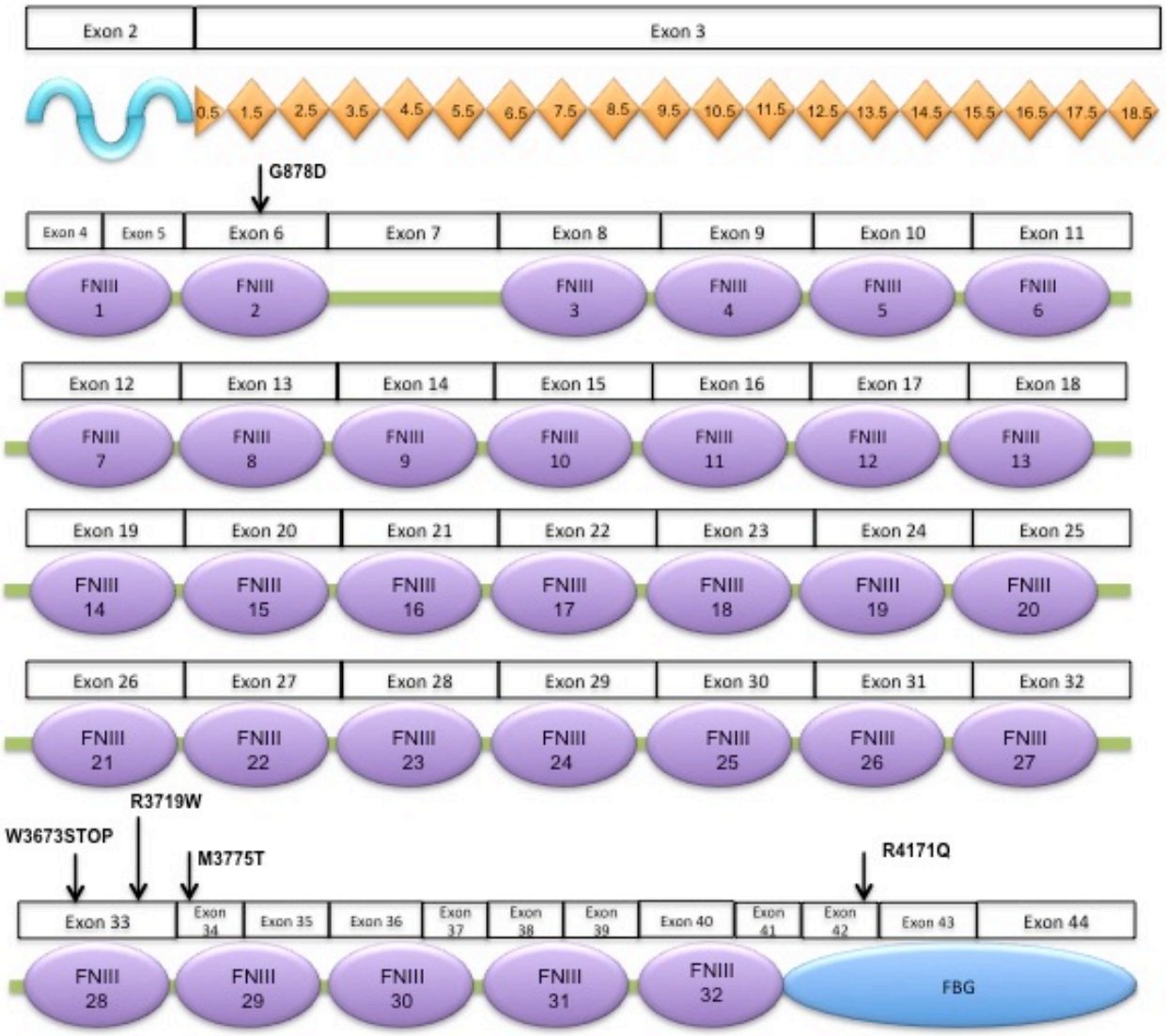

Figure 21 Schematic representation of TNXB and the location of identified rare putative-disease causing variants.

4 CHAPTER FOUR: Discussion

4.1 *Tnxb* mutant mice exhibit a bladder compliance defect

The newborn *Tnxb* mutant mice were found to have a bladder compliance defect that manifested more severely in the *Tnxb*$^{-/-}$ mice. Because compliance is a function of distensibility and tensile strength in the bladder, presence of a compliance defects indicates an imbalance between these biomechanical forces that essentially stems from faults in fibrillary collagens, elastic fibres, as well as the musculature of the bladder. Given the regulatory role of TNXB in assembly of collagen fibres and modulation of matrix homeostasis, as well as the reported dermatological and musculoskeletal phonotypes of *Tnxb* mutant mice, the newly characterized bladder compliance phenotype can be explained as a direct consequence of matrix defects. The bladder compliance assay will be repeated on a larger sample of *Tnxb*$^{-/-}$ mice.

We examined the *Tnxb* mRNA expression pattern in the urinary tract through RNA *in situ* hybridization (ISH), and reverse transcription quantitative PCR (RT-qPCR). While analysis of mRNA expression pattern for a secreted protein such as TNXB is not ideal, given the limitation we faced with respect to antibody specificity, it is a helpful tool to identify cells expressing *Tnxb* mRNA. At E15, *Tnxb* mRNA was detected in the undifferentiated mesenchyme of the kidney, the outer edges of the bladder and ureter smooth muscle, and the dermis of the skin. The expression profile in the skin is consistent with numerous studies that have investigated TNXB expression in mouse skin. The RNA ISH results will be repeated in E15, as well as newborn mice.

The RT-qPCR results suggest that starting from birth to adulthood, the bladder followed by the skin, has the highest levels of *Tnxb* mRNA. These results confirm that *Tnxb* mRNA is also expressed in the ureter and the kidney albeit in levels lower than the bladder and the skin. This analysis will be performed in E15 tissues as well.

To investigate the underlying cause of the bladder compliance defect observed in $Tnxb^{+/-}$ and $Tnxb^{-/-}$ mice, we evaluated the collagen, elastin and α-SMA content in the bladder and ureter of these mice in comparison with their WT littermates. Taking advantage of the inherent birefringence quality of collagen fibres, we evaluated the quality and quantity of collagen present in paraffin-embedded sections of newborn bladder, ureter and skin. Our results indicated the presence of a systemic defect in collagen deposition manifested by reduction in the amount of collagen present in the bladder, ureter and skin of $Tnxb^{+/-}$ and $Tnxb^{-/-}$ mice. This analysis will be repeated in newborn and E15 mice, and confirmed by Western blot analysis. Our evaluation of the elastin expression in these mice, pointed to a systemic defect in the deposition of elastin manifested by a decrease in the elastin signal detected using immunofluorescence. The described collagen defect translates to a decrease in tensile strength and tissue distensibility, while the reduction in elastin results in defects in recoil properties of the tissue. Together these defects compromise the ability of the bladder to withstand increasing intraluminal pressure during urine collection, causing bladder rupture and/or diverticula formation.

Furthermore, our analysis of bladder and ureter smooth muscle in $Tnxb^{+/-}$ and $Tnxb^{-/-}$ mice revealed that α-SMA is highly expressed especially in the bladder and ureter of $Tnxb^{-/-}$ mice. Analysis of bladder musculature using Masson's Trichrome staining revealed increased collagen deposition in the bladder musculature of $Tnxb^{-/-}$ mice. Increased α-SMA expression

has been long associated with pro-fibrotic environment within a tissue. Indeed, the increased deposition of collagen within the musculature could suggest increased stress on the smooth muscle cells prompting them to up-regulate α-SMA expression. It has been shown that TNXB regulates the bioavailability of TGF-β1, a pro-fibrotic cytokine, and down-regulates members of matrix metalloproteinase family (i.e. MMP-2, MMP-13) (259). Furthermore, TNXB deficiency has been associated with increased levels of TGF-β3 in humans. All these molecules are important drivers of pro-fibrotic responses in tissues, and are associated with increased rates of matrix turnover. Investigation of changes in the expression level of the above-mentioned molecules could shed light on the underlying cause of the increase in α-SMA expression and collagen deposition in bladder musculature. Because the onset of urine production in mouse is E15, it will be informative to perform similar analysis on embryonic tissue to pinpoint the onset of the above-mentioned defects, and to investigate whether any potential increase in matrix turnover is the cause or the effect of compliance defects.

4.2 The bladder and ureter of C3H mice exhibit increased tensile strength and decrease recoil

The C3H mice are a fully penetrant model for VUR without kidney malformations. In order to investigate the potential effect of VUR on the compliance properties of their bladders, and to contrast their compliance phenotype with the *Tnxb*$^{+/-}$ and *Tnxb*$^{-/-}$ mice that do not exhibit VUR, we performed the compliance assay in C3H newborn mice. Our results indicate that the bladder of C3H mice is able to withstand increasing intraluminal pressure better than non-refluxing B6 bladders. This could be partly attributed to the fact that the refluxing UVJ in the C3H mice allows some of the injected dye to travel towards the upper urinary tract, allowing for more volume to be injected into the bladder. However, given that the amount of dye that can reflux toward the upper urinary tract is very small, we evaluated the collagen, elastin and α-SMA content of the C3H bladders and ureters. Our analysis showed that the bladder and ureter of C3H mice has significantly more collagen, and therefore more tensile strength. We performed Western blot analysis to further breakdown the type of collagen fibres most abundantly found in the bladder and ureters of these mice. We found a significant increase in the amount of Col I fibres in the bladder, and Col III in the ureter of these mice. The thicker Col I fibres are the major contributors to tissue's tensile strength, while the thinner Col III fibres dictate distensibility. This translates into a stiffer bladder and a more lax ureter. Evaluation of elastin expression in the bladder and ureter of C3H mice, yielded an unexpected and interesting result, indicating reduction in recoil properties of these mice. We propose that these newly described characteristics of C3H bladder and ureter not only explain the compliance phenotype in these mice, but could also be causative of VUR. A stiff bladder with reduced recoil properties could hinder the occlusion of UVJ during

micturition and lead to VUR. At the same time a lax ureter with reduced recoil properties could lead to impaired peristalsis and be at higher risk of becoming dilated. The smooth muscle layer in the bladder and ureter of C3H mice expressed more α-SMA, and the bladder musculature had an increased amount of collagen fibres. Similar to the *Tnxb*$^{-/-}$ mice, these observations could be indicative of pro-fibrotic environment of C3H bladder, and requires further analysis, as suggested for *Tnxb*$^{-/-}$ mice.

4.3 The C3H mice harbour a putative-disease causing variant in *Rock2*

Based on the host of matrix-related phenotypes observed in the bladder and ureter of C3H mice, I surveyed the *Vurm1* locus for matrix-related genes, and conducted an *in silico* analysis to determine if the C3H mice harbour any putative disease-causing variants for these genes. I further examined the presence of these variants in the non-refluxing B6 strain as well other mouse models of VUR without kidney malformations. These analyses revealed the following deleterious variant: T16A in *Rock2.*

Rock2 is a serine/threonine kinase that is a downstream target of the small GTPases RhoA, RhoB, and RhoC. *Rock2* promotes actin-myosin-mediated contractile force generation by phosphorylating a variety of downstream target proteins. Its major downstream targets include the myosin-binding subunit of myosin light chain (MLC) phosphatase 1 (MYPT1), MLC2, LIM kinases, as well as Ezrin-radixin-moesin (ERM), thereby modulating actin cytoskeleton organization, stress fibre formation and smooth muscle cell contraction (260, 261). *Rock2* is expressed in the developing kidney and bladder (262-264). *Rock2*$^{-/-}$ mice die at E13.5, and exhibit a range of developmental defects that include placental and cardiovascular defects. Bladder smooth muscle contraction was disrupted in mice that

underwent a chemically induced down-regulation of *Rock2* (263, 265). Given the role of *Rock2* in modulation of smooth muscle contraction, a deleterious mutation in the gene can give rise to a malfunctioning protein that enhances smooth muscle contractility in the bladder. The increased contractility exerts additional mechanical force on the tissue, which is the prerequisite for α-SMA production (266). This could explain the increased α-SMA detected in the bladder and ureter of C3H mice. Interestingly, an increase in α-SMA expression further increases tissue contractility (267). I hypothesize that this leads to a cycle that ultimately results in increased mechanical force on the bladder musculature, which supports the UVJ, preventing proper occlusion of the UVJ during micturition and causing VUR.

It is important to consider that the variants identified in Table 3.2 and their predicted impact are the result of *in silico* analysis, which requires *in vivo* and *ex vivo* validation. The non-synonymous variants in Table 3.2 that are predicted to be tolerated might cause hindrances of varying degrees in protein function, and therefore should not be excluded from further exploration.

I hypothesize that multiple regulatory genes within the *Vurm1* locus are responsible for the VUR phenotype. To fully explore this hypothesis and further refine the locus, generation of congenic mice could prove crucial.

4.4 Children with VUR and generalized joint hypermobility harbour putative-disease causing variants in *TNXB*

Sanger sequencing of *TNXB* in a cohort of 47 paediatric patients with VUR identified five rare (i.e. MAF <1%) putative-disease causing variants: G878D, W3673STOP, R3791W, M3775T, R4171Q. These variants are found in the FNIII domain of TNXB, which regulates the assembly and deposition of collagen fibres. Therefore, these variants could affect the quantity and quality of collagen deposited in the various tissues. Except for M3775T, all other variants affect evolutionarily conserved amino acid residues, further supporting the damaging potential of these mutations.

The 9-point Beighton hypermobility score was used for the diagnosis of joint hypermobility in our cohort. The Beighton criteria were originally designed to assist in the clinical diagnosis of hypermobility in adults and not in children. Tofts and colleagues (2009) conducted a comprehensive literature review on the differential diagnosis of children with joint hypermobility, and reported major inconsistencies in diagnostic criteria (268). Another inadequacy of use of Beighton criteria in children arises from the inverse correlation of age with hypermobility (i.e. younger individuals are more hypermobile)(269). Consequently, an age limit has to be exerted on the criteria, which renders Beighton scoring ineffective in children younger than six years old. A recent reclassification of EDS subtypes has led to a more comprehensive evaluation of Beighton cut offs for pre-pubertal children, and sets the diagnosis cut off at a score of six out of nine (170). A final limitation of these criteria pertains to the fact that they only cover a sample of joints in the body through performance of five manoeuvres, leading to hypermobility being missed in joints not being tested (e.g. shoulders, hips, etc.), as well as skin features (e.g. hyperextensible skin, thin scar formation, etc.) being

ignored. Despite these inadequacies and due to lack of a better diagnostic system, we resorted to Beighton to evaluate the hypermobility status of the cohort. Because hypermobility testing required attendance of recruited children at a follow up clinic, we were unable to test all individuals included in the cohort (i.e. 85% were tested). However, we found hypermobility was highly prevalent in our cohort: 77.5% of those tested were hypermobile. This finding is consistent with previous studies that have reported a significant co-prevalence of VUR and joint hypermobility. Approximately 55% of hypermobile patients in our cohort were females, which is consistent with the higher prevalence of hypermobility in females(269).

Of the five damaging mutations described above, all with the exception of G878D are found in hypermobile individuals. The individual harbouring G878D was assigned a hypermobility score of 4. Given the limitations of Beighton criteria as described above, it is possible that this patient is hypermobile in joints not covered by these criteria.

Functional validation of the identified deleterious variants through various methods is a crucial in establishing causality vs. correlation. For instance, skin biopsies could be used to both perform histological analyses and to establish fibroblast cell lines to test for matrix defects. Gbadegesin and colleagues (2013) performed wound-healing assay and evaluated the activation of focal adhesion kinase in fibroblast cell lines from a patient with VUR harbouring a deleterious mutation in *TNXB*, in order to establish the effect of the mutation on cell migration and adhesion (36).

However, a number of limitations exist for such analyses. Firstly, given the fact that our cohort consists of paediatric patients, obtaining consent for skin biopsies might be challenging due to mild pain associated with the procedure. Secondly, we do not have a

validated commercially available TNXB antibody to properly probe for co-localization of this protein with other matrix components. Thirdly, while evaluation of the dermis and/or fibroblast cell line could be informative, the tissue microenvironment at the UVJ and the bladder are different from the skin, and need to be evaluated to prove that the variants result in a refluxing UVJ. Currently there are no UVJ cell lines; alternatively, human bladder cell lines could be used, however, cloning the *TNXB* gene could pose potential challenges given its size (i.e. 68kbps). Recently Tsoi and colleagues (2017), have described a new technique that utilized long-adapter single-stand oligonucleotide (LASSO) probes to capture and clone large DNA fragments (i.e. thousands of kbps) in a single reaction, making cloning of a 68kbps gene a possibility (270). Alternatively, the Crispr/Cas9 system could be used to generate knock-in human bladder cell lines, or knock-in mouse models harbouring the identified deleterious variants. However, given that the *Tnxb*$^{+/-}$ and *Tnxb*$^{-/-}$ mice do not reflux, incomplete phenotype recapitulation could occur.

5 CHAPTER FIVE: CONCLUSIONS AND FUTURE DIRECTIONS

Through the studies outlined herein, I investigated the association of matrix anomalies with the pathologies of BD and VUR. In my attempts to determine causality vs. correlation between these pathologies and matrix defects, I used three mouse lines: B6 as controls, *Tnxb*$^{+/-}$ and *Tnxb*$^{-/-}$ as models representing the skin phenotypes of EDS, and C3H as a model for VUR. I was able to determine that the bladder of the *Tnxb* mutant mice exhibits compliance defects associated with the reduction in the amount of collagen and elastic fibres present in their bladders. A number of studies have reported similar findings in the skin of these mice. These studies have evaluated the quality and strength of collagen fibres in the skin of these mice through electron microscopy and stress tests, respectively. To show that the bladder phenotype in the *Tnxb* mutant mice is a direct consequence of defects in collagen fibres, similar studies must be performed in the bladder.

In humans, compliance defects due to weakness in the bladder musculature, as well as obstruction of urethra can lead to BD. While there are no mouse models of BD, it would be interesting to partially occlude the urethra in the *Tnxb* mutant mice to evaluate whether BD can form over time.

In C3H mice, I showed that there is an increase in the amount of collagen fibres coupled with a decrease in the expression of elastin in the bladder and ureter. Furthermore these mice harbour a deleterious mutation in *Rock2,* which modulates smooth muscle contraction. I postulate that the increased stiffness caused by increased collagen expression, coupled with decreased recoil due to decreased elastin expression, could cause the UVJ in these mice to remain patent and therefore lead to VUR. Indeed the bladders of these mice show increased tensile strength, as they did not rupture during the compliance assay.

Performing electron microscopy to evaluate the quality and arrangement of collagen fibres, and a stress test on the bladder of the C3H could be informative. To conclusively establish that these changes affect the UVJ, the quality and quantity of collagen and elastic fibres in the UVJ must be examined. Give the size and location of the UVJ, laser capture microdissection could be use to accurately dissect the UVJ from the bladder thereby facilitating the examination of UVJ ECM microenvironment.

Both the C3H and *Tnxb* mutant mice exhibited increased α-SMA expression. To establish whether this increase is the effect of the smooth muscle experiencing fibrosis or it is a developmental defect compromising the function of the musculature, pro-fibrotic pathways such as the TGF-β1 and MMPs could be explored. In the case of the C3H mice, downstream effectors of *Rock2* that are known to modulate stress fibres and smooth muscle contraction could be explored. Furthermore, RNA sequencing could be performed to better evaluate the correlation of ECM-related genes identified in the *Vurm1* locus in C3H mice. Creation a congenic mouse line between the B6 and C3H could help further refine the *Vurm1* locus and fully explore whether defects in matrix-related genes are responsible for the VUR phenotype.

To further explore the association between matrix anomalies with BD and VUR, we sequenced *TNXB,* the gene known to cause clEDS in a cohort of children with VUR and BD. We identified five putative disease-causing variants; four in children who had a Beighton score of greater than six and were therefore hypermobile, and one in an non-hypermobile child. This study faced a number of limitations pertaining to the current protocol used to test children for hypermobility. Efforts are ongoing by various healthcare professionals to improve the hypermobility diagnostic criteria.

We hope to establish a causal correlation between TNXB-induced joint hypermobility and VUR, with the ultimate goal of improving the test for hypermobility and using it as a non-invasive test to diagnose children with VUR.

References

1. Williams G, Fletcher JT, Alexander SI, Craig JC. Vesicoureteral reflux. Journal of the American Society of Nephrology : JASN. 2008;19(5):847-62.
2. Hodson CJ, Edwards D. Chronic pyelonephritis and vesico-ureteric reflex. Clin Radiol. 1960;11:219-31.
3. Wolfish NM, Delbrouck NF, Shanon A, Matzinger MA, Stenstrom R, McLaine PN. Prevalence of hypertension in children with primary vesicoureteral reflux. J Pediatr. 1993;123(4):559-63.
4. Bailey RR, Lynn KL, Robson RA. End-stage reflux nephropathy. Ren Fail. 1994;16(1):27-35.
5. Viana R, Batourina E, Huang H, Dressler GR, Kobayashi A, Behringer RR, et al. The development of the bladder trigone, the center of the anti-reflux mechanism. Development. 2007;134(20):3763-9.
6. Murawski IJ, Gupta IR. Vesicoureteric reflux and renal malformations: a developmental problem. Clin Genet. 2006;69(2):105-17.
7. Lebowitz RL, Olbing H, Parkkulainen KV, Smellie JM, Tamminen-Mobius TE. International system of radiographic grading of vesicoureteric reflux. International Reflux Study in Children. Pediatr Radiol. 1985;15(2):105-9.
8. Smellie JM, Prescod NP, Shaw PJ, Risdon RA, Bryant TN. Childhood reflux and urinary infection: a follow-up of 10-41 years in 226 adults. Pediatr Nephrol. 1998;12(9):727-36.
9. Smellie JM, Jodal U, Lax H, Mobius TT, Hirche H, Olbing H, et al. Outcome at 10 years of severe vesicoureteric reflux managed medically: Report of the International Reflux Study in Children. J Pediatr. 2001;139(5):656-63.
10. Sjostrom S, Sillen U, Bachelard M, Hansson S, Stokland E. Spontaneous resolution of high grade infantile vesicoureteral reflux. The Journal of Urology. 2004;172(2):694-8; discussion 9.
11. Arlen AM, Garcia-Roig M, Weiss AD, Leong T, Cooper CS, Kirsch AJ. Vesicoureteral Reflux Index: 2-Institution Analysis and Validation. The Journal of Urology. 2015.
12. Agostiniani R, Mariotti P. The natural history of vesicoureteral reflux. J Matern Fetal Neonatal Med. 2011;24 Suppl 1:2-3.
13. Roshani H, Dabhoiwala NF, Verbeek FJ, Kurth KH, Lamers WH. Anatomy of ureterovesical junction and distal ureter studied by endoluminal ultrasonography in vitro. The Journal of Urology. 1999;161(5):1614-9.
14. Tanagho EA, Pugh RC. The anatomy and function of the ureterovesical junction. Br J Urol. 1963;35:151-65.
15. Noe HN, Wyatt RJ, Peeden JN, Jr., Rivas ML. The transmission of vesicoureteral reflux from parent to child. The Journal of Urology. 1992;148(6):1869-71.
16. Noe HN. The long-term results of prospective sibling reflux screening. The Journal of Urology. 1992;148(5 Pt 2):1739-42.
17. Parekh DJ, Pope JCt, Adams MC, Brock JW, 3rd. Outcome of sibling vesicoureteral reflux. The Journal of Urology. 2002;167(1):283-4.
18. Wan J, Greenfield SP, Ng M, Zerin M, Ritchey ML, Bloom D. Sibling reflux: a dual center retrospective study. The Journal of Urology. 1996;156(2 Pt 2):677-9.

19. Pirker ME, Colhoun E, Puri P. Renal scarring in familial vesicoureteral reflux: is prevention possible? The Journal of Urology. 2006;176(4 Pt 2):1842-6; discussion 6.
20. Burger RH. A theory on the nature of transmission of congenital vesicoureteral reflux. The Journal of Urology. 1972;108(2):249-54.
21. Chapman CJ, Bailey RR, Janus ED, Abbott GD, Lynn KL. Vesicoureteric Reflux - Segregation Analysis. American Journal of Medical Genetics. 1985;20(4):577-84.
22. Eccles MR, Bailey RR, Abbott GD, Sullivan MJ. Unravelling the genetics of vesicoureteric reflux: A common familial disorder. Human Molecular Genetics. 1996;5:1425-9.
23. Lambert HJ, Stewart A, Gullett AM, Cordell HJ, Malcolm S, Feather SA, et al. Primary, Nonsyndromic Vesicoureteric Reflux and Nephropathy in Sibling Pairs: A United Kingdom Cohort for a DNA Bank. Clin J Am Soc Nephro. 2011;6(4):760-6.
24. Sanna-Cherchi S, Reese A, Hensle T, Caridi G, Izzi C, Kim YY, et al. Familial vesicoureteral reflux: Testing replication of linkage in seven new multigenerational kindreds. Journal of the American Society of Nephrology. 2005;16(6):1781-7.
25. van Eerde AM, Koeleman BP, van de Kamp JM, de Jong TP, Wijmenga C, Giltay JC. Linkage study of 14 candidate genes and loci in four large Dutch families with vesico-ureteral reflux. Pediatr Nephrol. 2007;22(8):1129-33.
26. Pasch A, Hoefele J, Grimminger H, Hacker HW, Hildebrandt F. Multiple urinary tract malformations with likely recessive inheritance in a large Somalian kindred. Nephrol Dial Transplant. 2004;19(12):3172-5.
27. Weng PL, Sanna-Cherchi S, Hensle T, Shapiro E, Werzberger A, Caridi G, et al. A recessive gene for primary vesicoureteral reflux maps to chromosome 12p11-q13. Journal of the American Society of Nephrology : JASN. 2009;20(7):1633-40.
28. Middleton GW, Howards SS, Gillenwater JY. Sex-linked familial reflux. The Journal of Urology. 1975;114(1):36-9.
29. Naseri M, Ghiggeri GM, Caridi G, Abbaszadegan MR. Five cases of severe vesico-ureteric reflux in a family with an X-linked compatible trait. Pediatric Nephrology. 2010;25(2):349-52.
30. de Vargas A, Evans K, Ransley P, Rosenberg AR, Rothwell D, Sherwood T, et al. A family study of vesicoureteric reflux. J Med Genet. 1978;15(2):85-96.
31. Pournasiri Z, Madani A, Zandi H, Salehpour S, Abdollah Gorji F, Ahmadzahe A. Relationship of generalized joint hypermobility with vesicoureteral reflux and urinary tract infection. Iran J Kidney Dis. 2014;8(3):189-93.
32. Beiraghdar F, Rostami Z, Panahi Y, Einollahi B, Teimoori M. Vesicourethral reflux in pediatrics with hypermobility syndrome. Nephrourol Mon. 2013;5(4):924-7.
33. Adib N, Davies K, Grahame R, Woo P, Murray KJ. Joint hypermobility syndrome in childhood. A not so benign multisystem disorder? Rheumatology (Oxford). 2005;44(6):744-50.
34. van Eerde AM, Verhoeven VJ, de Jong TP, van de Putte EM, Giltay JC, Engelbert RH. Is joint hypermobility associated with vesico-ureteral reflux? An assessment of 50 patients. BJU Int. 2012;109(8):1243-8.
35. Elahi S, Homstad A, Vaidya H, Stout J, Hall G, Wu G, et al. Rare variants in tenascin genes in a cohort of children with primary vesicoureteric reflux. Pediatr Nephrol. 2016;31(2):247-53.

36. Gbadegesin RA, Brophy PD, Adeyemo A, Hall G, Gupta IR, Hains D, et al. TNXB mutations can cause vesicoureteral reflux. Journal of the American Society of Nephrology : JASN. 2013;24(8):1313-22.
37. Kaufman CS, Butler MG. Mutation in TNXB gene causes moderate to severe Ehlers-Danlos syndrome. World J Med Genet. 2016;6(2):17-21.
38. Demirdas S, Dulfer E, Robert L, Kempers M, van Beek D, Micha D, et al. Recognizing the tenascin-X deficient type of Ehlers-Danlos syndrome: a cross-sectional study in 17 patients. Clin Genet. 2017;91(3):411-25.
39. Sakiyama T, Kubo A, Sasaki T, Yamada T, Yabe N, Matsumoto K, et al. Recurrent gastrointestinal perforation in a patient with Ehlers-Danlos syndrome due to tenascin-X deficiency. J Dermatol. 2015;42(5):511-4.
40. Hendriks AG, Voermans NC, Schalkwijk J, Hamel BC, van Rossum MM. Well-defined clinical presentation of Ehlers-Danlos syndrome in patients with tenascin-X deficiency: a report of four cases. Clin Dysmorphol. 2012;21(1):15-8.
41. Ismail A, Hamad B, Kaabi AA, Nagaar OA, Bhat V, Zamar JA. Congenital bladder diverticula as a cause of bladder outlet obstruction in children. Eur J Pediatr Surg. 2011;21(5):345-7.
42. Pieretti RV, Pieretti-Vanmarcke RV. Congenital bladder diverticula in children. J Pediatr Surg. 1999;34(3):468-73.
43. Berrocal T, Lopez-Pereira P, Arjonilla A, Gutierrez J. Anomalies of the distal ureter, bladder, and urethra in children: embryologic, radiologic, and pathologic features. Radiographics. 2002;22(5):1139-64.
44. Psutka SP, Cendron M. Bladder diverticula in children. J Pediatr Urol. 2013;9(2):129-38.
45. Barrett DM, Malek RS, Kelalis PP. Observations on vesical diverticulum in childhood. The Journal of Urology. 1976;116(2):234-6.
46. Blane CE, Zerin JM, Bloom DA. Bladder diverticula in children. Radiology. 1994;190(3):695-7.
47. Garat JM, Angerri O, Caffaratti J, Moscatiello P, Villavicencio H. Primary congenital bladder diverticula in children. Urology. 2007;70(5):984-8.
48. Levard G, Aigrain Y, Ferkadji L, Elghoneimi A, Pichon J, Boureau M. Urinary bladder diverticula and the Ehlers-Danlos syndrome in children. J Pediatr Surg. 1989;24(11):1184-6.
49. Lee H, Lee YS, Im YJ, Han SW. Vesicoureteral reflux and bladder dysfunction. Transl Androl Urol. 2012;1(3):153-9.
50. Macedo A, Jr., Garrone G, Ottoni SL, Oliveira DE, Souza GR, Cruz ML. Primary congenital bladder diverticula: Where does the ureter drain? Afr J Paediatr Surg. 2015;12(4):280-5.
51. Rawat J, Rashid KA, Kanojia RP, Kureel SN, Tandon RK. Diagnosis and management of congenital bladder diverticulum in infancy and childhood: experience with nine cases at a tertiary health center in a developing country. Int Urol Nephrol. 2009;41(2):237-42.
52. Yu W, Hill WG. Defining protein expression in the urothelium: a problem of more than transitional interest. Am J Physiol Renal Physiol. 2011;301(5):F932-42.
53. Wu XR, Kong XP, Pellicer A, Kreibich G, Sun TT. Uroplakins in urothelial biology, function, and disease. Kidney Int. 2009;75(11):1153-65.

54. Minsky BD, Chlapowski FJ. Morphometric analysis of the translocation of lumenal membrane between cytoplasm and cell surface of transitional epithelial cells during the expansion-contraction cycles of mammalian urinary bladder. The Journal of Cell Biology. 1978;77(3):685-97.
55. Lewis SA, de Moura JL. Incorporation of cytoplasmic vesicles into apical membrane of mammalian urinary bladder epithelium. Nature. 1982;297(5868):685-8.
56. Hicks RM. The fine structure of the transitional epithelium of rat ureter. The Journal of Cell Biology. 1965;26(1):25-48.
57. Porter KR, Kenyon K, Badenhausen S. Specializations of the unit membrane. Protoplasma. 1967;63(1):262-74.
58. Hu P, Deng FM, Liang FX, Hu CM, Auerbach AB, Shapiro E, et al. Ablation of uroplakin III gene results in small urothelial plaques, urothelial leakage, and vesicoureteral reflux. The Journal of Cell Biology. 2000;151(5):961-72.
59. Kong XT, Deng FM, Hu P, Liang FX, Zhou G, Auerbach AB, et al. Roles of uroplakins in plaque formation, umbrella cell enlargement, and urinary tract diseases. J Cell Biol. 2004;167(6):1195-204.
60. Lazzeri M. The physiological function of the urothelium--more than a simple barrier. Urol Int. 2006;76(4):289-95.
61. Lilly JD, Parsons CL. Bladder surface glycosaminoglycans is a human epithelial permeability barrier. Surg Gynecol Obstet. 1990;171(6):493-6.
62. Parsons CL, Boychuk D, Jones S, Hurst R, Callahan H. Bladder surface glycosaminoglycans: an epithelial permeability barrier. The Journal of Urology. 1990;143(1):139-42.
63. Parsons CL, Stauffer C, Schmidt JD. Bladder-surface glycosaminoglycans: an efficient mechanism of environmental adaptation. Science. 1980;208(4444):605-7.
64. Janssen DA, van Wijk XM, Jansen KC, van Kuppevelt TH, Heesakkers JP, Schalken JA. The distribution and function of chondroitin sulfate and other sulfated glycosaminoglycans in the human bladder and their contribution to the protective bladder barrier. The Journal of Urology. 2013;189(1):336-42.
65. Noordzij JW, Dabhoiwala NF. A view on the anatomy of the ureterovesical junction. Scand J Urol Nephrol. 1993;27(3):371-80.
66. Gearhart JP, Canning DA, Gilpin SA, Lam EE, Gosling JA. Histological and histochemical study of the vesicoureteric junction in infancy and childhood. Br J Urol. 1993;72(5 Pt 1):648-54.
67. Hutch JA. Theory of maturation of the intravesical ureter. The Journal of Urology. 1961;86:534-8.
68. Andersson KE, Arner A. Urinary bladder contraction and relaxation: physiology and pathophysiology. Physiol Rev. 2004;84(3):935-86.
69. Tanaka ST, Ishii K, Demarco RT, Pope JCt, Brock JW, 3rd, Hayward SW. Endodermal origin of bladder trigone inferred from mesenchymal-epithelial interaction. The Journal of Urology. 2010;183(1):386-91.
70. Aitken KJ, Bagli DJ. The bladder extracellular matrix. Part I: architecture, development and disease. Nat Rev Urol. 2009;6(11):596-611.
71. Alali S, Aitken KJ, Schroder A, Gribble A, Bagli DJ, Vitkin IA. Assessment of local structural disorders of the bladder wall in partial bladder outlet obstruction using polarized light imaging. Biomed Opt Express. 2014;5(2):621-9.

72. Andersson KE, Sjogren C. Aspects on the physiology and pharmacology of the bladder and urethra. Prog Neurobiol. 1982;19(1-2):71-89.
73. Gabella G, Uvelius B. Urinary bladder of rat: fine structure of normal and hypertrophic musculature. Cell and Tissue Research. 1990;262(1):67-79.
74. DeLancey JO. Anatomy and embryology of the lower urinary tract. Obstet Gynecol Clin North Am. 1989;16(4):717-31.
75. Dressler GR. The cellular basis of kidney development. Annu Rev Cell Dev Biol. 2006;22:509-29.
76. Yu J, Carroll TJ, McMahon AP. Sonic hedgehog regulates proliferation and differentiation of mesenchymal cells in the mouse metanephric kidney. Development. 2002;129(22):5301-12.
77. Batourina E, Choi C, Paragas N, Bello N, Hensle T, Costantini FD, et al. Distal ureter morphogenesis depends on epithelial cell remodeling mediated by vitamin A and Ret. Nature Genetics. 2002;32(1):109-15.
78. Deng FM, Liang FX, Tu L, Resing KA, Hu P, Supino M, et al. Uroplakin IIIb, a urothelial differentiation marker, dimerizes with uroplakin Ib as an early step of urothelial plaque assembly. The Journal of Cell Biology. 2002;159(4):685-94.
79. Wankel B, Ouyang J, Guo X, Hadjiolova K, Miller J, Liao Y, et al. Sequential and compartmentalized action of Rabs, SNAREs, and MAL in the apical delivery of fusiform vesicles in urothelial umbrella cells. Mol Biol Cell. 2016;27(10):1621-34.
80. Airik R, Bussen M, Singh MK, Petry M, Kispert A. Tbx18 regulates the development of the ureteral mesenchyme. J Clin Invest. 2006;116(3):663-74.
81. Baker LA, Gomez RA. Embryonic development of the ureter and bladder: acquisition of smooth muscle. The Journal of Urology. 1998;160(2):545-50.
82. Caubit X, Lye CM, Martin E, Core N, Long DA, Vola C, et al. Teashirt 3 is necessary for ureteral smooth muscle differentiation downstream of SHH and BMP4. Development. 2008;135(19):3301-10.
83. Mahoney ZX, Sammut B, Xavier RJ, Cunningham J, Go G, Brim KL, et al. Discs-large homolog 1 regulates smooth muscle orientation in the mouse ureter. Proc Natl Acad Sci U S A. 2006;103(52):19872-7.
84. Iizuka-Kogo A, Ishidao T, Akiyama T, Senda T. Abnormal development of urogenital organs in Dlgh1-deficient mice. Development. 2007;134(9):1799-807.
85. Miyazaki Y, Oshima K, Fogo A, Hogan BL, Ichikawa I. Bone morphogenetic protein 4 regulates the budding site and elongation of the mouse ureter. The Journal of clinical investigation. 2000;105(7):863-73.
86. Raatikainen-Ahokas A, Hytonen M, Tenhunen A, Sainio K, Sariola H. BMP-4 affects the differentiation of metanephric mesenchyme and reveals an early anterior-posterior axis of the embryonic kidney. Dev Dyn. 2000;217(2):146-58.
87. Miyazaki Y, Oshima K, Fogo A, Ichikawa I. Evidence that bone morphogenetic protein 4 has multiple biological functions during kidney and urinary tract development. Kidney international. 2003;63(3):835-44.
88. Bohnenpoll T, Bettenhausen E, Weiss AC, Foik AB, Trowe MO, Blank P, et al. Tbx18 expression demarcates multipotent precursor populations in the developing urogenital system but is exclusively required within the ureteric mesenchymal lineage to suppress a renal stromal fate. Developmental Biology. 2013;380(1):25-36.

89. Lye CM, Fasano L, Woolf AS. Ureter myogenesis: putting Teashirt into context. Journal of the American Society of Nephrology : JASN. 2010;21(1):24-30.
90. Wang Z, Wang DZ, Pipes GC, Olson EN. Myocardin is a master regulator of smooth muscle gene expression. Proceedings of the National Academy of Sciences of the United States of America. 2003;100(12):7129-34.
91. Chen J, Kitchen CM, Streb JW, Miano JM. Myocardin: a component of a molecular switch for smooth muscle differentiation. J Mol Cell Cardiol. 2002;34(10):1345-56.
92. Jenkins D, Caubit X, Dimovski A, Matevska N, Lye CM, Cabuk F, et al. Analysis of TSHZ2 and TSHZ3 genes in congenital pelvi-ureteric junction obstruction. Nephrol Dial Transplant. 2010;25(1):54-60.
93. Airik R, Trowe MO, Foik A, Farin HF, Petry M, Schuster-Gossler K, et al. Hydroureternephrosis due to loss of Sox9-regulated smooth muscle cell differentiation of the ureteric mesenchyme. Hum Mol Genet. 2010;19(24):4918-29.
94. Trowe MO, Shah S, Petry M, Airik R, Schuster-Gossler K, Kist R, et al. Loss of Sox9 in the periotic mesenchyme affects mesenchymal expansion and differentiation, and epithelial morphogenesis during cochlea development in the mouse. Developmental Biology. 2010;342(1):51-62.
95. Martin E, Caubit X, Airik R, Vola C, Fatmi A, Kispert A, et al. TSHZ3 and SOX9 regulate the timing of smooth muscle cell differentiation in the ureter by reducing myocardin activity. PloS One. 2013;8(5):e63721.
96. Thomas JC, DeMarco RT, Pope JCt. Molecular biology of ureteral bud and trigonal development. Curr Urol Rep. 2005;6(2):146-51.
97. Haraguchi R, Motoyama J, Sasaki H, Satoh Y, Miyagawa S, Nakagata N, et al. Molecular analysis of coordinated bladder and urogenital organ formation by Hedgehog signaling. Development. 2007;134(3):525-33.
98. Avni EF, Gallety E, Rypens F, Hall M, Dedeire S, Schulman CC. A hypothesis for the higher incidence of vesico-ureteral reflux and primary megaureters in male babies. Pediatr Radiol. 1992;22(1):1-4.
99. Cuckow PM, Nyirady P, Winyard PJ. Normal and abnormal development of the urogenital tract. Prenat Diagn. 2001;21(11):908-16.
100. Huang YC, Chen F, Li X. Clarification of mammalian cloacal morphogenesis using high-resolution episcopic microscopy. Developmental Biology. 2016;409(1):106-13.
101. Baskin L, DiSandro M, Li Y, Li W, Hayward S, Cunha G. Mesenchymal-epithelial interactions in bladder smooth muscle development: effects of the local tissue environment. The Journal of Urology. 2001;165(4):1283-8.
102. Baskin LS, Hayward SW, Young P, Cunha GR. Role of mesenchymal-epithelial interactions in normal bladder development. The Journal of Urology. 1996;156(5):1820-7.
103. Shiroyanagi Y, Liu B, Cao M, Agras K, Li J, Hsieh MH, et al. Urothelial sonic hedgehog signaling plays an important role in bladder smooth muscle formation. Differentiation. 2007;75(10):968-77.
104. Yucel S, Liu W, Cordero D, Donjacour A, Cunha G, Baskin LS. Anatomical studies of the fibroblast growth factor-10 mutant, Sonic Hedge Hog mutant and androgen receptor mutant mouse genital tubercle. Adv Exp Med Biol. 2004;545:123-48.
105. Liu W, Li Y, Cunha S, Hayward G, Baskin L. Diffusable growth factors induce bladder smooth muscle differentiation. In Vitro Cell Dev Biol Anim. 2000;36(7):476-84.

106. Belaguli NS, Schildmeyer LA, Schwartz RJ. Organization and myogenic restricted expression of the murine serum response factor gene. A role for autoregulation. The Journal of Biological Chemistry. 1997;272(29):18222-31.
107. Browning CL, Culberson DE, Aragon IV, Fillmore RA, Croissant JD, Schwartz RJ, et al. The developmentally regulated expression of serum response factor plays a key role in the control of smooth muscle-specific genes. Developmental Biology. 1998;194(1):18-37.
108. Wang DZ, Li S, Hockemeyer D, Sutherland L, Wang Z, Schratt G, et al. Potentiation of serum response factor activity by a family of myocardin-related transcription factors. Proceedings of the National Academy of Sciences of the United States of America. 2002;99(23):14855-60.
109. Du KL, Ip HS, Li J, Chen M, Dandre F, Yu W, et al. Myocardin is a critical serum response factor cofactor in the transcriptional program regulating smooth muscle cell differentiation. Mol Cell Biol. 2003;23(7):2425-37.
110. Li J, Shiroyanagi Y, Lin G, Haqq C, Lin CS, Lue TF, et al. Serum response factor, its cofactors, and epithelial-mesenchymal signaling in urinary bladder smooth muscle formation. Differentiation. 2006;74(1):30-9.
111. Jarvelainen H, Sainio A, Koulu M, Wight TN, Penttinen R. Extracellular matrix molecules: potential targets in pharmacotherapy. Pharmacol Rev. 2009;61(2):198-223.
112. Koo HP, Macarak EJ, Chang SL, Rosenbloom J, Howard PS. Temporal expression of elastic fiber components in bladder development. Connect Tissue Res. 1998;37(1-2):1-11.
113. Aitken KJ, Bagli DJ. The bladder extracellular matrix. Part II: regenerative applications. Nat Rev Urol. 2009;6(11):612-21.
114. Gordon MK, Hahn RA. Collagens. Cell Tissue Res. 2010;339(1):247-57.
115. Ottani V, Raspanti M, Ruggeri A. Collagen structure and functional implications. Micron. 2001;32(3):251-60.
116. Gelse K, Poschl E, Aigner T. Collagens--structure, function, and biosynthesis. Adv Drug Deliv Rev. 2003;55(12):1531-46.
117. Martin R, Waldmann L, Kaplan DL. Supramolecular assembly of collagen triblock peptides. Biopolymers. 2003;70(4):435-44.
118. Birk DE, Fitch JM, Babiarz JP, Doane KJ, Linsenmayer TF. Collagen fibrillogenesis in vitro: interaction of types I and V collagen regulates fibril diameter. J Cell Sci. 1990;95 (Pt 4):649-57.
119. Wenstrup RJ, Florer JB, Brunskill EW, Bell SM, Chervoneva I, Birk DE. Type V collagen controls the initiation of collagen fibril assembly. The Journal of Biological Chemistry. 2004;279(51):53331-7.
120. Mouw JK, Ou G, Weaver VM. Extracellular matrix assembly: a multiscale deconstruction. Nat Rev Mol Cell Biol. 2014;15(12):771-85.
121. Liu X, Wu H, Byrne M, Krane S, Jaenisch R. Type III collagen is crucial for collagen I fibrillogenesis and for normal cardiovascular development. Proc Natl Acad Sci U S A. 1997;94(5):1852-6.
122. Henkel W, Glanville RW. Covalent crosslinking between molecules of type I and type III collagen. The involvement of the N-terminal, nonhelical regions of the alpha 1 (I) and alpha 1 (III) chains in the formation of intermolecular crosslinks. Eur J Biochem. 1982;122(1):205-13.

123. Bao G, Kamm RD, Thomas W, Hwang W, Fletcher DA, Grodzinsky AJ, et al. Molecular Biomechanics: The Molecular Basis of How Forces Regulate Cellular Function. Mol Cell Biomech. 2010;3(2):91-105.
124. Sherratt MJ. Tissue elasticity and the ageing elastic fibre. Age (Dordr). 2009;31(4):305-25.
125. Gosline J, Lillie M, Carrington E, Guerette P, Ortlepp C, Savage K. Elastic proteins: biological roles and mechanical properties. Philos Trans R Soc Lond B Biol Sci. 2002;357(1418):121-32.
126. Kielty CM, Sherratt MJ, Shuttleworth CA. Elastic fibres. J Cell Sci. 2002;115(Pt 14):2817-28.
127. Liu X, Zhao Y, Gao J, Pawlyk B, Starcher B, Spencer JA, et al. Elastic fiber homeostasis requires lysyl oxidase-like 1 protein. Nature Genetics. 2004;36(2):178-82.
128. Kielty CM. Elastic fibres in health and disease. Expert Rev Mol Med. 2006;8(19):1-23.
129. Kielty CM, Shuttleworth CA. Fibrillin-containing microfibrils: structure and function in health and disease. Int J Biochem Cell Biol. 1995;27(8):747-60.
130. Milewicz DM, Grossfield J, Cao SN, Kielty C, Covitz W, Jewett T. A mutation in FBN1 disrupts profibrillin processing and results in isolated skeletal features of the Marfan syndrome. J Clin Invest. 1995;95(5):2373-8.
131. Kielty CM, Wess TJ, Haston L, Ashworth JL, Sherratt MJ, Shuttleworth CA. Fibrillin-rich microfibrils: elastic biopolymers of the extracellular matrix. J Muscle Res Cell Motil. 2002;23(5-6):581-96.
132. Hyytiainen M, Penttinen C, Keski-Oja J. Latent TGF-beta binding proteins: extracellular matrix association and roles in TGF-beta activation. Crit Rev Clin Lab Sci. 2004;41(3):233-64.
133. Rifkin DB. Latent transforming growth factor-beta (TGF-beta) binding proteins: orchestrators of TGF-beta availability. The Journal of Biological Chemistry. 2005;280(9):7409-12.
134. Huang J, Davis EC, Chapman SL, Budatha M, Marmorstein LY, Word RA, et al. Fibulin-4 deficiency results in ascending aortic aneurysms: a potential link between abnormal smooth muscle cell phenotype and aneurysm progression. Circ Res. 2010;106(3):583-92.
135. Yanagisawa H, Schluterman MK, Brekken RA. Fibulin-5, an integrin-binding matricellular protein: its function in development and disease. J Cell Commun Signal. 2009;3(3-4):337-47.
136. Choudhury R, McGovern A, Ridley C, Cain SA, Baldwin A, Wang MC, et al. Differential regulation of elastic fiber formation by fibulin-4 and -5. The Journal of Biological Chemistry. 2009;284(36):24553-67.
137. Papke CL, Yanagisawa H. Fibulin-4 and fibulin-5 in elastogenesis and beyond: Insights from mouse and human studies. Matrix Biol. 2014;37:142-9.
138. Yanagisawa H, Davis EC. Unraveling the mechanism of elastic fiber assembly: The roles of short fibulins. Int J Biochem Cell Biol. 2010;42(7):1084-93.
139. Sillen U. Bladder dysfunction in children with vesico-ureteric reflux. Acta Paediatr Suppl. 1999;88(431):40-7.
140. Sillen U. Bladder dysfunction and vesicoureteral reflux. Adv Urol. 2008:815472.
141. Lee BR, Silver RI, Partin AW, Epstein JI, Gearhart JP. A quantitative histologic analysis of collagen subtypes: the primary obstructed and refluxing megaureter of childhood. Urology. 1998;51(5):820-3.

142. Sokolis DP. Multiaxial mechanical behaviour of the passive ureteral wall: experimental study and mathematical characterisation. Comput Methods Biomech Biomed Engin. 2012;15(11):1145-56.
143. Rassoli A, Shafigh M, Seddighi A, Seddighi A, Daneshparvar H, Fatouraee N. Biaxial mechanical properties of human ureter under tension. Urol J. 2014;11(3):1678-86.
144. Shilo Y, Pichamuthu JE, Averch TD, Vorp DA. Evaluation of the tensile strength of the human ureter--preliminary results. J Endourol. 2014;28(12):1470-3.
145. Escala JM, Keating MA, Boyd G, Pierce A, Hutton JL, Lister J. Development of elastic fibres in the upper urinary tract. The Journal of Urology. 1989;141(4):969-73.
146. Andersson KE, McCloskey KD. Lamina propria: the functional center of the bladder? Neurourol Urodyn. 2014;33(1):9-16.
147. Chang SL, Howard PS, Koo HP, Macarak EJ. Role of type III collagen in bladder filling. Neurourol Urodyn. 1998;17(2):135-45.
148. Macarak EJ, Howard PS. The role of collagen in bladder filling. Adv Exp Med Biol. 1999;462:215-23; discussion 25-33.
149. Tokhmafshan F, Brophy PD, Gbadegesin RA, Gupta IR. Vesicoureteral reflux and the extracellular matrix connection. Pediatric Nephrology. 2016.
150. Mohamed M, Voet M, Gardeitchik T, Morava E. Cutis Laxa. Adv Exp Med Biol. 2014;802:161-84.
151. Morava E, Guillard M, Lefeber DJ, Wevers RA. Autosomal recessive cutis laxa syndrome revisited. Eur J Hum Genet. 2009;17(9):1099-110.
152. Alehossein M, Pourgholami M, Kamrani K, Soltani M, Yazdi A, Salamati P. Radiologic findings in cutis laxa syndrome and unusual association with hypertrophic pyloric stenosis. Iran J Radiol. 2013;10(2):94-8.
153. Agha A, Sakati NO, Higginbottom MC, Jones KL, Jr., Bay C, Nyhan WL. Two forms of cutis laxa presenting in the newborn period. Acta Paediatr Scand. 1978;67(6):775-80.
154. Robertson SP, Bankier A. Sotos syndrome and cutis laxa. J Med Genet. 1999;36(1):51-6.
155. Kielty CM, Davies SJ, Phillips JE, Jones CJ, Shuttleworth CA, Charles SJ. Marfan syndrome: fibrillin expression and microfibrillar abnormalities in a family with predominant ocular defects. J Med Genet. 1995;32(1):1-6.
156. Robinson PN, Godfrey M. The molecular genetics of Marfan syndrome and related microfibrillopathies. J Med Genet. 2000;37(1):9-25.
157. Clunie GJ, Mason JM. Visceral diverticula and the Marfan syndrome. Br J Surg. 1962;50:51-2.
158. de Silva DG, Gunawardena TP, Law FM. Unusual complications in siblings with marfanoid phenotype. Arch Dis Child. 1996;75(3):247-8.
159. Al-Hakim W, Goldsmith DJ. Bilateral popliteal aneurysms complicating adult polycystic kidney disease in a patient with a marfanoid habitus. Postgrad Med J. 2003;79(934):474-5.
160. Sakai LY, Keene DR, Renard M, De Backer J. FBN1: The disease-causing gene for Marfan syndrome and other genetic disorders. Gene. 2016;591(1):279-91.
161. Stromme P, Bjornstad PG, Ramstad K. Prevalence estimation of Williams syndrome. J Child Neurol. 2002;17(4):269-71.
162. Pober BR. Williams-Beuren syndrome. N Engl J Med. 2010;362(3):239-52.

163. Stoermer J, Olbing H, Hentrich F, Even K, Galal O, Bachmann J. [Syndrome of supravalvular aortic stenosis (Williams-Beuren syndrome) in association with changes in the kidney and efferent urinary tract]. Monatsschr Kinderheilkd. 1984;132(2):110-2.
164. Pober BR, Lacro RV, Rice C, Mandell V, Teele RL. Renal findings in 40 individuals with Williams syndrome. Am J Med Genet. 1993;46(3):271-4.
165. Pankau R, Partsch CJ, Winter M, Gosch A, Wessel A. Incidence and spectrum of renal abnormalities in Williams-Beuren syndrome. Am J Med Genet. 1996;63(1):301-4.
166. Sugayama SM, Koch VH, Furusawa EA, Leone C, Kim CA. Renal and urinary findings in 20 patients with Williams-Beuren syndrome diagnosed by fluorescence in situ hybridization (FISH). Rev Hosp Clin Fac Med Sao Paulo. 2004;59(5):266-72.
167. Morris CA, Leonard CO, Dilts C, Demsey SA. Adults with Williams syndrome. Am J Med Genet Suppl. 1990;6:102-7.
168. Callewaert B, Malfait F, Loeys B, De Paepe A. Ehlers-Danlos syndromes and Marfan syndrome. Best Pract Res Clin Rheumatol. 2008;22(1):165-89.
169. De Paepe A, Malfait F. The Ehlers-Danlos syndrome, a disorder with many faces. Clin Genet. 2012;82(1):1-11.
170. Malfait F, Francomano C, Byers P, Belmont J, Berglund B, Black J, et al. The 2017 international classification of the Ehlers-Danlos syndromes. American journal of medical genetics Part C, Seminars in Medical Genetics. 2017;175(1):8-26.
171. Wenstrup RJ, Florer JB, Cole WG, Willing MC, Birk DE. Reduced type I collagen utilization: a pathogenic mechanism in COL5A1 haplo-insufficient Ehlers-Danlos syndrome. J Cell Biochem. 2004;92(1):113-24.
172. Malfait F, Wenstrup RJ, De Paepe A. Clinical and genetic aspects of Ehlers-Danlos syndrome, classic type. Genet Med. 2010;12(10):597-605.
173. Malfait F, De Coster P, Hausser I, van Essen AJ, Franck P, Colige A, et al. The natural history, including orofacial features of three patients with Ehlers-Danlos syndrome, dermatosparaxis type (EDS type VIIC). American Journal of Medical Genetics Part A. 2004;131(1):18-28.
174. Symoens S, Malfait F, Renard M, Andre J, Hausser I, Loeys B, et al. COL5A1 signal peptide mutations interfere with protein secretion and cause classic Ehlers-Danlos syndrome. Hum Mutat. 2009;30(2):E395-403.
175. Zalis EG, Roberts DC. Ehlers-Danlos syndrome with a hypoplastic kidney, bladder diverticulum, and diaphragmatic hernia. Arch Dermatol. 1967;96(5):540-4.
176. Burrows NP, Monk BE, Harrison JB, Pope FM. Giant bladder diverticulum in Ehlers-Danlos syndrome type I causing outflow obstruction. Clin Exp Dermatol. 1998;23(3):109-12.
177. Cuckow PM, Blackhall RJ, Mouriquand PD. Huge bladder diverticula associated with Ehlers-Danlos syndrome. J R Soc Med. 1994;87(5):290-1.
178. Berger J, Lang E, Schaeffer EM. Urological radiographic manifestations of the Ehlers-Danlos syndrome. The Journal of Urology. 2007;178(4 Pt 1):1490.
179. Jorion JL, Michel M. Spontaneous rupture of bladder diverticula in a girl with Ehlers-Danlos syndrome. J Pediatr Surg. 1999;34(3):483-4.
180. Handa S, Sethuraman G, Mohan A, Sharma VK. Ehlers-Danlos syndrome with bladder diverticula. Br J Dermatol. 2001;144(5):1084-5.

181. Shukla AR, Bellah RA, Canning DA, Carr MC, Snyder HM, Zderic SA. Giant bladder diverticula causing bladder outlet obstruction in children. The Journal of Urology. 2004;172(5 Pt 1):1977-9.
182. Eadie DG, Wilkins JL. Bladder-neck obstruction and the Ehlers-Danlos syndrome. Br J Urol. 1967;39(3):353-8.
183. Kuivaniemi H, Peltonen L, Palotie A, Kaitila I, Kivirikko KI. Abnormal copper metabolism and deficient lysyl oxidase activity in a heritable connective tissue disorder. J Clin Invest. 1982;69(3):730-3.
184. Breivik N, Refsum S, Jr., Oppedal BR, Vesterhus P. Ehlers-Danlos syndrome and diverticula of the bladder. Z Kinderchir. 1985;40(4):243-6.
185. Schippers E, Dittler HJ. Multiple hollow organ dysplasia in Ehlers-Danlos syndrome. J Pediatr Surg. 1989;24(11):1181-3.
186. Kahn T, Reiser M, Gmeinwieser J, Heuck A. The Ehlers-Danlos syndrome, type IV, with an unusual combination of organ malformations. Cardiovasc Intervent Radiol. 1988;11(5):288-91.
187. Bade JJ, Ypma AF, van Elk P, Mensink HJ. A pelvic mass: bladder diverticulum with haemorrhage in Ehlers-Danlos patient. Scand J Urol Nephrol. 1994;28(3):319-21.
188. Stage KH, Tank ES. Primary congenital bladder diverticula in boys. Urology. 1992;40(6):536-8.
189. Kumar S, Jayant K, Barapatra Y, Rani J, Agrawal S. Giant Urinary Bladder Diverticula presenting as Epigastric Mass and Dyspepsia. Nephrourol Mon. 2014;6(4):e18918.
190. Ghosh AK, O'Bryan T. Ehlers-Danlos syndrome with reflux nephropathy. Nephron. 1995;70(2):266.
191. Remvig L, Jensen DV, Ward RC. Epidemiology of general joint hypermobility and basis for the proposed criteria for benign joint hypermobility syndrome: review of the literature. J Rheumatol. 2007;34(4):804-9.
192. Beighton P, De Paepe A, Steinmann B, Tsipouras P, Wenstrup RJ. Ehlers-Danlos syndromes: revised nosology, Villefranche, 1997. Ehlers-Danlos National Foundation (USA) and Ehlers-Danlos Support Group (UK). Am J Med Genet. 1998;77(1):31-7.
193. Forleo LH, Hilario MO, Peixoto AL, Naspitz C, Goldenberg J. Articular hypermobility in school children in Sao Paulo, Brazil. J Rheumatol. 1993;20(5):916-7.
194. Larsson LG, Baum J, Mudholkar GS, Srivastava DK. Hypermobility: prevalence and features in a Swedish population. Br J Rheumatol. 1993;32(2):116-9.
195. Decoster LC, Vailas JC, Lindsay RH, Williams GR. Prevalence and features of joint hypermobility among adolescent athletes. Arch Pediatr Adolesc Med. 1997;151(10):989-92.
196. Rikken-Bultman DG, Wellink L, van Dongen PW. Hypermobility in two Dutch school populations. Eur J Obstet Gynecol Reprod Biol. 1997;73(2):189-92.
197. Bristow J, Tee MK, Gitelman SE, Mellon SH, Miller WL. Tenascin-X: a novel extracellular matrix protein encoded by the human XB gene overlapping P450c21B. J Cell Biol. 1993;122(1):265-78.
198. Lethias C, Descollonges Y, Boutillon MM, Garrone R. Flexilin: a new extracellular matrix glycoprotein localized on collagen fibrils. Matrix biology : journal of the International Society for Matrix Biology. 1996;15(1):11-9.
199. Lethias C, Carisey A, Comte J, Cluzel C, Exposito JY. A model of tenascin-X integration within the collagenous network. FEBS Lett. 2006;580(26):6281-5.

200. Bristow J, Carey W, Egging D, Schalkwijk J. Tenascin-X, collagen, elastin, and the Ehlers-Danlos syndrome. American journal of medical genetics Part C, Seminars in Medical Genetics. 2005;139C(1):24-30.
201. Veit G, Hansen U, Keene DR, Bruckner P, Chiquet-Ehrismann R, Chiquet M, et al. Collagen XII interacts with avian tenascin-X through its NC3 domain. The Journal of Biological Chemistry. 2006;281(37):27461-70.
202. Egging D, van den Berkmortel F, Taylor G, Bristow J, Schalkwijk J. Interactions of human tenascin-X domains with dermal extracellular matrix molecules. Arch Dermatol Res. 2007;298(8):389-96.
203. Minamitani T, Ikuta T, Saito Y, Takebe G, Sato M, Sawa H, et al. Modulation of collagen fibrillogenesis by tenascin-X and type VI collagen. Experimental Cell Research. 2004;298(1):305-15.
204. Burch GH, Gong Y, Liu W, Dettman RW, Curry CJ, Smith L, et al. Tenascin-X deficiency is associated with Ehlers-Danlos syndrome. Nature Genetics. 1997;17(1):104-8.
205. Schalkwijk J, Zweers MC, Steijlen PM, Dean WB, Taylor G, van Vlijmen IM, et al. A recessive form of the Ehlers-Danlos syndrome caused by tenascin-X deficiency. N Engl J Med. 2001;345(16):1167-75.
206. Voermans NC, Jenniskens GJ, Hamel BC, Schalkwijk J, Guicheney P, van Engelen BG. Ehlers-Danlos syndrome due to tenascin-X deficiency: muscle weakness and contractures support overlap with collagen VI myopathies. American Journal of Medical Genetics Part A. 2007;143A(18):2215-9.
207. Voermans NC, Altenburg TM, Hamel BC, de Haan A, van Engelen BG. Reduced quantitative muscle function in tenascin-X deficient Ehlers-Danlos patients. Neuromuscul Disord. 2007;17(8):597-602.
208. Voermans NC, Verrijp K, Eshuis L, Balemans MC, Egging D, Sterrenburg E, et al. Mild muscular features in tenascin-X knockout mice, a model of Ehlers-danlos syndrome. Connect Tissue Res. 2011;52(5):422-32.
209. Lindor NM, Bristow J. Tenascin-X deficiency in autosomal recessive Ehlers-Danlos syndrome. American journal of medical genetics Part A. 2005;135(1):75-80.
210. Mao JR, Taylor G, Dean WB, Wagner DR, Afzal V, Lotz JC, et al. Tenascin-X deficiency mimics Ehlers-Danlos syndrome in mice through alteration of collagen deposition. Nature Genetics. 2002;30(4):421-5.
211. Zweers MC, Bristow J, Steijlen PM, Dean WB, Hamel BC, Otero M, et al. Haploinsufficiency of TNXB is associated with hypermobility type of Ehlers-Danlos syndrome. Am J Hum Genet. 2003;73(1):214-7.
212. Egging DF, van Vlijmen I, Starcher B, Gijsen Y, Zweers MC, Blankevoort L, et al. Dermal connective tissue development in mice: an essential role for tenascin-X. Cell Tissue Res. 2006;323(3):465-74.
213. Zweers MC, Hakim AJ, Grahame R, Schalkwijk J. Joint hypermobility syndromes: the pathophysiologic role of tenascin-X gene defects. Arthritis Rheum. 2004;50(9):2742-9.
214. Zweers MC, van Vlijmen-Willems IM, van Kuppevelt TH, Mecham RP, Steijlen PM, Bristow J, et al. Deficiency of tenascin-X causes abnormalities in dermal elastic fiber morphology. J Invest Dermatol. 2004;122(4):885-91.
215. Zweers MC, Schalkwijk J, van Kuppevelt TH, van Vlijmen-Willems IM, Bergers M, Lethias C, et al. Transplantation of reconstructed human skin on nude mice: a model system

to study expression of human tenascin-X and elastic fiber components. Cell and Tissue Research. 2005;319(2):279-87.
216. Chiquet-Ehrismann R, Kalla P, Pearson CA, Beck K, Chiquet M. Tenascin interferes with fibronectin action. Cell. 1988;53(3):383-90.
217. Fujie S, Maita H, Ariga H, Matsumoto K. Tenascin-X induces cell detachment through p38 mitogen-activated protein kinase activation. Biol Pharm Bull. 2009;32(10):1795-9.
218. Matsumoto K, Takayama N, Ohnishi J, Ohnishi E, Shirayoshi Y, Nakatsuji N, et al. Tumour invasion and metastasis are promoted in mice deficient in tenascin-X. Genes Cells. 2001;6(12):1101-11.
219. Matsumoto K, Sato T, Oka S, Inokuchi J, Ariga H. Comparison of the compositions of phospholipid-associated fatty acids in wild-type and extracellular matrix tenascin-X-deficient mice. Biol Pharm Bull. 2004;27(9):1447-50.
220. Ikuta T, Ariga H, Matsumoto KI. Effect of tenascin-X together with vascular endothelial growth factor A on cell proliferation in cultured embryonic hearts. Biol Pharm Bull. 2001;24(11):1320-3.
221. Alcaraz LB, Exposito JY, Chuvin N, Pommier RM, Cluzel C, Martel S, et al. Tenascin-X promotes epithelial-to-mesenchymal transition by activating latent TGF-beta. J Cell Biol. 2014;205(3):409-28.
222. Springer MS, Murphy WJ. Mammalian evolution and biomedicine: new views from phylogeny. Biol Rev Camb Philos Soc. 2007;82(3):375-92.
223. Chen F, Guo R, Itoh S, Moreno L, Rosenthal E, Zappitelli T, et al. First mouse model for combined osteogenesis imperfecta and Ehlers-Danlos syndrome. J Bone Miner Res. 2014;29(6):1412-23.
224. Cooper TK, Zhong Q, Krawczyk M, Tae HJ, Muller GA, Schubert R, et al. The haploinsufficient Col3a1 mouse as a model for vascular Ehlers-Danlos syndrome. Vet Pathol. 2010;47(6):1028-39.
225. Wenstrup RJ, Florer JB, Davidson JM, Phillips CL, Pfeiffer BJ, Menezes DW, et al. Murine model of the Ehlers-Danlos syndrome. col5a1 haploinsufficiency disrupts collagen fibril assembly at multiple stages. The Journal of Biological Chemistry. 2006;281(18):12888-95.
226. Costantini F, Shakya R. GDNF/Ret signaling and the development of the kidney. Bioessays. 2006;28(2):117-27.
227. Jain S. The many faces of RET dysfunction in kidney. Organogenesis. 2009;5(4):177-90.
228. Srinivas S, Wu Z, Chen CM, D'Agati V, Costantini F. Dominant effects of RET receptor misexpression and ligand-independent RET signaling on ureteric bud development. Development. 1999;126(7):1375-86.
229. Yu OH, Murawski IJ, Myburgh DB, Gupta IR. Overexpression of RET leads to vesicoureteric reflux in mice. American Journal of Physiology Renal Physiology. 2004;287(6):F1123-30.
230. Dressler GR, Deutsch U, Chowdhury K, Nornes HO, Gruss P. Pax2, a new murine paired-box-containing gene and its expression in the developing excretory system. Development. 1990;109(4):787-95.
231. Murawski IJ, Myburgh DB, Favor J, Gupta IR. Vesico-ureteric reflux and urinary tract development in the Pax2 1Neu+/- mouse. Am J Physiol Renal Physiol. 2007;293(5):F1736-45.

232. Sanyanusin P, Schimmenti LA, McNoe LA, Ward TA, Pierpont ME, Sullivan MJ, et al. Mutation of the PAX2 gene in a family with optic nerve colobomas, renal anomalies and vesicoureteral reflux. Nature Genetics. 1995;9(4):358-64.
233. Sanyanusin P, McNoe LA, Sullivan MJ, Weaver RG, Eccles MR. Mutation of PAX2 in two siblings with renal-coloboma syndrome. Human Molecular Genetics. 1995;4(11):2183-4.
234. Favor J, Sandulache R, Neuhauser-Klaus A, Pretsch W, Chatterjee B, Senft E, et al. The mouse Pax2(1Neu) mutation is identical to a human PAX2 mutation in a family with renal-coloboma syndrome and results in developmental defects of the brain, ear, eye, and kidney. Proceedings of the National Academy of Sciences of the United States of America. 1996;93(24):13870-5.
235. Hains D, Sims-Lucas S, Kish K, Saha M, McHugh K, Bates CM. Role of fibroblast growth factor receptor 2 in kidney mesenchyme. Pediatr Res. 2008;64(6):592-8.
236. Hains DS, Sims-Lucas S, Carpenter A, Saha M, Murawski I, Kish K, et al. High incidence of vesicoureteral reflux in mice with Fgfr2 deletion in kidney mesenchyma. The Journal of Urology. 2010;183(5):2077-84.
237. Nishimura H, Yerkes E, Hohenfellner K, Miyazaki Y, Ma J, Hunley TE, et al. Role of the angiotensin type 2 receptor gene in congenital anomalies of the kidney and urinary tract, CAKUT, of mice and men. Mol Cell. 1999;3(1):1-10.
238. Yerkes E, Nishimura H, Miyazaki Y, Tsuchida S, Brock JW, 3rd, Ichikawa I. Role of angiotensin in the congenital anomalies of the kidney and urinary tract in the mouse and the human. Kidney Int Suppl. 1998;67:S75-7.
239. Oshima K, Miyazaki Y, Brock JW, 3rd, Adams MC, Ichikawa I, Pope JCt. Angiotensin type II receptor expression and ureteral budding. The Journal of Urology. 2001;166(5):1848-52.
240. Pedersen A, Skjong C, Shawlot W. Lim 1 is required for nephric duct extension and ureteric bud morphogenesis. Developmental Biology. 2005;288(2):571-81.
241. Desalle R, Chicote JU, Sun TT, Garcia-Espana A. Generation of divergent uroplakin tetraspanins and their partners during vertebrate evolution: identification of novel uroplakins. BMC Evolutionary Biology. 2014;14:13.
242. Garcia-Espana A, Chung PJ, Zhao X, Lee A, Pellicer A, Yu J, et al. Origin of the tetraspanin uroplakins and their co-evolution with associated proteins: implications for uroplakin structure and function. Mol Phylogenet Evol. 2006;41(2):355-67.
243. Hu P, Meyers S, Liang FX, Deng FM, Kachar B, Zeidel ML, et al. Role of membrane proteins in permeability barrier function: uroplakin ablation elevates urothelial permeability. American journal of physiology Renal physiology. 2002;283(6):F1200-7.
244. Murawski IJ, Watt CL, Gupta IR. Vesico-ureteric reflux: using mouse models to understand a common congenital urinary tract defect. Pediatric Nephrology. 2011;26(9):1513-22.
245. Murawski IJ, Maina RW, Malo D, Guay-Woodford LM, Gros P, Fujiwara M, et al. The C3H/HeJ inbred mouse is a model of vesico-ureteric reflux with a susceptibility locus on chromosome 12. Kidney Int. 2010;78(3):269-78.
246. Sargent MA. What is the normal prevalence of vesicoureteral reflux? Pediatr Radiol. 2000;30(9):587-93.
247. Muensterer OJ. Comprehensive ultrasound versus voiding cysturethrography in the diagnosis of vesicoureteral reflux. Eur J Pediatr. 2002;161(8):435-7.

248. Chand DH, Rhoades T, Poe SA, Kraus S, Strife CF. Incidence and severity of vesicoureteral reflux in children related to age, gender, race and diagnosis. The Journal of Urology. 2003;170(4 Pt 2):1548-50.
249. Exeter D, Connell DA. Skeletal muscle: functional anatomy and pathophysiology. Semin Musculoskelet Radiol. 2010;14(2):97-105.
250. Murawski IJ, Watt CL, Gupta IR. Assessing urinary tract defects in mice: methods to detect the presence of vesicoureteric reflux and urinary tract obstruction. Methods Mol Biol. 2012;886:351-62.
251. Hellemans J, Vandesompele J. Selection of reliable reference genes for RT-qPCR analysis. Methods Mol Biol. 2014;1160:19-26.
252. Bustin SA, Wittwer CT. MIQE: A Step Toward More Robust and Reproducible Quantitative PCR. Clin Chem. 2017.
253. Hellemans J, Mortier G, De Paepe A, Speleman F, Vandesompele J. qBase relative quantification framework and software for management and automated analysis of real-time quantitative PCR data. Genome Biol. 2007;8(2):R19.
254. Karolchik D, Hinrichs AS, Furey TS, Roskin KM, Sugnet CW, Haussler D, et al. The UCSC Table Browser data retrieval tool. Nucleic Acids Res. 2004;32(Database issue):D493-6.
255. El Andalousi J, Murawski IJ, Capolicchio JP, El-Sherbiny M, Jednak R, Gupta IR. A single-center cohort of Canadian children with VUR reveals renal phenotypes important for genetic studies. Pediatr Nephrol. 2013;28(9):1813-9.
256. Tee MK, Thomson AA, Bristow J, Miller WL. Sequences promoting the transcription of the human XA gene overlapping P450c21A correctly predict the presence of a novel, adrenal-specific, truncated form of tenascin-X. Genomics. 1995;28(2):171-8.
257. Tasian G, Cunha G, Baskin L. Smooth muscle differentiation and patterning in the urinary bladder. Differentiation. 2010;80(2-3):106-17.
258. Smits-Engelsman B, Klerks M, Kirby A. Beighton score: a valid measure for generalized hypermobility in children. J Pediatr. 2011;158(1):119-23, 23 e1-4.
259. Morissette R, Merke DP, McDonnell NB. Transforming growth factor-beta (TGF-beta) pathway abnormalities in tenascin-X deficiency associated with CAH-X syndrome. Eur J Med Genet. 2014;57(2-3):95-102.
260. Kang JH, Jiang Y, Toita R, Oishi J, Kawamura K, Han A, et al. Phosphorylation of Rho-associated kinase (Rho-kinase/ROCK/ROK) substrates by protein kinases A and C. Biochimie. 2007;89(1):39-47.
261. Hartmann S, Ridley AJ, Lutz S. The Function of Rho-Associated Kinases ROCK1 and ROCK2 in the Pathogenesis of Cardiovascular Disease. Front Pharmacol. 2015;6:276.
262. Michael L, Sweeney DE, Davies JA. A role for microfilament-based contraction in branching morphogenesis of the ureteric bud. Kidney International. 2005;68(5):2010-8.
263. Wibberley A, Chen Z, Hu E, Hieble JP, Westfall TD. Expression and functional role of Rho-kinase in rat urinary bladder smooth muscle. Br J Pharmacol. 2003;138(5):757-66.
264. Meyer TN, Schwesinger C, Sampogna RV, Vaughn DA, Stuart RO, Steer DL, et al. Rho kinase acts at separate steps in ureteric bud and metanephric mesenchyme morphogenesis during kidney development. Differentiation. 2006;74(9-10):638-47.
265. Thumkeo D, Keel J, Ishizaki T, Hirose M, Nonomura K, Oshima H, et al. Targeted disruption of the mouse rho-associated kinase 2 gene results in intrauterine growth retardation and fetal death. Mol Cell Biol. 2003;23(14):5043-55.

266. Zhao XH, Laschinger C, Arora P, Szaszi K, Kapus A, McCulloch CA. Force activates smooth muscle alpha-actin promoter activity through the Rho signaling pathway. Journal of Cell Science. 2007;120(Pt 10):1801-9.
267. Hinz B, Celetta G, Tomasek JJ, Gabbiani G, Chaponnier C. Alpha-smooth muscle actin expression upregulates fibroblast contractile activity. Mol Biol Cell. 2001;12(9):2730-41.
268. Tofts LJ, Elliott EJ, Munns C, Pacey V, Sillence DO. The differential diagnosis of children with joint hypermobility: a review of the literature. Pediatr Rheumatol Online J. 2009;7:1.
269. Castori M, Camerota F, Celletti C, Danese C, Santilli V, Saraceni VM, et al. Natural history and manifestations of the hypermobility type Ehlers-Danlos syndrome: a pilot study on 21 patients. American Journal of Medical Genetics Part A. 2010;152A(3):556-64.
270. Lorenzo Tosi VS, Yunlong Yang, Dongli Guan, Polina Shpilker, Nicola Segata, H. Benjamin Larman & Biju Parekkadan. Long-adapter single-strand oligonucleotide probes for the massively multiplexed cloning of kilobase genome regions. Nature. 2017;1(0092).